The design and testing of magnets for nuclear magnetic resonance imaging.

Evans, P. R.

Award date:
1984

Awarding institution:
University of Bath

THE DESIGN AND TESTING OF MAGNETS
FOR
NUCLEAR MAGNETIC RESONANCE IMAGING

submitted by P.R.Evans

for the degree of Ph.D.

of the University of Bath

1984

P. R. Evans

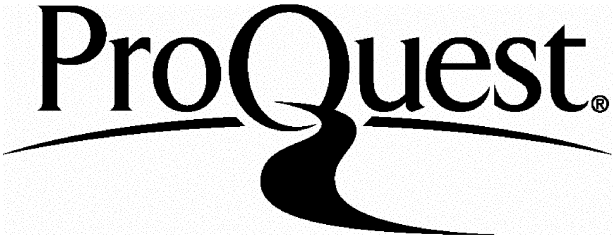

ABSTRACT

Recently, images of the inside of the human body have been produced non-invasively using nuclear magnetic resonance (nmr). The technique involves placing the patient in a strong, homogeneous magnetic field. The heart of any nmr imaging system is the magnet that produces this field and this thesis is concerned with the design and testing of such magnets.

Various computer programs have been written that allow the designer to model a magnet either in terms of axisymmetric coils, or in terms of the discrete conductors that simulate the actual form of the winding. The axisymmetric program automatically optimises the design so as to produce a uniform field, and the data from this program may be used directly to generate an appropriate helical or spiral winding. These programs not only allow the designer to produce a suitable design, but also to put tolerances on the dimensions of the conductors and formers that support the winding. The problem of removing inhomogeneities produced by dimensional inaccuracies and surrounding ferromagnetic materials is also considered.

A nmr probe system has been developed that allows the homogeneity of a magnet to be assessed independently of the stability of its power supply. The probe has been used for field measurements in a magnet designed using the above techniques, and the results are presented.

To my Mother and Father
for all their support and
encouragement.

ACKNOWLEDGEMENTS

My thanks go to Professor J.F.Eastham for his guidance and supervision during this work, and to Dr.I.R.Young, without whom this work would not have been undertaken. May I also thank Dr.D.Rodger and Dr.M.Burl for their help, and their novel approaches to solving problems. I am grateful to Mr.M.D.Evans for the use of his word processing facilities.

The work was supported by an S.R.C. Industrial Studentship, with the cooperation of EMI's Central Research Laboratory.

INDEX

LIST OF SYMBOLS

A	area of coil
A_n, a_{nm}	harmonic amplitude
b_{nm}	harmonic amplitude
B	bandwidth
B_o	static magnetic field
B_1	rf magnetic field
B_{eff}	combined B_o and B_1
c_{nm}	weighted harmonic amplitude
d_{nm}	weighted harmonic amplitude
E	2nd kind complete elliptic integral
E_c	coil voltage
E_n	noise voltage
g	magnetogyric ratio
H	magnetic field
I	spin number
$\hbar$	Planck's constant / 2π
K	1st kind complete elliptic integral
k	Boltzmann's constant, modulus of elliptic integral
k_c	complementary modulus of elliptic integral
L	coil inductance
M	magnetisation
M'	magnetisation in rotating frame

M_o	static magnetisation
m	degree of Legendre function
N	spin density
n	order of Legendre function or polynomial
P_n	Legendre polynomial
P_{nm}	Legendre function
p	filling factor or integer
Q	quality factor of coil
q	integer
r	spherical radius
r_o	measurement radius
s	rms signal to noise ratio
T	absolute temperature, or period of time
T_1	spin-lattice relaxation time
T_2'	observed 'spin-spin' relaxation time
T_2	intrinsic spin-spin relaxation time
T_2^*	inhomogeneity component of 'spin-spin' relaxation time
u	magnetic moment, or cos θ
u'	magnetic moment in rotating frame
u_o	permeability of free space
V	magnetostatic potential
V_c	coil volume

w	angular frequency
w_o	angular Larmor frequency
w_{err}	error in angular frequency
X,Y,Z	shorthand notation for spherical harmonics
x,y,z	Cartesian coordinates
x',y',z'	Cartesian coordinates in rotating frame
θ	spherical coordinate
ϕ	spherical and cylindrical coordinate of azimuth
ρ	cylindrical coordinate of radius
Π	3rd kind complete elliptic integral

INTRODUCTION

There is an obvious need for painless, non-invasive methods for producing images of the inside of the human body. Various forms of radiation have been used for this purpose, including X-rays, gamma rays and ultrasound. For many years, virtually the only method of producing these images has been to expose the body to X-rays, and record the presence of those rays that pass through the body on a photographic film. The major drawbacks in the usefulness of the resulting images are that the soft tissues within the body are often obscured by surrounding bone, and that there is little contrast between normal and diseased tissue.

In 1972, EMI invented the Brain Scanner [i], followed later by a body scanner. These machines rotate an X-ray tube around the patient, and measure the rays that pass through the patient with a suitable detector. The data is stored in a computer, and from it a picture of a transverse "slice" through the patient is reconstructed

This technique, known as Computed Tomography, marked a great step forward in the diagnosis of many diseases because of its ability to obtain unobscured images of the internal organs, and the increased contrast between different tissues that could be achieved. The most

notable area of application is probably within the brain, where both of these factors allow conditions that were previously undetectable to be readily diagnosed. However, the major drawback with the method is that there is a risk to the patient in exposing him to X-ray radiation. Tomographic techniques employing gamma rays are also used, but these also present a risk to the patient as they use ionising radiation.

The use of ultrasound [ii] has the benefit of being safer. It is used routinely used for the examination of unborn children. Ultrasound pulses are applied to the patient, and reflections from the internal bones and organs received as echoes. These are then processed to yield an image, either on a storage tube or a television monitor. However, this technique also suffers from problems caused by dense bone, and the differentiation between diseased and normal tissue is not good.

More recently, scans have been made using nuclear magnetic resonance (nmr). This technique exploits the properties of the minute magnetic moment of certain atomic nuclei . Usually, the nucleus concerned is that of hydrogen, because this is the most abundant element in the body suitable for nmr scanning. The images therefore highlight any substances with a high water or fat content.

The technique involves placing the patient in a strong (0.1-2.0 Tesla), homogeneous magnetic field. The nuclei are then able to resonate at a frequency, usually between 1 and 100MHz, that is proportional to the magnitude of the field. Radio frequency pulses are applied at the resonant frequency that excite the nuclei , and these in turn induce a small voltage in a pickup coil. In addition to the rf pulses, well defined disturbances to the field homogeneity are produced, and these allow the position of the source of the induced voltage to be determined. A picture may then be displayed that maps out the volume density of hydrogen nuclei throughout the region that is scanned. The process is described more thoroughly in chapter 1.

The major advantages of the method are that it is regarded as completely safe, and the problems of an area of interest being obscured by bone simply does not occur because such materials do not reflect or absorb the rf fields that are used. However, the most significant advantage over other methods is that, since the atomic nucleii are intimately linked with the chemical structure of materials, information about the chemical composition of organs may be obtained. Thus the differences between healthy and diseased tissue may be readily seen. Furthemore, the sequence of rf pulses may be altered so

as to emphasise these differences.

The heart of any nmr imaging system is the magnet in which the patient is placed. For fields above about 0.2 Tesla, superconducting magnets operating in persistent mode are usually used. Below this figure magnets may be constructed from conventional copper or aluminium windings. It is essential that the field is as homogeneous as possible, a variation of less than 50 parts per million being necessary for most scanning methods

The magnet itself is usually constructed from coaxial, circular coils. Typical arrangements are a long solenoid with a "correction coil" at each end, or four coils spaced over the surface of a sphere. This thesis is concerned with the design and testing of such magnets. The major part of this work has been the writing of computer programs that model the magnet windings and obtain accurate field values. The first of these is a fast interactive program that uses axisymmetric loops, solenoids and thick section coils as models. Automatic optimisation of the coil geometry is performed so as to produce a uniform field. The design may then be evaluated in terms of its field uniformity, conductor weight and dissipation (if resistive). The next stage in the design is the accurate modelling of the actual windings. A

second program allows effects such as helical or spiral pitch, ovality and coil interconnections to be modelled. These programs not only allow the user to design a suitable magnet, but to put mechanical tolerances on the placement of the conductors and the dimensions of the formers that support the winding.

Inevitably, a real magnet will have a reduced homogeneity compared with its design performance. This may either be due to mechanical tolerances in its construction, or the effects of ferromagnetic materials in the building that contains the magnet. The above programs may be used to design specially shaped coils to remove this inhomogeneity. Alternatively, some of these effects may be removed by deliberately moving individual coils of the magnet away from their designed positions. A third program is used to model these movements.

An accurate field measurement device is needed in order to set up any nmr imaging magnet. A novel magnetometer has been developed that uses the nmr effect. One advantage of the system is that, by using one probe as a reference and the other for measurement, the homogeneity of a magnet may be assessed independently of the stability of its power supply.

The design and measurement methods have been used in a number of applications. However, a full scale resistive

magnet has been designed, built and tested using the software and measurement techniques described here. This magnet has proved itself to be capable of being used for nmr imaging, and measured results from it are presented in the final chapter.

CHAPTER1. THE NMR EFFECT.

1.1 Introduction.

The nmr effect is due to certain atomic nuclei possessing spin, which results in the nuclei having a magnetic dipole moment. It is the properties of this moment that are exploited in an nmr scanner. The most common nucleus used for nmr imaging is that of hydrogen. This is due to the abundance of hydrogen within the body, and the relatively large magnetic moment of the proton.

This chapter looks at the basic physics of nmr, the behaviour of a single magnetic moment being considered before the behaviour of matter in bulk. An experimental procedure is considered, together with the information that may be gained about nmr relaxation times. One technique for producing images of the human body is then described, and this allows a broad specification for a nmr imaging magnet to be drawn up in terms of its physical dimensions, field magnitude and field homogeneity. Some of the equations derived in this chapter will also be of use in future chapters.

The use of quantum mechanics has been avoided even though it gives a more accurate model of nmr. For present purposes classical mechanics suffices, as this allows the

effect to be explained with the aid of a few simple diagrams.

A more general, though early, account of the concepts of nmr is given by Andrew [1.1], whilst Slichter [1.2] provides a more rigorous, up to date approach. The literature on nmr imaging is rapidly expanding, but the papers of Young et al [1.3] describe early scanning hardware, pulse sequences and clinical results. A more comprehensive collection of papers on the present state of the art is given in reference [1.4].

1.2 Isolated moments and the rotating frame.

An atomic nucleus that has spin will have a magnetic dipole moment $\underline{u}$ in addition to a mechanical moment. The ratio of these two moments is known as the magnetogyric ratio, g. It may take positive or negative values depending whether the moments are aligned parallel or anti-parallel. If this magnetic moment is placed in a magnetic field $\underline{B}_o$, that is defined as being parallel to the z axis, it will experience a torque equal to $\underline{u} \times \underline{B}_o$. This torque causes the moment to precess around the z axis (fig 1.1). Equating the rate of change of angular momentum to the applied torque yields:

$$d/dt\ (\underline{u}/g) = \underline{u} \times \underline{B}_o \qquad (1.1)$$

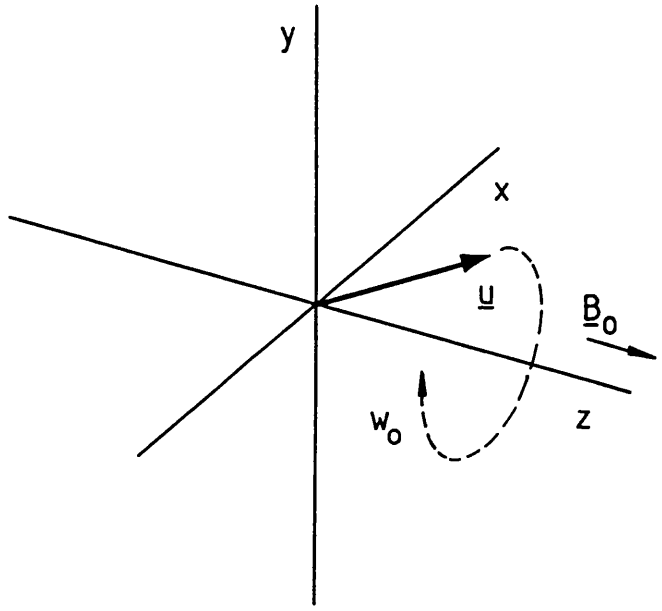

Fig.1.1 A magnetic moment precesses about the applied field

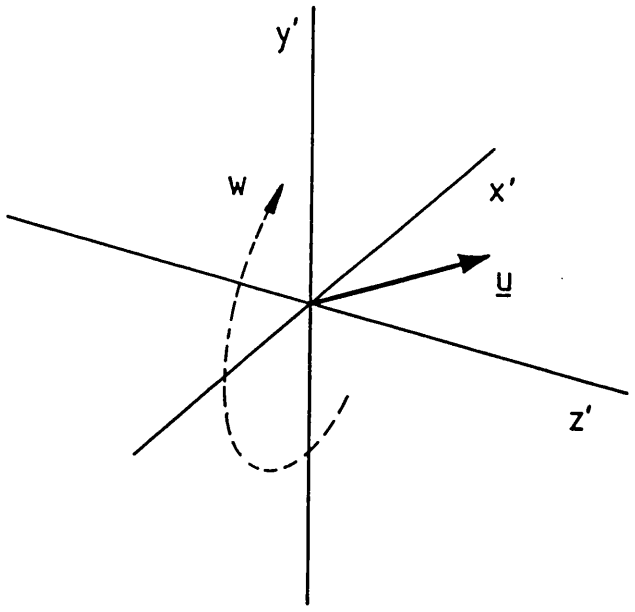

Fig.1.2 Viewed from a rotating frame the moment appears stationary when $w=w_o$

The angular velocity of the moment may be denoted by a vector $\underline{w}_o$. The rate of change of $\underline{u}$ will then be given by:

$$d\underline{u}/dt = \underline{w}_o \times \underline{u} \qquad (1.2)$$

Comparison of 1.1 and 1.2 shows that:

$$\underline{w}_o = - g \underline{B}_o \qquad (1.3)$$

Thus the moment will precess around the z axis at a well defined frequency, known as the Larmor frequency, that is directly proportional to the value of the $\underline{B}_o$ field.

It is necessary to consider the effect of a second field rotating about the z axis, and so it will be useful to look at the moment from a rotating set of axes. Let the coordinates (x',y',z') rotate at angular frequency $\underline{w}$, with the z and z' axes coincident (fig 1.2). If the moment viewed from these axes is $\underline{u}'$ then its equation of motion will be

$$d\underline{u}'/dt = (\underline{w}_o - \underline{w}) \times \underline{u}' \qquad (1.4)$$

Combining equations 1.3 and 1.4 gives

$$d\underline{u}'/dt = g \underline{u}' \times (\underline{B}_o + \underline{w}/g) \qquad (1.5)$$

As the angular frequency of the rotating axes approaches the Larmor frequency the term in the brackets will approach zero, and the moment, viewed from the rotating axes, will precess more slowly and eventually stop when $\underline{w} = \underline{w}_o$.

If a field $\underline{B}_1$, rotating at the Larmor frequency, is now applied such that $\underline{B}_1$ lies along the x' axis, the moment $\underline{u}'$ will be subjected to a torque $\underline{u}' \times \underline{B}_1$. This causes $\underline{u}'$ to precess around the x' axis with frequency $\underline{w}_1 = -g\,\underline{B}_1$, describing a circle in the y'-z' plane (fig 1.3). Thus the angle of precession of $\underline{u}$ around the z axis may be altered by the application of the $\underline{B}_1$ field. The equation for the moment in the rotating frame has now become

$$d\underline{u}'/dt = g\,\underline{u}' \times (\underline{B}_o + \underline{w}/g + \underline{B}_1) \qquad (1.6)$$

and $\underline{u}'$ precesses around an "effective" field given by

$$\underline{B}_{eff} = \underline{B}_o + \underline{w}/g + \underline{B}_1 \qquad (1.7)$$

If $\underline{w} \neq \underline{w}_o$, and given that $\underline{u}'$ lies along z' at t=0, the moment describes a cone whose surface includes the z axis (fig 1.4). The vertex angle of the cone will vary with $\underline{w}$, since $\underline{w}$ varies the direction (and magnitude) of $\underline{B}_{eff}$. For this situation to approximate the case where $\underline{w} = \underline{w}_o$, the condition

$$B_o - w/g \ll B_1 \qquad (1.8)$$

must be fulfilled. If this is not the case, however, and w is far from the Larmor frequency, the vertex angle of the described cone will be very small and the effect of B_1 may be neglected. A resonance condition therefore exists in the sense that the spin system is only disturbed if the frequency of the applied B_1 field is close to the Larmor frequency.

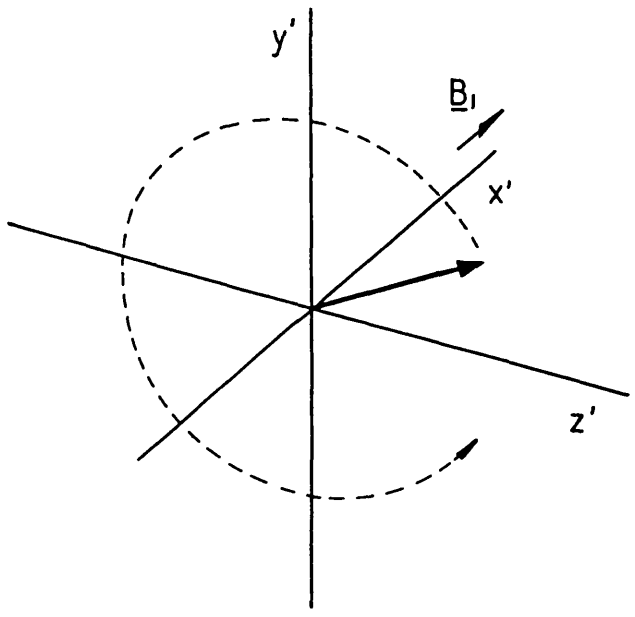

Fig.1.3 The B_1 field causes the moment to rotate in the y'-z' plane

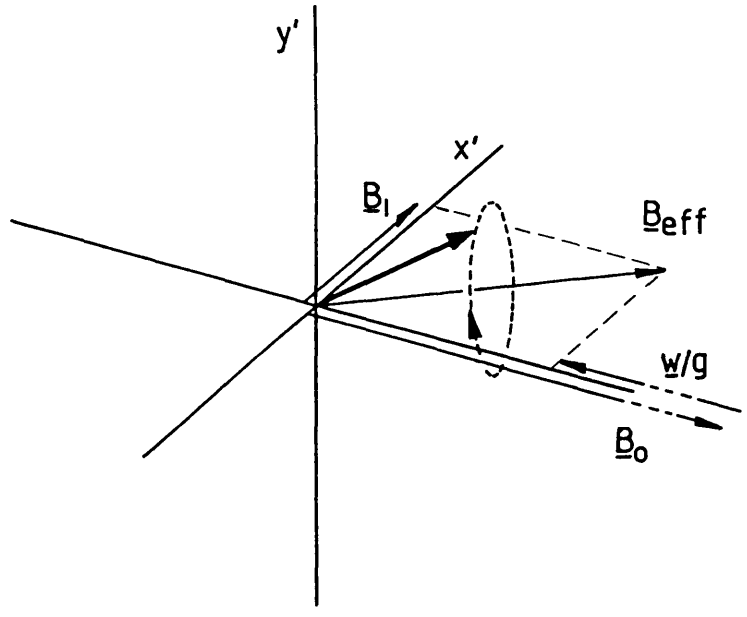

Fig.1.4 Off tune the moment precesses about B_{eff}

1.3 Nmr in matter.

After the $\underline{B}_o$ field is applied to a suitable material, quantum mechanics dictates that the nuclear spins will be in one of two states, the populations of which will be given by the Boltzmann distribution. The difference in populations gives rise to a net "static magnetisation", $\underline{M}_o$, which is given by

$$\underline{M}_o = \frac{N g^2 \hbar^2 I(I+1)}{3 k T} \underline{B}_o \qquad (1.9)$$

where N = no. nucleii per m^3 $\hbar$ = Planck's constant/2π

I = spin number k = Boltzmann's constant

T = absolute temperature of spin system

Application of the B_1 field will disturb the magnetisation as previously described, which will precess in accordance with

$$d\underline{M}'/dt = g \underline{M}' \times \underline{B}_{eff} \qquad (1.10)$$

However, the actual field seen by a particular moment will not only depend on $\underline{B}_o$, but on the field due to its neighbours. Thus there is a tendency for the spins to precess at slightly different frequencies. As a result the net magnetisation in the x-y plane decays (fig 1.5). The effect will be exponential for a single population of spins, and the time constant T_2 is called the "spin-spin

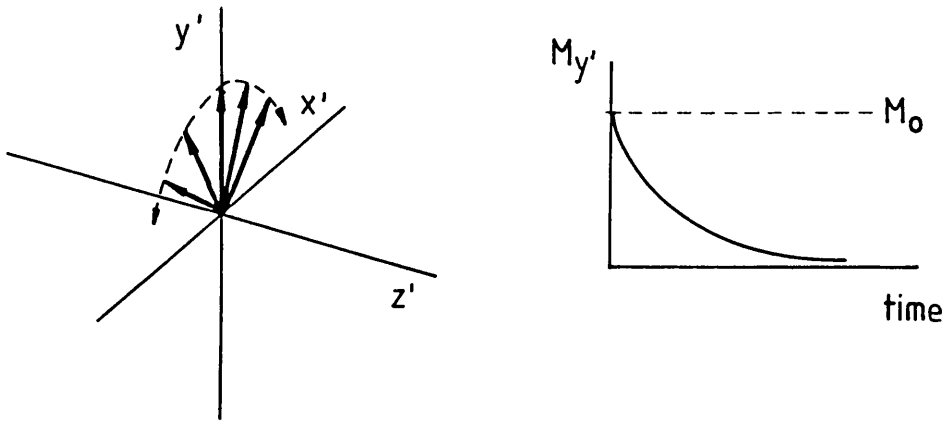

Fig.1.5 M_y' decays with time constant T_2

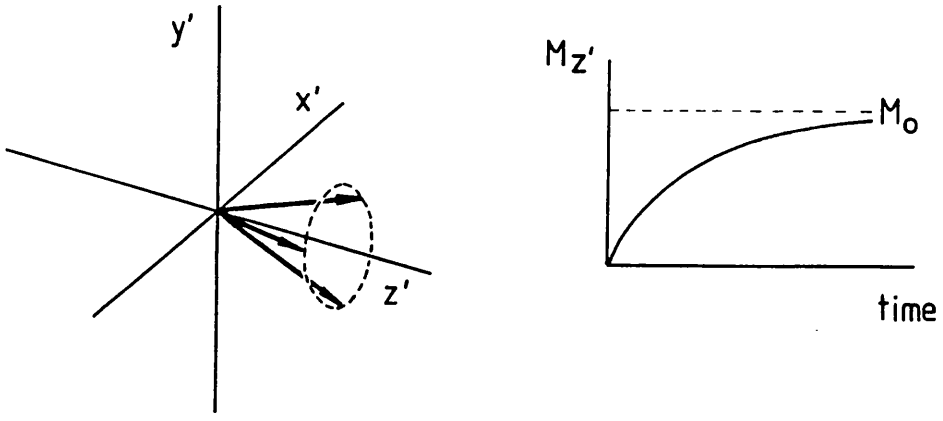

Fig.1.6 M_z' increases with time constant T_1

relaxation time". A similar effect is produced by non-uniformities in B_o, so T_2' is defined as an "observed" time constant which may be resolved into two parts:

$$1/T_2' = 1/T_2 + 1/T_2^* \qquad (1.11)$$

where T_2 is the intrinsic relaxation time for the material, and T_2^* represents the time constant arising from field inhomogeneity. Also, there will be a thermal interaction between the spins and their surrounding chemical "lattice", which results in the z component of the magnetisation returning exponentially towards M_o (fig 1.6). The associated time constant is known as the "spin-lattice relaxation time", and is denoted by T_1. It is the same time constant with which M_o built up upon the initial application of B_o.

The complete equation of motion in the rotating frame thus becomes

$$\frac{d\underline{M}'}{dt} = g\,\underline{M}' \times [\underline{B}_o + \underline{w}/g + \underline{B}_1] - \frac{[M_x'\underline{x}' + M_y'\underline{y}']}{T_2'} - \frac{[M_z' - M_o]\,\underline{z}'}{T_1} \qquad (1.12)$$

This is known as the Bloch equation after the co-discoverer of nmr who proposed it [1.5]. If necessary it may be solved for simple cases as three simultaneous differential equations by means of the Laplace transform. For more complex problems numerical solution may be used.

However, enough detail of nmr processes has been given already so that a typical experiment can be described without actually solving this equation.

1.4 Experimental procedure.

A sample with an abundance of suitable molecules (eg. water) is placed in a strong magnetic field (fig. 1.7). Coils are arranged around the sample for applying $\underline{B}_1$ and detecting the rotating magnetisation.

The magnetogyric ratio for hydrogen is 42.6MHz/Tesla, so that a $\underline{B}_o$ field of 0.1T produces resonance at a fairly convenient 4.26 MHz. The field needs to be homogeneous so that the resonance occurs at the same frequency throughout the sample volume.

The rotating $\underline{B}_1$ field is produced by an oscillating field of magnitude $2B_1$, which may be resolved into two contra-rotating components, each of magnitude B_1. One component, as far as the spins are concerned, will be rotating in phase. The other will be rotating in the wrong direction at twice the speed, and thus has negligible effect. This oscillating field may be produced by a pair of Helmholtz coils spaced around the sample.

By applying B_1, the static magnetisation, M_o, induced in the sample by B_o, may be rotated from lying along the z axis to precessing in the x-y plane. The moments are then said to have been "flipped by 90

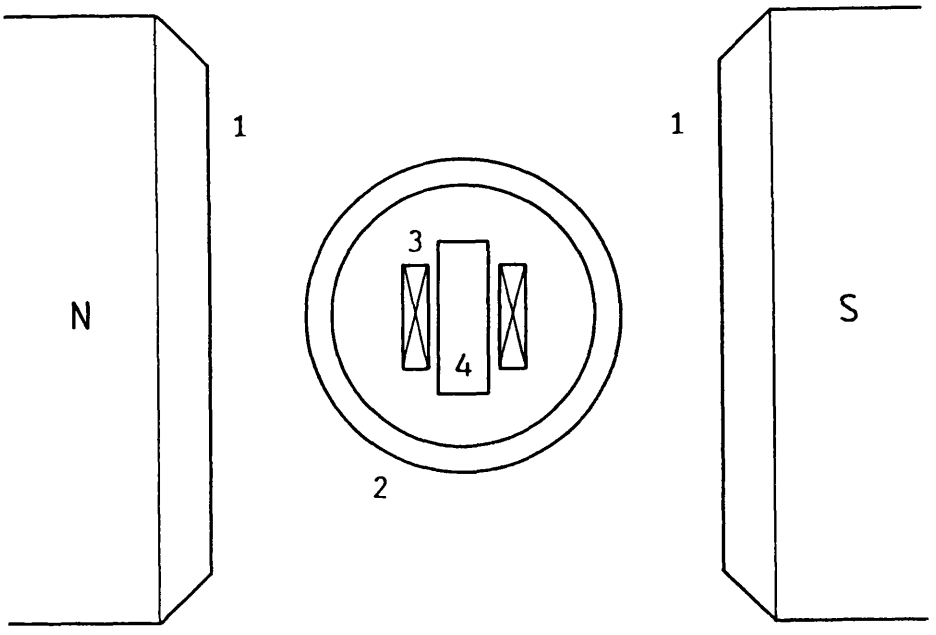

Key:
1. Magnet poles
2. Helmholtz coils for B_1
3. Solenoidal pickup coil
4. Sample

Fig.1.7 Typical experimental arrangement

degrees" with a "90 degree pulse". This is of course providing that the time taken is short compared with T_1 and T_2', and that the frequency of B_1 is close to the Larmor frequency, as given by relation 1.8 .

The pickup coil around the sample has its axis in the x-y plane, and a sinusoidal voltage will be induced in it by the precessing magnetisation. It is this signal

that provides information about the nuclear spin system. The coil is generally tuned and connected to a low noise rf receiver. It is also convenient to place it perpendicular to the B_1 coil so as to avoid overloading the receiver during B_1 pulses.

A typical sequence of events for observing an nmr signal would therefore be to place the sample in the B_o field long enough for the static magnetisation to build up. The B_1 field is then applied to flip the magnetisation into the x-y plane, producing a signal at the receiver output. This signal then decays with time constant T_2', and is known as a "free induction decay" (f.i.d.). It is now necessary to wait for the magnetisation to build up again in the z direction, with time constant T_1, before the process can be repeated. If the sequence is repeated too quickly, a magnetisation much less than M_o will be flipped into the x-y plane, and consequently the received signal will be smaller. The sample is then tending towards "saturation".

1.5 Determination of T_1 & T_2

The time constants that govern the nmr process may be determined using the same experimental equipment as above, but with a different sequence of B_1 pulses.

In order to find T_1 a "180 degree pulse" is used to rotate the magnetisation into the negative z direction

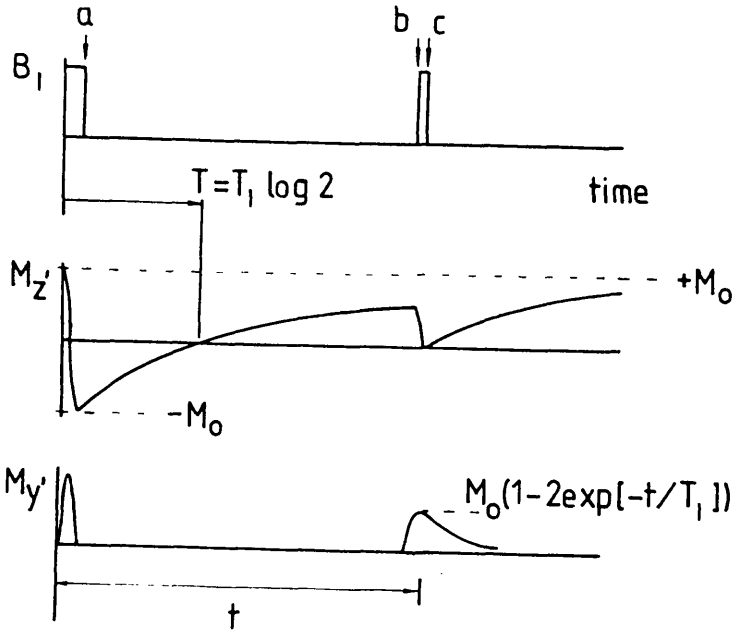

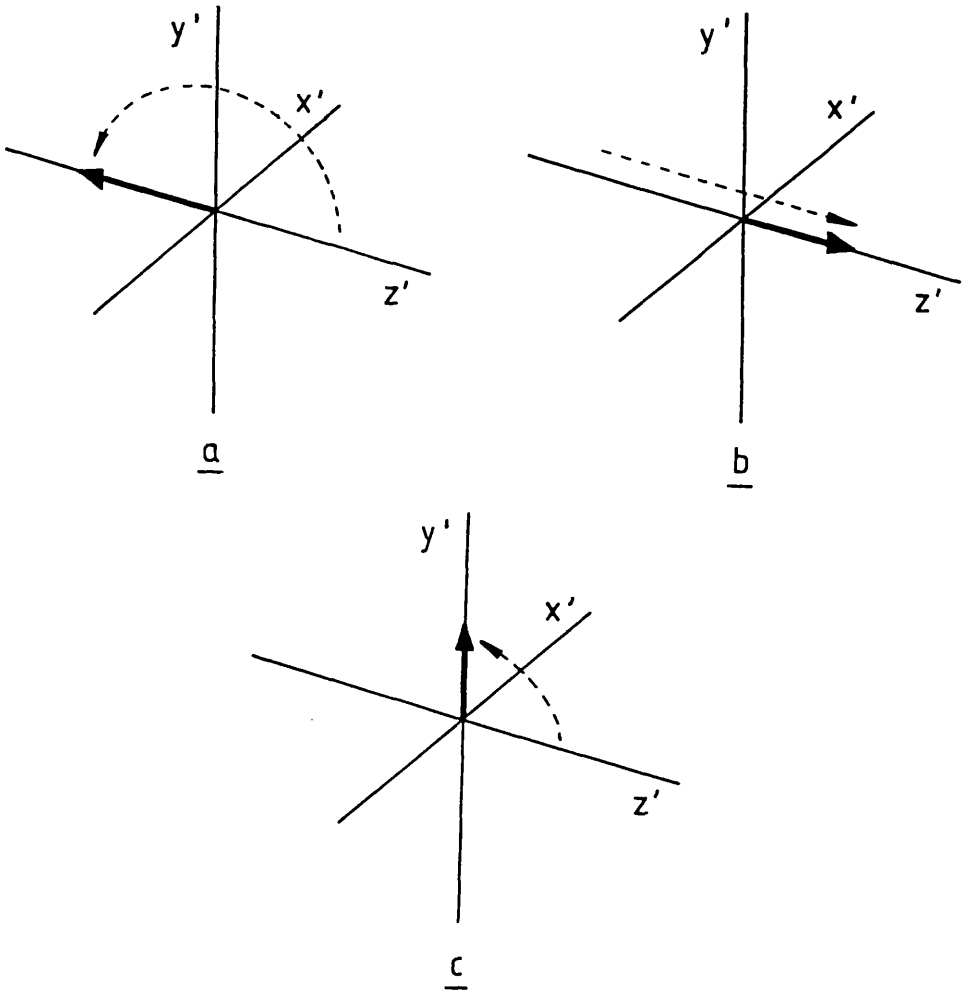

Fig.1.8 The Inversion Recovery sequence

such that $M_z = -M_o$ (fig 1.8). M_z then returns exponentially to its initial value of $+M_o$ with time constant T_1, according to the equation

$$M_z = M_o\,(1 - 2\exp(-t/T_1)) \qquad (1.13)$$

A 90 degree pulse is then applied after a time T. This flips M_z at that instant into the x-y plane, and a free induction decay is observed. If T is adjusted such that this signal is zero, then T_1 will be given by

$$T_1 = T \,/\, \ln(2) \qquad (1.14)$$

The procedure is known as an "inversion recovery sequence" and gives a very quick way of finding T_1.

To find T_2, a 90 degree pulse is applied to the sample, and a free induction decay observed, after which the spins are spread out in the x'-y' plane (fig 1.9). The rate of decay will be determined by T_2' which is usually shorter than T_2 because of field non-uniformities. After a time T, a 180 degree pulse is used to turn this "pancake" of spins over, however their sense of precession remains unchanged. Thus, instead of continuing to fan out, the spins "re-phase" until they are aligned again along the negative y' axis, and then they "dephase" once again. The result is an "echo" that appears at a time 2T after the initial 90 degree pulse, and so the process is known as a "spin echo sequence".

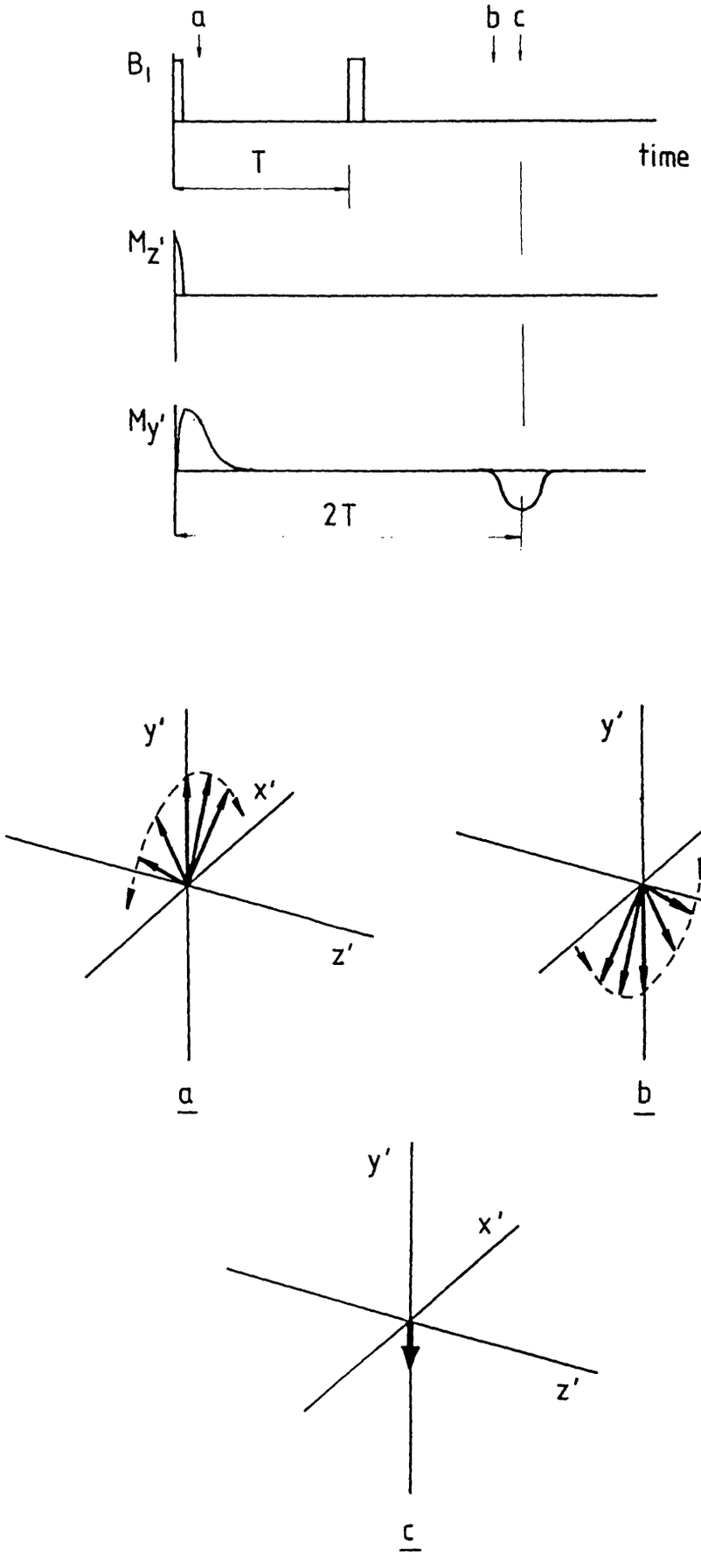

Fig.1.9 The Spin Echo sequence

The magnitude of the echo will be smaller than the original f.i.d. by a factor that depends on T_2, T_1 and T. However, if T_1 is long compared with T_2 then the amplitude of the echo will be smaller than the original f.i.d. by a factor of $\exp(-2T/T_2)$.

Values of T_1 and T_2 vary enormously for different materials. In the case of solids T_1 may be as long as an hour whilst T_2 may be in the order of tens of microseconds. However, for liquids and wet tissues within the body, relaxation times usually have much more convenient values. For example, in pure water $T_1 \doteq T_2 \doteq 3.5$secs. In tissues T_2 is usually in the order of tens of milliseconds, and T_1 hundreds of milliseconds.

1.6 Signal to noise ratio of nmr experiments.

The signal appearing across the tuned pickup coil will be given by

$$E_c = - n A p Q u_o (dM_y/dt) \qquad (1.15)$$

where

E_c = voltage across coil

A = cross sectional area of coil

n = no. of turns

Q = quality factor of coil

p = fraction of coil filled by sample

Since $M_y = M_o \cos(w_o t)$, the signal will, from equations 1.9 and 1.15, have a peak value of

$$E_{c(peak)} = \frac{n\ A\ p\ Q\ u_o\ N\ g\ \hbar^2\ I(I+1)\ w_o}{3\ k\ T} \qquad (1.16)$$

If it is assumed that most of the energy of the magnetic field is stored within the volume of the coil (V_c) such that $1/2(Li^2) \doteq 1/2(V_c B^2/u_o)$, then the nA term in the above formula may be replaced by $(LV_c/u_o)^{1/2}$ yielding

$$E_{c(peak)} = \frac{(\ u_o\ L\ V_c\ )^{1/2}\ p\ Q\ N\ g\ \hbar^2\ I(I+1)\ w_o^{\ 2}}{3\ k\ T} \qquad (1.17)$$

In order to estimate the magnitude of this voltage take $L=10^{-6}$ H, $V_c = 10^{-6}$ m^3, $p = 1$, $Q = 100$, $N = 10^{28}$ m^{-3} $w_o = 25\times10^6$ r/s, $g = 2.7\times10^8$ rad/sT and $I = 1/2$. These are fairly typical values for a small sample of water, and when substituted into 1.17 give $E_c = 127$ μV. Thus some care needs to be taken when processing these small signals.

In low field systems, the main noise contribution in the system will be due to the resistance of the coil, and is given by

$$E_n = \sqrt{4\ k\ T\ B\ R_p} \qquad (1.18)$$

where E_n = rms noise voltage B = bandwidth of system

R_p = equivalent parallel resistance of coil

Letting $R_p = Q\, w_o\, L$ and making allowance for the noise figure F of the receiver, an expression for the signal to noise ratio of the nmr experiment may be obtained from 1.17 and 1.18.

$$S/N = \frac{(u_o\, V_c\, Q)^{1/2} \rho N\, g\, \hbar^2\, I(I+1)\, w_o^{3/2}}{6\, \sqrt{2}\, B^{1/2}\, F\, (k\, T)^{3/2}} \qquad (1.19)$$

Using the previous typical values along with $B = 10^4$ Hz and $F = 1.25$ (2dB), the signal to noise ratio $E_c/E_n = 112$. This figure, of course, is only valid immediately after a 90 degree pulse. It then reduces exponentially to zero with time constant T_2'.

From 1.19 it is evident that experiments should be carried out at the highest possible frequency, and hence field, 100 MHz being typical in a spectrometer. However, for scanning purposes such frequencies are impractical since the outer layers of the body absorb a large portion of the rf energy supplied in the B_1 pulse, and this makes it difficult to excite the nuclei uniformly throughout the region of interest. As a result most scanners operate between 1 and 80MHz.

1.7 Steady State NMR.

All the methods described so far have used B_1 pulses to obtain a transient nmr signal. However, a steady

signal may be obtained by the application of a continuous, low level B_1 field. In fact, this is how much of the work was carried out in the early years of nmr experiments. The Bloch equation (1.12) may solved for steady state conditions by setting $d\underline{M}'/dt=0$. This results in the following expressions for the three components of magnetisation

$$M_{x'} = \frac{g\, B_1\, T_2'\, (w-w_o)\, M_o}{1 + T_2'^2(w-w_o)^2 + g^2 B_1^2 T_1 T_2'}$$

$$M_{y'} = \frac{g\, B_1\, T_2'\, M_o}{1 + T_2'^2(w-w_o)^2 + g^2 B_1^2 T_1 T_2'}$$

$$M_{z'} = \frac{1 + T_2'^2(w-w_o)^2\, M_o}{1 + T_2'^2(w-w_o)^2 + g^2 B_1^2 T_1 T_2'} \qquad (1.20)$$

For cases where

$$g^2\, B_1^2\, T_1\, T_2' \ll 1 \qquad (1.21)$$

the magnetisation in the x'-y' plane increases linearly with increasing B_1, and hence the received signal increases. If $w=w_o$ it can be shown that M_y' is at a maximum when $g^2 B_1^2 T_1 T_2' = 1$, taking the value

$$M_y' = \frac{M_o\, (T_2'/T_1)^{1/2}}{2} \qquad (1.22)$$

The term $g^2B_1{}^2T_1T_2'$ is generally known as the "saturation factor". If it is increased beyond unity all the magnetisation components are reduced and the sample becomes saturated. Since T_2' cannot be longer than T_1, then the largest possible value of M_y' is $M_o/2$, when $T_1=T_2'$. The variation of the magnetisation components with B_1 frequency for this case is shown in fig 1.10.

The arrangement of fig.1.7 may be used for steady state nmr experiments. If the B_1 field is given by $2B_1\cos(wt)$, then the magnetisation that induces a signal in the pickup coil will be given by

$$M_y = M_x'\sin(wt) + M_y'\cos(wt) \qquad (1.23)$$

Thus there is a component of the received signal proportional to M_y' and in phase with B_1, and an out of phase component proportional to M_x'.

Now it is inevitable that there will be some leakage flux from the B_1 coil into the pickup coil. This leakage may be many times the magnitude of the flux of M_y, but this fact may be used to advantage. The M_y' term will cause amplitude modulation of the leakage signal, and to a first order the M_x' term will only cause phase modulation (see fig 1.11). So by using an a.m. receiver the phase modulation, and hence the M_x' term, will be ignored. Sweeping the frequency of B_1 will therefore produce a resonance signal at the receiver output of the form shown in fig. 1.10.2.

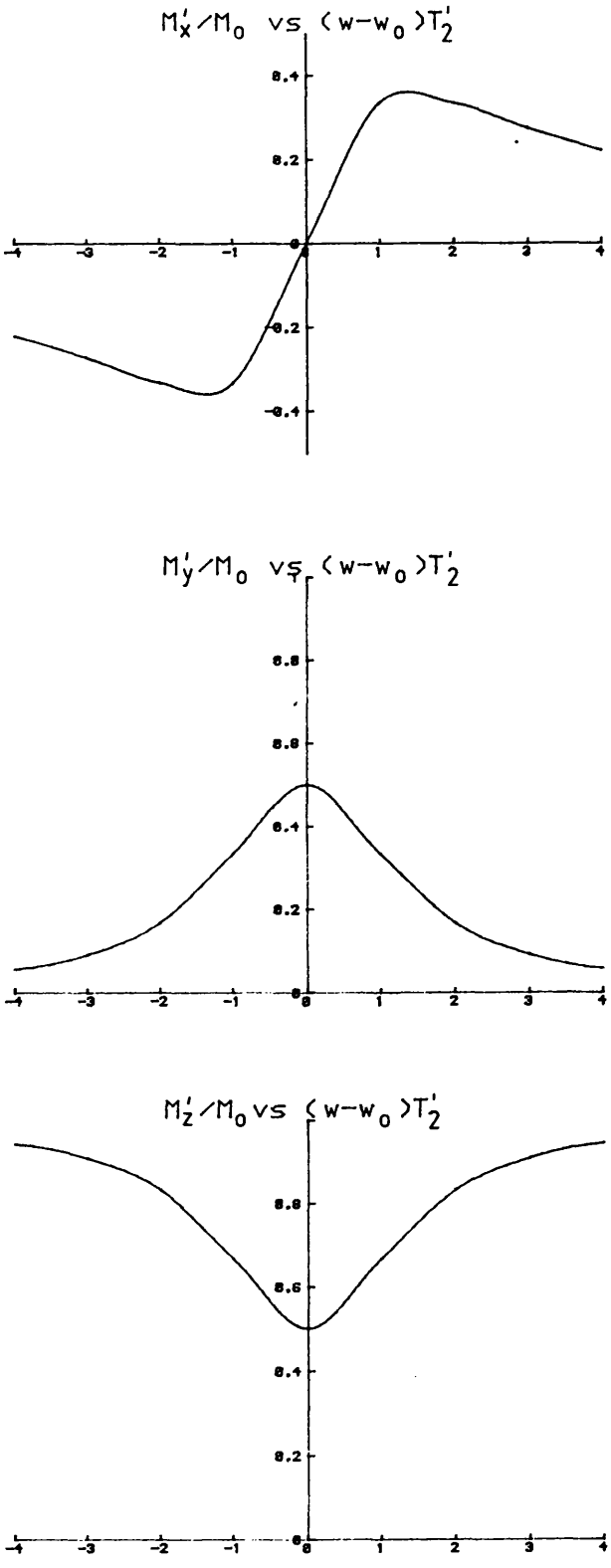

Fig.1.10 Variation of magnetisation components with frequency

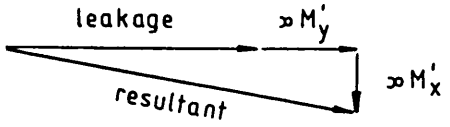

Fig.1.11 M_x' produces phase modulation of B_1 leakage

This was the technique used by Bloch in his work [1.5], although a modification to the method also allowed the M_x' component to be resolved. An alternative approach taken by Bloembergen, Purcell and Pound [1.6] was to use a single transmit/receive coil and balance out the unwanted signal components using a bridge circuit. Again signals proportional to M_x' and M_y' could be obtained.

1.8 A Basic NMR Scanner.

The procedure for obtaining an nmr signal from a patient is essentially the same as the pulsed methods described above. The patient is placed in a uniform B_o field with a tightly coupled pickup coil around him. A further coil set provides the exciting B_1 field. This allows a signal to be obtained, but does not give any information about where the resonating material is positioned in space. To accomplish this, three further

sets of coils are required. Each set produces a linear variation of the B_o field along one of the Cartesian axes, and they are known as the x, y and z gradients respectively.

The patient is generally laid along the z axis, and a picture made of a "slice" of resonating material in the x-y plane. Thus the first process is to excite only those nucleii in the required slice. This is accomplished by performing the excitation with B_1 whilst the z gradient is applied. The gradient has the effect of making the Larmor frequencies of the nucleii within the patient a function of position along the z axis, so the resonating frequency of a particular nucleus will be given by

$$w = g\ B_o + g\ z\ (dB_z/dz) \qquad (1.24)$$

where dB_z/dz is the effect of the z gradient.

The envelope of the B_1 pulse is shaped so as to produce a well defined spectrum. The width of this spectrum in conjunction with the amplitude of the z gradient then defines the width of the slice of material that is excited within the patient (fig 1.12). So by an appropriate choice of parameters a slice, typically of width 1cm, may be given a 90 degree flip. However, the nucleii have been dephased by the z gradient and have to be rephased by the application of this gradient in the reverse direction. The whole of this "slice selection" process needs to be short in comparison with T_2', and

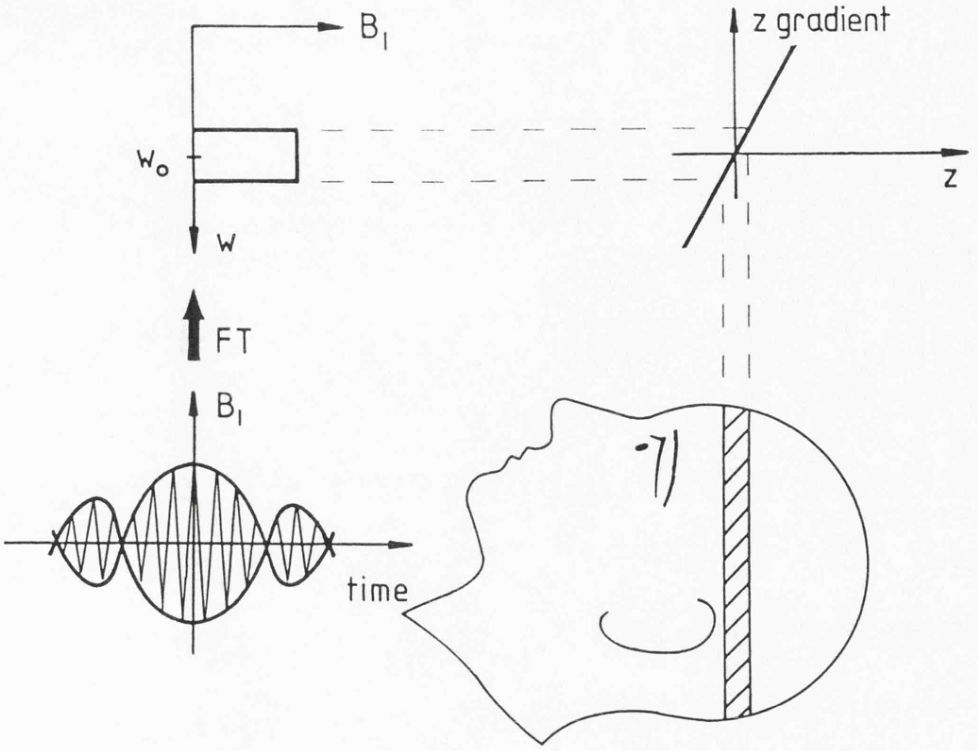

Fig.1.12 Slice selection is performed with a shaped B_1 pulse and a field gradient

typically takes place in less than 5mS.

Having defined a slice, some form of encoding needs to take place in the x-y plane. Various point-scan and line-scan methods have been used where the picture is built up point by point or line by line. However, these techniques are inefficient as they throw away information from the rest of the slice whilst concentrating on a particular point or line. This results in very long scan times. Quicker methods have been developed that build up data from the whole slice, either with respect to a rectangular or polar set of coordinates. The polar method will be described as it is easier to visualise. In fact

it is derived from the techniques used in X-ray brain and body scanners.

The x and y gradients are driven so that they produce a fixed amplitude "r gradient" at a varying angle θ. Without any r gradient the whole of the selected slice would resonate at a single frequency if T_2' effects were ignored. However, when the r gradient is applied, the individual moments precess at a frequencies dependent on their position in the gradient field. This significantly shortens the decay of the signal, from which a spectrum may be produced by Fourier analysis. The amplitude of this spectrum is a measure of the quantity of resonating material along the direction of the r gradient (fig. 1.13). After a pause to allow M_z to build up again, the slice selection process and r gradient is again applied, this time at a new angle θ. The whole process is repeated with θ varying between 0 and 180 degrees, typically in 1 degree intervals, and a set of spectra is obtained.

These spectra are now "back-projected" so as to form an image of the original object (fig.1.14). In practice some form of spatial filtering has to be performed in order to avoid artifacts in the pictures caused by the finite number of projections. The resulting image may now be displayed on a video monitor.

The above sequence of events builds up a picture that displays a map of the quantity of resonating

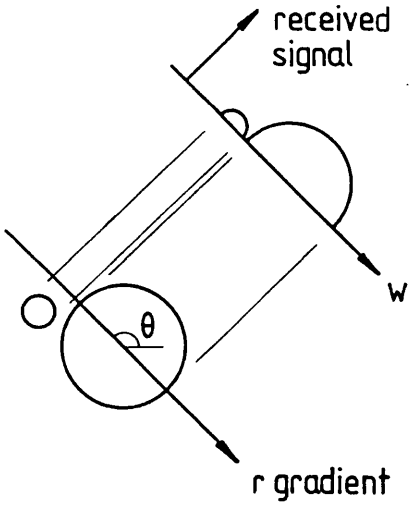

Fig.1.13 The r-gradient is used to obtain sets of spectra

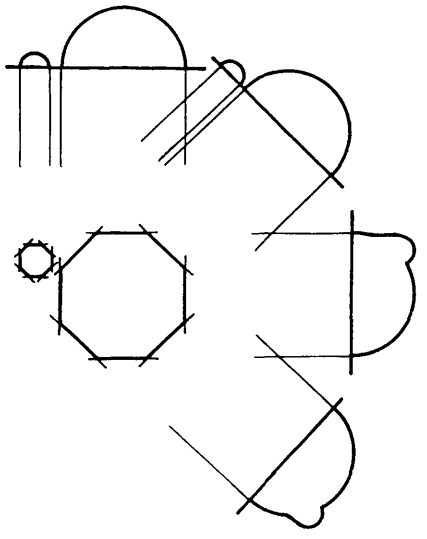

Fig.1.14 Back-projection of the spectra allows the image to be reconstructed

material throughout the slice of the patient. However, this picture is modified by T_1 and T_2' effects. Similarly pictures based on T_1 and T_2 may be made using the inversion recovery and spin echo techniques described earlier, but these in turn depend on the quantity of resonating material present. For a fuller description of these techniques see [1.3].

1.9 Required Magnet Characteristics.

A typical magnet will consist of coaxial circular coils where the patient lies along the axis. Although a clear bore of 0.6m diameter might be all that is required to accommodate a patient, a 1m bore is generally required in order to fit in the gradient and r.f. coils.

The field magnitude needed to produce good nmr images is still a much debated subject. Systems have been built that work at anything from 0.025 to 2.0 Tesla. Image quality at 1.5 Tesla is not markedly different from machines operating at 0.15 to 0.5 Tesla, however, a high field may give the option of performing phosphorus spectroscopy with a reasonable signal to noise ratio.

The factor that field magnitude most affects is the technology with which the magnet is constructed. An air-cored, resistive magnet for whole-body scanning that is not excessively heavy becomes prohibitively expensive to run above somewhere between 0.1 and 0.2 Tesla. This is

because of the power dissipation and the cost of removing the unwanted heat. A superconducting magnet therefore becomes essential if high fields are required. For the present work it is assumed that the magnets described are resistive. Although the physical characteristics of the two types will inevitably be different, the mathematical methods used for modelling and design are identical. Thus there is little loss in generality by considering only resistive magnets. The required field magnitude will be assumed to be 0.1 Tesla.

In order to quantify the required field homogeneity assume that a defect in the field manifests itself as a linear gradient in the x-y plane in the direction of θ = 0 degrees. When the r gradient is at θ=0 the gradients will add. The resulting spectrum, and hence the scanned object, will then appear wider than without the error gradient. Similarly, when θ = 180 degrees the gradients will subtract and the object appears smaller. The picture elements (pixels) will therefore overlap when they are back-projected and reduce the resolution of the picture.

If a maximum overlap of half a pixel is allowed at the picture edge, then the error in the positioning of a pixel produced by the error gradient must be less than a quarter of a pixel width, so that

$$\frac{\text{error gradient}}{\text{r gradient}} < \frac{1}{4}\,\frac{\text{pixel width}}{\text{picture width}} \qquad (1.25)$$

Typically, the picture will consist of 256x256 pixels, the r gradient will be 1mT at a point corresponding to the picture edge, and the main B_o field will have a value in the order of 100mT. The error gradient must therefore be less than about 10uT at the picture edge, which corresponds to 10ppm of the B_o field. So for a practical scanning device the field homogeneity should not be worse than $\pm$ 10ppm throughout the volume that is to be scanned.

If B_o is increased to 1T and the r gradient magnitude remains unchanged, then the allowable 10uT field error required to keep the resolution constant now corresponds to a $\pm$1ppm field error. Therefore operating at high fields also requires a tighter control of the field homogeneity. Obviously the effect of field errors may be reduced by increasing the amplitude of the r gradient. However, this would increase the bandwidth of the received signal and so increase the amount of noise in the pictures. Noise may in turn be reduced by signal averaging, but this increases the time taken for a complete scan. A balance therefore has to be struck between picture resolution, noise and scan time. This is by no means an easy matter. For the present work, however, a uniformity requirement of $\pm$10ppm or better will be assumed over a volume of 50cms diameter for body scans, and 30cms for head scans.

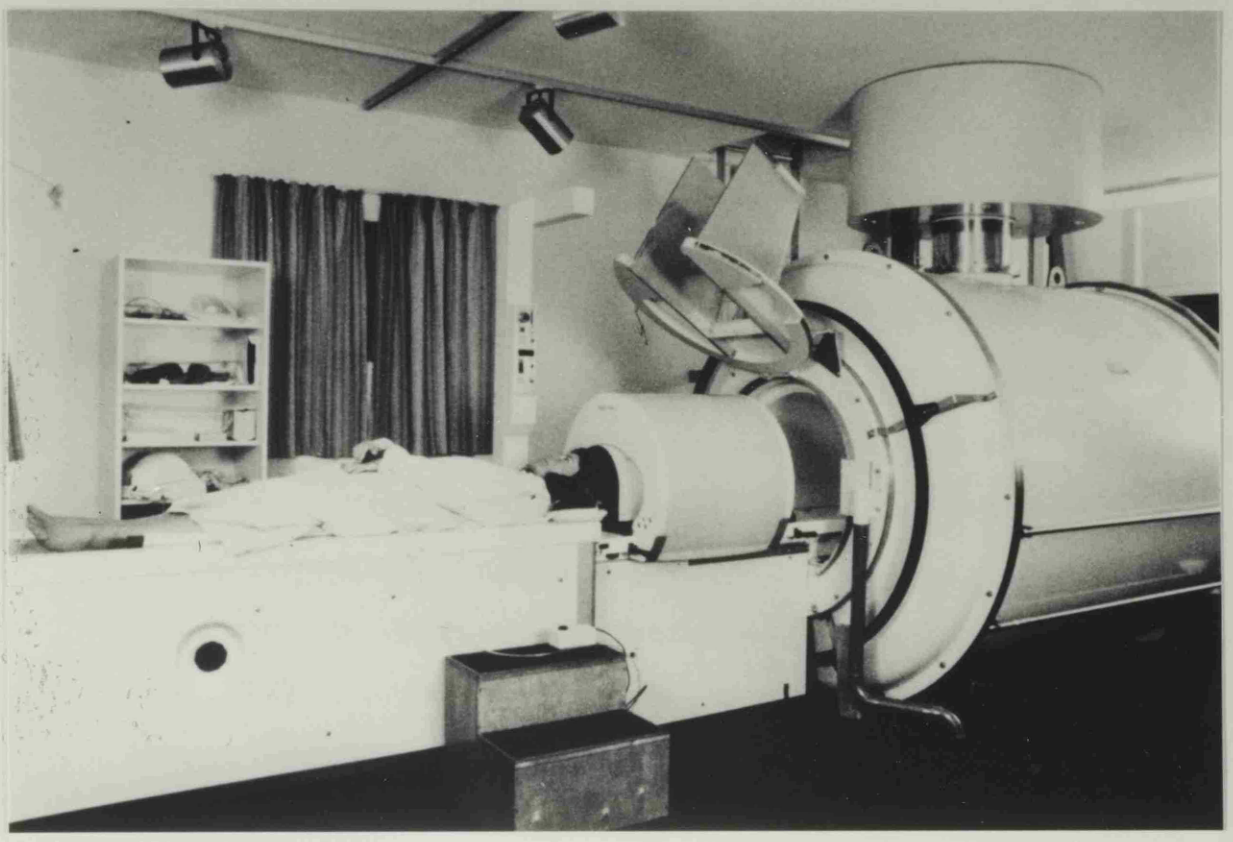

The NEPTUNE Scanner at Hammersmith Hospital, London.

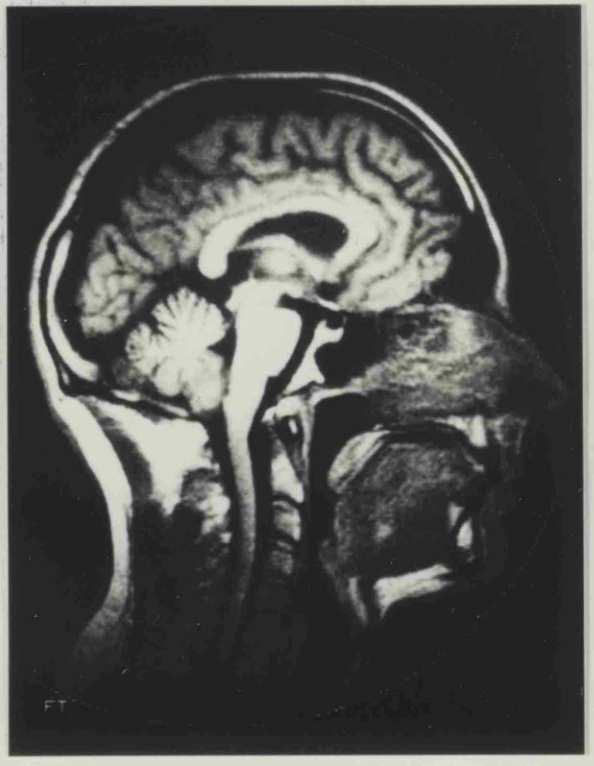

Head scan using an inversion recovery sequence

CHAPTER 2. NMR PROBE SYSTEMS.

2.1 Introduction.

In order to set up and test nmr magnet systems some form of accurate magnetometer must be available. A Hall effect probe is usually the first device considered when magnetic fields are to be measured, and they can certainly measure changes in field of the order of 1 part in 10^5. However, they are sensitive to orientation so the accuracy of their mechanical positioning usually limits the field accuracy that can be achieved. On the other hand a nmr probe is relatively insensitive to orientation and an accuracy of 1 ppm can be achieved fairly readily.

A conventional nmr probe locks an oscillator to the signal obtained from a continuously excited sample of suitable material. The oscillator frequency can be readily measured and so the field magnitude may be determined. Since the probe has to be operated continuously it is difficult to operate in conjunction with an nmr scanner. For this reason a pulsed nmr probe system has been developed that may be incorporated into a scanner with the minimum of hardware. It also lends itself to the measurement of pulsed field gradients.

The probe may be tuned by an automatic system using the lock-in technique of the conventional probe. For this reason the workings of a steady state type of nmr probe are described first.

2.2 A conventional nmr probe.

The block diagram for a typical probe system is shown in fig.2.1. A small sample of resonant material such as water, grease, or wax, has a tuned coil wound around it and is connected to an amplifier and receiver. The low level B_1 signal used for continuously exciting the sample comes from a voltage controlled oscillator, and is fed to the coil via a bridge network (section 1.7). If the vco is swept over a range of frequencies the output of the receiver will vary as a typical resonance curve of the form 1.10.2

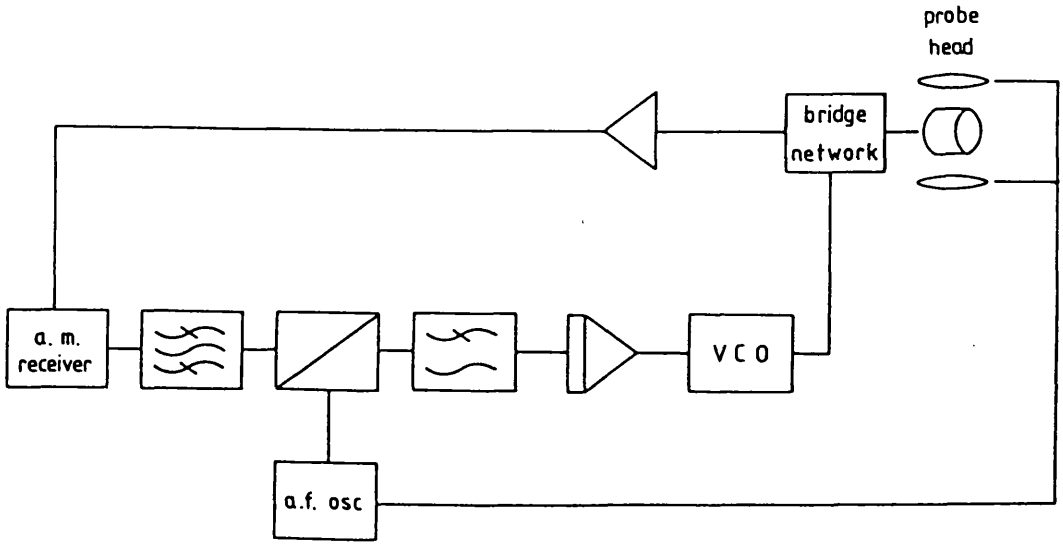

Fig.2.1 Block diagram of a conventional probe

A set of Helmholtz coils around the probe is used to move the nmr resonance with respect to the B_1 frequency by altering the B_o field slightly. These coils are driven by an audio frequency signal. If the B_1 frequency is just above the nmr resonance (fig 2.2) the output of the receiver will have the audio signal superimposed upon it. When the B_1 frequency is below the nmr resonance the audio signal is still present but has the opposite phase. By phase sensitive detection of this a.f. signal at the receiver output it is possible to derive a control signal that is positive or negative depending on which side of the resonance the injected signal lies.

The receiver output is bandpass filtered before phase sensitive detection to remove noise, and the d.c. component, which can cause dynamic range problems. Filtering is required after the detector to remove the twice frequency component produced by the multiplication process. The resulting control signal is fed to the vco via an integrator, which causes the B_1 frequency to move towards that of the nmr resonance.

When the two frequencies are the same the a.c. component at the output of the receiver will be at twice the audio frequency that modulates the sample, (fig. 2.2) and will be removed by the filters. The detector output will therefore be zero and so the integrator holds the vco at that frequency. This frequency can then be measured and converted to a field magnitude by

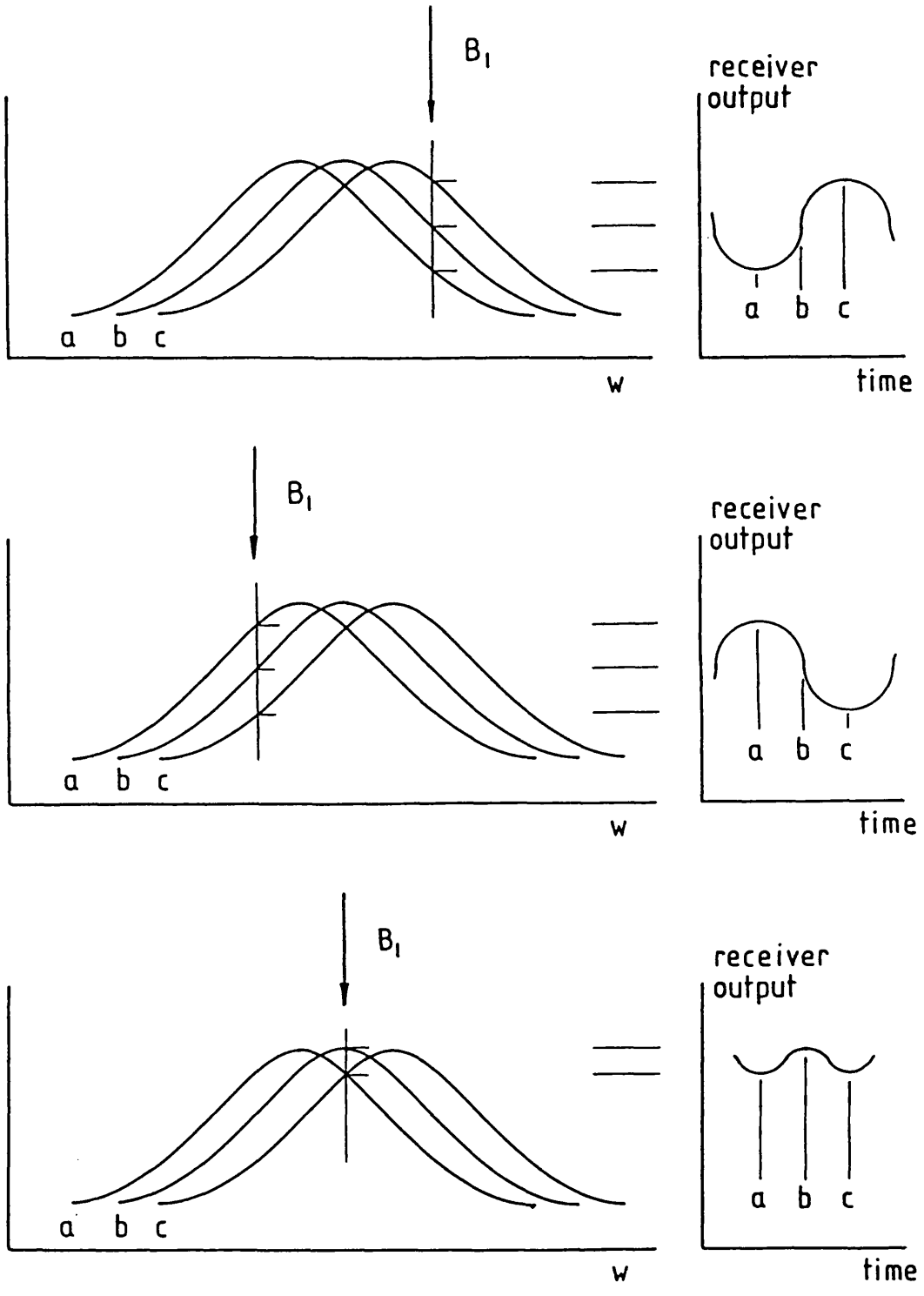

Fig.2.2 Receiver output when the resonance is modulated by an audio frequency

dividing it by the magnetogyric ratio of the nuclei concerned.

Thus, once the B_1 frequency is near that of the nmr resonance this circuit will lock-in until the two frequencies are the same. Once locked the probe may be moved provided that any change in field that may occur happens sufficiently slowly that the change can be tracked. In order to achieve lock in the first place it is usually necessary to sweep the vco across a range of frequencies to find the resonance.

2.3 A pulsed nmr probe.

As with the conventional probe, the object of the system is to determine the frequency of a nmr signal from a small sample of a suitable material. A free induction decay is produced from the sample in the manner described in section 1.4. The resulting signal is fed to a receiver where it is amplified, quadrature demodulated and filtered. The frequency of the signal appearing at the receiver outputs will be the difference between the nmr frequency and the demodulation frequency. Quadrature outputs are necessary to determine whether it is a "positive" or "negative" frequency. This difference is calculated and then added (or subtracted) to the known

demodulation frequency in order to give the frequency of the resonance. The magnitude of the field will then be given by $B_o = w_o/g$.

The difference frequency may be calculated by noting the phase of the demodulated signal immediately after the B_1 pulse, and then at some later time during the f.i.d. It will be given simply by the change in phase divided by the elapsed time. Since the signals are noisy and decaying exponentially, there will be an optimum length of time for the measurement to take place. Moreover, since the rate of decay is dependent on the uniformity of the field that the probe is placed in, this measurement time will vary from point to point.

To consider the frequency errors produced in this system the received signals are assumed, reasonably, to be contaminated by Gaussian noise. The noise will introduce both amplitude modulation, which is of no consequence, and phase modulation. If s is the rms voltage signal to noise ratio (as given by eq.1.19) then assuming that the phase of the uncontaminated signal is zero degrees, the probability density function of the noisy signal's phase will be given by

$$p(\theta) = \frac{\exp(-s^2)}{2\pi} + \frac{1}{2}\sqrt{\frac{s^2}{\pi}}\cos\theta \exp(-s^2\sin^2\theta)(1+\mathrm{erf}(s\cos\theta)) \qquad (2.1)$$

(from Schwarz [2.1])

This expression may be simplified by assuming that $s^2 \gg 1$, and restricting evaluation of the function to $\theta < 5$ degrees. Hence, $\sin\theta \doteq \theta$, $\cos\theta \doteq 1$, and $\mathrm{erf}(s\cos\theta) \doteq 1$, whereupon

$$p(\theta) \doteq \frac{\exp(-s^2\theta^2)}{(\pi / s^2)^{1/2}} \qquad (2.2)$$

This is a Gaussian distribution with zero mean, and a variance of $1/2s^2$. If the original signal does not have a zero phase angle, the distribution will simply have its mean shifted to a new value.

The phase measurement immediately after the B_1 pulse will therefore have a rms error of $1/s\sqrt{2}$ radians, whilst the later measurement has an error of $\exp(T/T_2')/s\sqrt{2}$ rads, where T is the period between the two measurements. Since the variances of the phases add when the two measurements are subtracted, the rms frequency error produced by the noise will, on average, be given by

$$w_{err} = \frac{(1 + \exp(2T/T_2'))^{1/2}}{\sqrt{2}\, s\, T} \qquad (2.3)$$

A plot of w_{err} versus measurement time for the case when s=100, and T_2'=0.01s is shown in fig 2.3. The optimum measurement time is approximately 1.11 times T_2', although from the plot it is clear that a variation of -50% to +100% in the measurement time does not increase the error by more than 30%.

If the $1cm^3$ sample described in chapter 1 were used as a field probe, then it would have an rms frequency error of 0.29Hz, assuming a T_2' of 10 ms. This corresponds to a field error of better than 0.1ppm at 0.1 Tesla. This sort of field probe is therefore quite suitable for measuring field uniformity to the required accuracy.

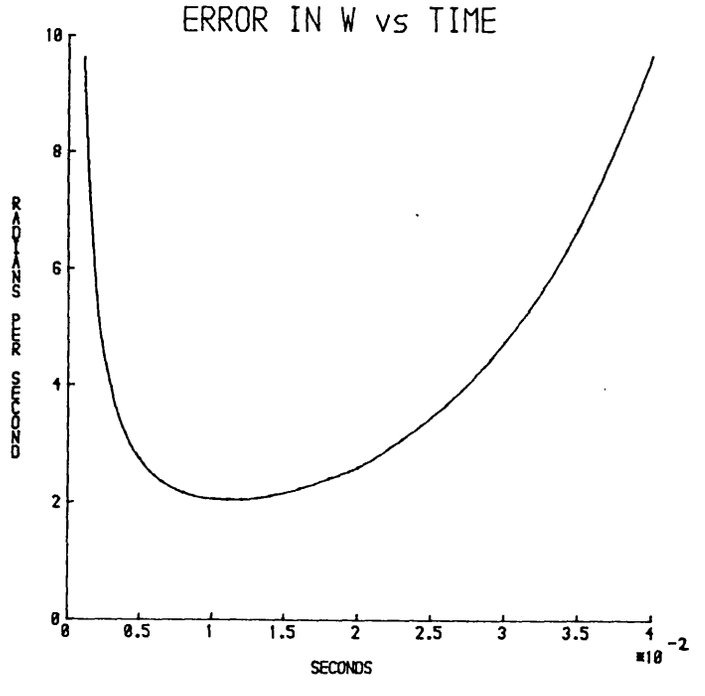

Fig.2.3 Variation of frequency error with measurement time

2.4 A stand alone pulsed nmr probe system

When making measurements on a resistive magnet it can be difficult to separate the effects of drift in the magnet from drift in the power supply current. By constructing a system with one probe used as a fixed reference and the other moveable it is possible to virtually eliminate the effects of power supply drift by looking at the difference between probe measurements rather than their absolute values.

The probes are based around a sample of oil contained in a perspex tube 6.5mm diameter and 5mm long. Oil is used because its T_1 of 50ms allows the probe to be pulsed quickly if required, with little saturation occuring. The pickup coil consists of copper wire close wound on the outside of the tube, the number of turns being chosen so as to provide a sensible value of inductance for tuning purposes, in this case 9uH. Filling factor for the coil is 0.6, and the quality factor, Q, is measured to be 40 at 3MHz. A metre length of twinax connects the probe to a balanced preamplifier with fet inputs, and a 100 ohm line connects this amplifier to the receiver. The sample tube slides into a former on which are wound the Helmholtz coils for the B_1 field. This former is 22mm diameter and 16mm long, and so the complete probe forms a compact unit (photograph on page 50). In order to reduce the number of adjustments that have to be made in setting up the system

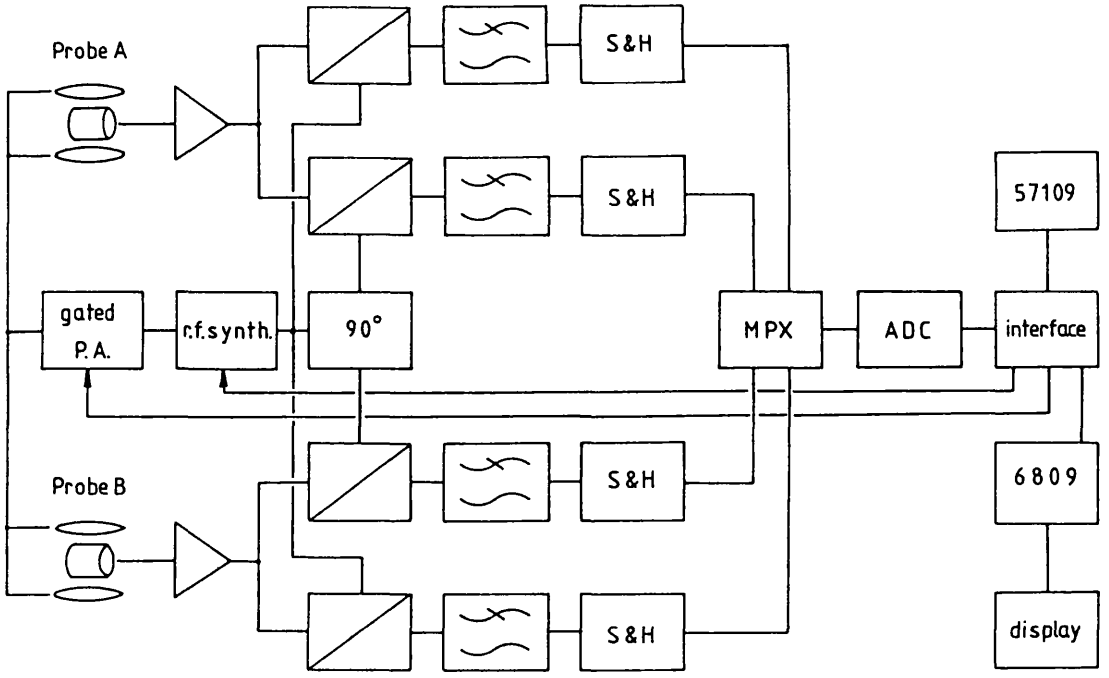

Fig.2.4 Block diagram of a pulsed nmr probe

these coils are not tuned. Instead they are connected via 50ohm line and terminating network to the output of a 30 watt broadband amplifier.

The receiver is a trf design with the reference frequency being provided by a digitally programable, crystal-locked synthesiser. This reference frequency is divided by four and produces the sin and cos signals at the demodulation frequency that are required for producing quadrature outputs. Baseband filtering is provided by 6 pole filters with a cutoff frequency of 5kHz.

The receiver outputs are fed to a data collection and conversion system along with the outputs from the second probe. These four signals are sampled at the same instant and converted into 8 bit binary words in turn. Processing of these samples is accomplished with a Motorola MC6809 microprocessor in conjunction with a National Semiconductors MM57109 Number-Oriented Processor that performs all the numerical calculations, albeit rather slowly. A counter keeps track of the number of samples taken since the processor does not operate sufficiently fast. Counters also note the number of quadrants that the phasor representing the signal has passed through in order to resolve phase ambiguities.

Upon starting the system the operator is asked for a frequency from which to start looking for a nmr signal. The probe samples are subjected to a 90 degree pulse and the receiver outputs monitored. If a signal is not detected from either probe the receiver is retuned to a frequency 3kHz higher and the process repeated. In this manner a resonance will be excited 3 times whilst within the bandwidth of the receiver, so it is impossible for the signal to be missed.

Having found a signal, sampling is performed until the f.i.d. with the shorter time constant has fallen to the required fraction of its original level. The number processor performs the required calculations and the frequencies of the two signals are displayed, along with

their difference in parts per million. Before repeating the sequence, the synthesiser is retuned to lie halfway between the two signal frequencies. If only one signal is present then only one figure for frequency is displayed, and the synthesiser is tuned as close to the signal frequency as possible. The circuit diagrams for the complete system are given in appendix 2.1.

2.5 Performance of the stand alone system.

An expression for the rms signal to noise ratio of an nmr experiment has been given in eq. 1.19, and it is worthwhile comparing this theoretical value with measurements made on the actual system.

A quantity not readily available is the noise factor of the preamplifier, since no detailed noise measurements have been performed upon it. However, using the maufacturers typical figures of 10nV/√Hz noise voltage, and negligible noise current for the input fets, a noise figure of 1.39 (2.9dB) may be calculated. The figure applies when the preamplifier is used with the coils described earlier that have an equivalent R_p of 6.8kohms at 3MHz. This rather poor noise figure is due to the low impedance of the coil. If Q were increased then R_p would also increase along with its noise voltage. The noise voltage of the preamplifier would then be a smaller fraction of the total noise, giving a corresponding improvement in noise figure. This does not mean that the

signal to noise ratio has worsened because the signal voltage will have increased in proportion to Q, whilst the noise voltage will only have increased as $Q^{1/2}$. So putting the following data into equation 1.19

$V_c = 1.66 \times 10^{-7}$ m^3 $\quad$ $g = 2.67 \times 10^{8}$ rad/sec/Tesla

$p = 0.6$ $\quad$ $\hbar = 1.06 \times 10^{-34}$ J/rad/sec

$Q = 40$ $\quad$ $I = 1/2$

$N = 6.69 \times 10^{28}$ m^{-3} $\quad$ $kT = 4 \times 10^{-21}$ J (at 290K)

$w_o = 18.85 \times 10^{6}$ rad/sec $\quad$ $F = 1.39$

$B = 10^{4}$ Hz

yields an rms signal to noise ratio of 71 at the beginning of an f.i.d. This compares with measured values of 62 and 73 for the two probes. Despite several attempts to discover the cause, the reason for the discrepancy between the two measured values has not been discovered. The differential nature of the multistage preamplifier makes it quite difficult to track down the problem. Neverthless, equation 1.19 does appear to give a reasonable estimate of the signal to noise ratio of the nmr experiment.

Having obtained these measured values, equation 2.3 may be used to calculate the likely frequency error that is intoduced by the noise. With a measurement time of 17ms, errors of 1.65 and 1.94 rad/sec are obtained. Thus the combined probe measurements will give rise to an apparent frequency error of 0.14ppm at 3MHz. In order to compare this with observed errors displayed by the

microprocessor system a set of 45 measurements were taken and the standard deviation found. The rms field error was found to be 0.15ppm and agrees well with the expected value.

The reason for using a pair of probes was to eliminate the effect of power supply drift. Deliberately changing the magnet current by 7000ppm did not change the results displayed by the probe system, and so this objective has been achieved.

The system takes about 2 seconds to process and display each measurement, with most of the time being spent performing numerical calculations. This makes the instrument rather tedious to use as it is tempting to look at a couple of consecutive readings in case rf interference has caused spurious results. Replacing the numerical processor with an AMD Am9511 would reduce the calculation time to 200ms, making the instrument much easier to use.

2.6 An automatically tuned probe system.

A set of field probes has also been developed for the "NEPTUNE" scanner, installed at Hammersmith Hospital, London. The intention is to provide a quick check on field uniformity before scanning, in case any ferrous material has accidentally been brought into the vicinity

of the magnet. Also, they are used for calibrating the r gradients. A further requirement is that their tuning should be made automatic in order to minimise the amount of setting up that is required by an operator.

A set of four probes is provided, all in the x-y plane, with one along each of the +x, -x, +y and -y axes. They are mounted in the structure that surrounds the patient and contains the B_1 and pickup coils. Since they are already in the main B_1 field there is no need to supply them with individual B_1 coils. The probe head has thus become quite a simple device.

As the probes are to be used in the presence of the r gradient they must have a small cross section in the x-y plane. Thus each probe consists of an oil sample in a 1mm internal diameter glass tube, 20mm long, and overwound with a copper wire coil. The coils are made tuneable between 8 and 10MHz by the use of varicap diodes.

Preamplifiers are housed inside the trolley on which the patient is moved into the magnet, and these are connected via 100 ohm lines to a receiver. This receiver has only two channels, and so switching is provided so that the central computer can select either a pair of vertically spaced probes, or a pair of horizontally spaced ones. Apart from this it is virtually identical to the receiver/data conversion system described previously. Processing is performed in this case, however, by the

central computer rather than a stand alone microprocessor system.

The circuitry required to automatically tune the probes fits around the receiver and does not interfere with its working in any way. It is assumed that an nmr signal has already been found using the main pick-up coil, and that the main B_1 coils are continuously excited at a low level so that this frequency can be picked up by the probe coils. A lock-in circuit now adjusts the voltages supplied to the varicap diodes that tune the probes so that the received signals are at a maximum.

The lock-in works in the same manner as that of the conventional nmr probe. Its block diagram is shown in fig. 2.5 and the cicuit diagrams are in appendix 2.1. The injected signal is picked up by the probe and passed through the receiver system. Since the receiver has quadrature outputs a square root of the sum of squares circuit is used to obtain the signal magnitude. In order to move the probe tuning closer to the frequency of the injected signal the varicap voltage is modulated with a 100Hz signal from a Wien bridge oscillator. The resulting modulation at the receiver output is phase sensitive detected, filtered, and converted to a pair of logic signals. One of these signals indicates that the detector output is positive, and the other that it is negative. The circuits that produce these signals have a dead band about zero volts as well as hysteresis. This is to avoid

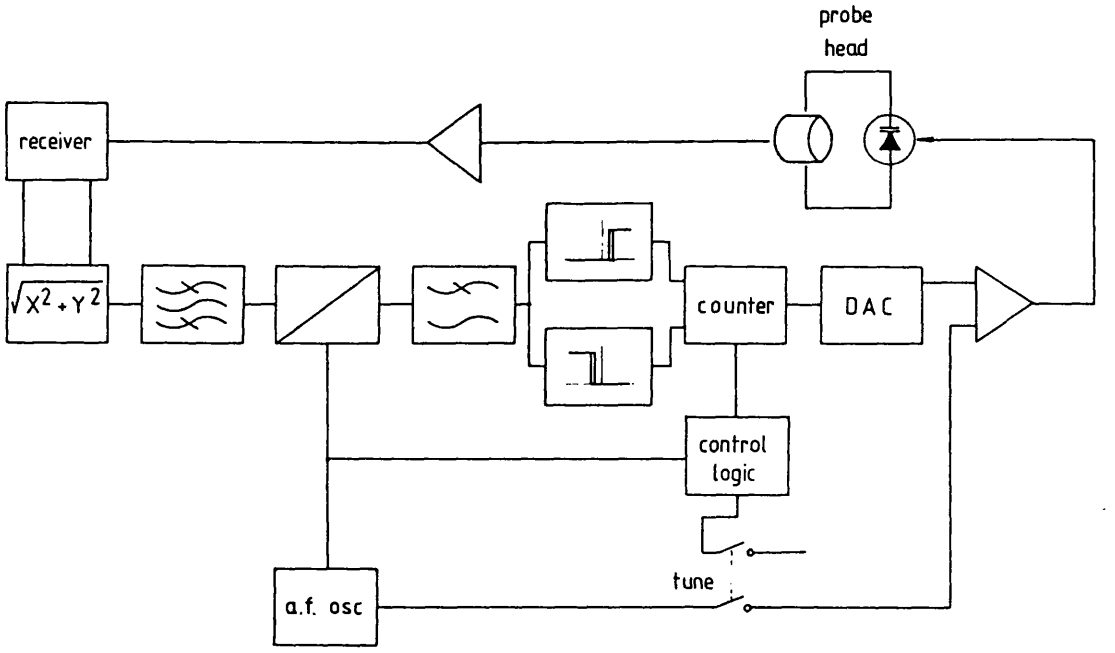

Fig.2.5 Block diagram of the automatic tuning system

any noise causing spurious results, or hunting when the probe is in tune.

These logic signals in turn drive an up/down counter connected to a digital to analogue converter. This replaces the integrator of the lock-in circuit, and it allows the correct varicap voltage to be maintained when the tuning process has stopped and the probes revert to their normal mode of operation.

When the automatic tuning process is initiated the counter is cleared and then slowly incremented, forcing the probe to sweep through its tuning range. When the injected signal is picked up by the receiver the lock-in

takes control. A lamp is lit when tuning is complete, indicated by both of the logic signals being false. The system manages to tune the probe to within 1dB of its maximum sensitivity.

2.7 Conclusions.

The agreement of measured values for signal to noise ratio and measurement accuracy with the theoretically derived values is encouraging. It suggests that it is possible to design nmr probes for use at a particular field magnitude, and be reasonably confident that they will perform to the required accuracy.

The pulsed nmr probe is quite a sophisticated instrument. It can search for a resonance, make measurements for an optimum length of time and display the results. Other useful features include freedom from drift in the absolute value of the field when two probes are used, and the ability to make the instrument self tuning. All this makes such an instrument very easy to use, with the minimum of setting up required by the operator. It is also apparent that as a stand alone unit it contains a large amount of hardware.

However, when used in conjunction with a complete scanning system, the receiver, data collection system, and computer will already be be present. The extra measurement hardware is therefore reduced to the probe

head itself (with or without B_1 coils) a preamplifier, and any tuning equipment. If tuning is performed manually then the equipment required is minimal, even when compared with the conventional continuously-excited probe.

The presence of general purpose nmr and computing systems allows various other improvements to be made. In the case of the NEPTUNE probes a least squares fit is performed on many data points in order to determine the rate of change of phase. This results in a large increase in measurement accuracy. Also, measurements have been taken of the pulsed fields from gradient coils in order to study the effects of eddy currents in the aluminium formers of the magnet. Thus the pulsed probes lend themselves to applications for which it is unlikely that a conventional probe could be used.

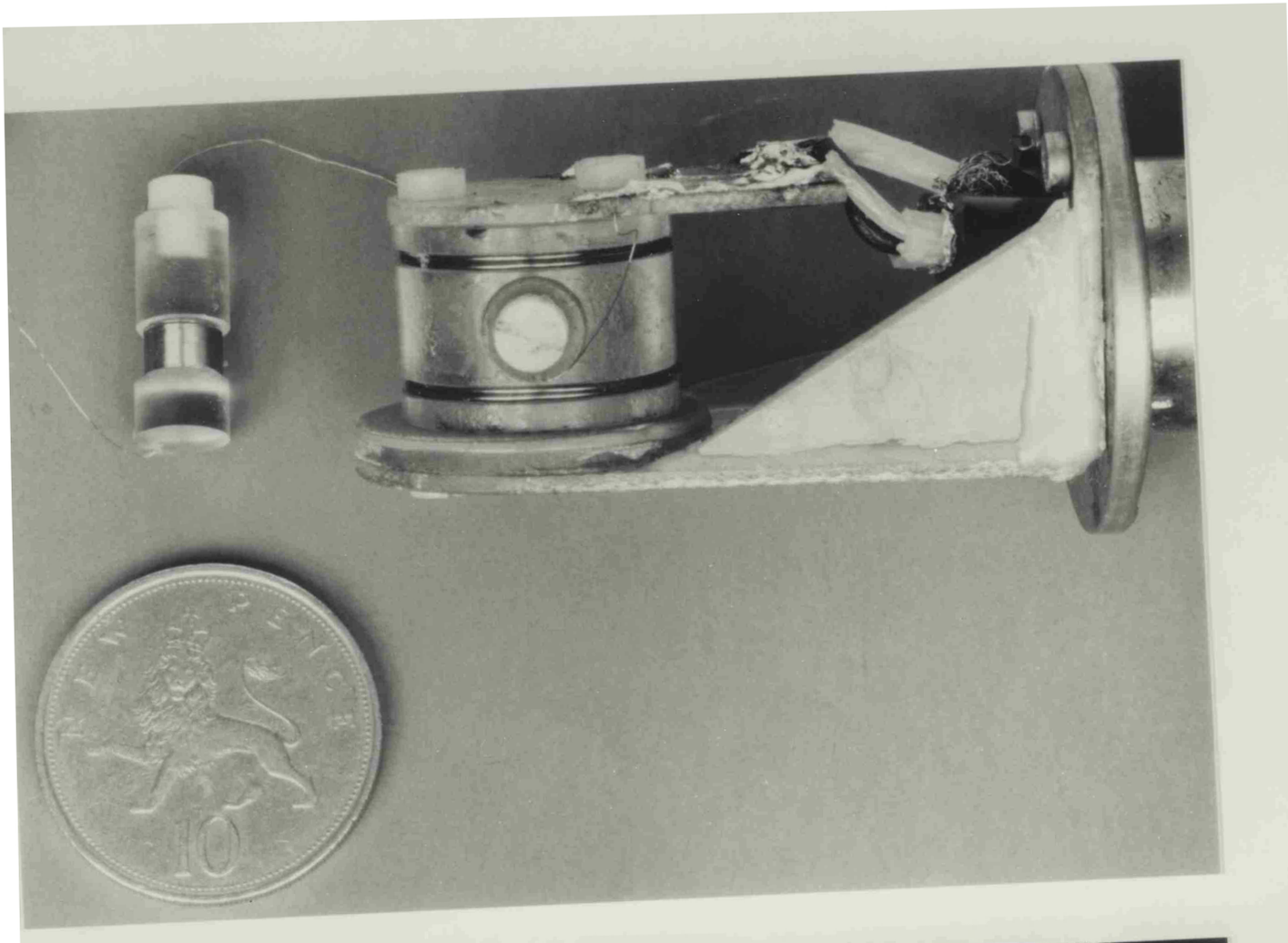

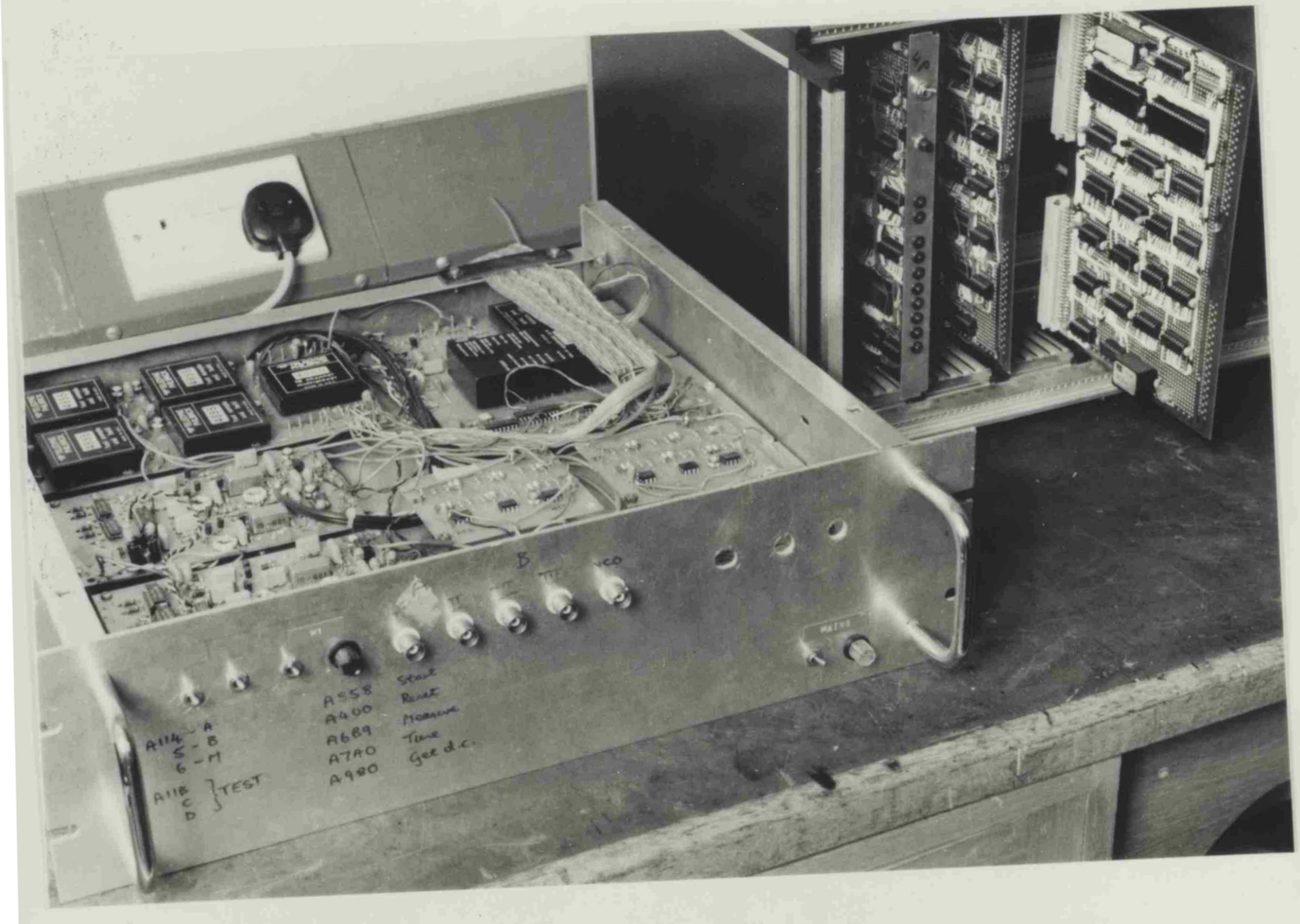

An NMR Probe

Electronics for a stand alone probe system

CHAPTER3 THE DESIGN OF AXISYMMETRIC, IRON FREE, MAGNET SYSTEMS.

3.1 Introduction

In order to design magnets that produce highly homogeneous fields it is not only necessary to be able to calculate those fields accurately and efficiently, but also to have a well defined method for arriving at a coil geometry that produces the required homogeneity. Only axisymmetric coil systems are dealt with here since they are more easily realised in practice. At the same time the field calculations are easier than for a more general three dimensional coil shape.

It is useful to represent the central field region by a spherical harmonic series. The number of terms required to obtain a given accuracy is small, and so the process is quite efficient. Also, it turns out that the design of a magnet reduces to adjusting the coil dimensions until some of the coefficients of the series vanish. In practice this involves solving a set of non-linear equations which may be accomplished using an optimisation routine.

This chapter describes the theory behind an interactive computer program that uses these techniques to arrive at suitable designs for nmr imaging magnets, and presents a selection of results from the program.

3.2 Field calculations using spherical harmonics.

It would be natural, when talking of axisymmetric magnets, to use cylindrical coordinates. However, in order to use spherical harmonics a spherical coordinate system is essential. To avoid confusion between cylindrical and spherical radii the spherical system will have coordinates (r,θ,ϕ), and the cylindrical system (ρ,ϕ,z). The relationship between these coordinates is shown in figure 3.1.

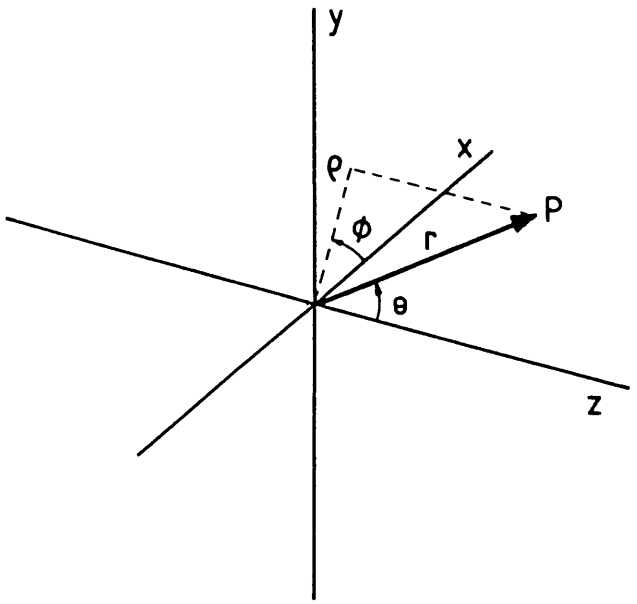

Fig.3.1 The relationship between Cartesian, cylindrical and spherical coordinates

For a current free region a magnetic potential V may be defined that satisfies Laplace's equation div(grad V)=0. The solution of this equation in the spherical coordinate system will be an infinite series of spherical harmonics. (as in Smythe [3.1]) For the particular case where V is axisymmetric and finite on the axis

$$V = \sum_{n=0}^{\infty} A_n \, r^n \, P_n(\cos \theta) \qquad (3.1)$$

where $P_n(x)$ is the Legendre polynomial of order n, and A_n is a coefficient dependent on coil geometry.

Differentiating this expression axially and radially yields the required field components

$$H_z = -\frac{\partial V}{\partial z} = \sum_{n=1}^{\infty} A_n \, n \, r^{n-1} \, P_{n-1}(\cos \theta) \qquad (3.2.1)$$

$$H_\rho = -\frac{\partial V}{\partial \rho} = \sum_{n=1}^{\infty} A_n \, \sin\theta \, r^{n-1} \, P_{n-1}'(\cos\theta) \qquad (3.2.2)$$

where P_n' is the first derivative of P_n.

It can be seen that a spherical harmonic series also describes H_z, whilst a different series, involving P_n', describes H_ρ but with the same coefficients A_n. So once a single set of coefficients has been found, both axial and radial field components may be calculated. Over the region of interest the H_ρ component can be shown to be at least four orders of magnitude less than H_z. Its contribution to the field modulus is therefore negligible

and will in future be ignored. Also the harmonic series will be taken as that for H_z, and not for V, as this is the quantity of interest. This is done so as to avoid H_z components with even symmetry having odd subscripts, and vice versa. The expressions for field are thus

$$H_z = \sum_{n=0}^{\infty} a_n r^n P_n(u) \qquad (3.3.1)$$

$$H_\rho = -\sin\theta \sum_{n=0}^{\infty} \frac{a_n r^n P_n'(u)}{(n+1)} \qquad (3.3.2)$$

where $u=\cos\theta$.

So, having found a general solution to Laplaces equation, a particular solution may be found by matching boundary conditions and equating coefficients. In this case the most useful boundary is the z axis. On axis, equation 3.3.1 reduces to

$$H_z = \sum_{n=0}^{\infty} a_n z^n \qquad (3.4)$$

since $P_n(\pm 1) = (\pm 1)^n$. Also, a Maclaurin expansion for the field about the origin will be given by

$$H_z = \sum_{n=0}^{\infty} H_{zo}^{(n)} z^n \qquad (3.5)$$

where $H_{zo}^{(n)}$ is the nth derivative of H_z evaluated at the origin. This gives the key to finding the a_n s for any

axisymmetric coil system. An expression for H_z, on axis, can usually be found quite readily by using the Biot-Savart law. The coefficients of the harmonic series may then be calculated by the repeated differentiation of the expression and equating the coefficients of the formulae in equations 3.4 and 3.5. Once the coefficients have been calculated, the field may be calculated anywhere throughout the region where eqs. 3.3 are valid, namely a sphere, with the origin as its centre, that does not enclose any current. In practice this is limited by the number of terms that are necessary to obtain convergence to the required accuracy.

Garrett[3.2] has taken expressions for the coefficients for basic coil shapes and recast them in terms of the Legendre polynomials. This greatly eases computation of the coefficients, and they are summarised in Appendix 3.1. It is clear that the expressions for the a_n's do not involve the position of the point at which the field is required. Likewise the equations 3.3 for evaluating the field do not involve the positions of the coils generating the field once the coefficients are known. Calculating the a_n's and evaluating the field components therefore forms two completely separate processes. This can result in economies in the computational effort required.

It is possible to derive coefficients for an equivalent series valid outside the current regions.

However, this still leaves the problem of calculating the field accurately near and inside windings. The exterior problem is therefore best left to an elliptic integral approach. (section 3.6)

3.3 The Legendre polynomials.

The Legendre polynomials arise from the series solution of Legendre's equation, which in turn arises from the product solution of Laplace's equation in spherical coordinates. The first few orders of polynomial are given by

$$P_0(u) = 1$$
$$P_1(u) = u$$
$$P_2(u) = 1/2(3u^2 - 1)$$
$$P_3(u) = 1/2(5u^3 - 3u)$$
$$P_4(u) = 1/8(35u^4 - 30u^2 + 3)$$
$$P_5(u) = 1/8(63u^5 - 70u^3 + 15u) \ldots \qquad (3.6)$$

It can be seen that the order of any of the terms is the same as the degree of the polynomial. Also, the odd order terms have odd symmetry, whilst the even orders have even symmetry.

For calculation purposes the use of these expressions directly is undesirable because of the need to store large tables of coefficients. Instead recurrence formulae are used that allow the next term of the series to be expressed as a function of the previous two.

Recurrence formulae are also available for evaluating the first derivatives P_n'. Since the first two members of these series are simple, the whole series may be calculated efficiently up to any given order. A table of useful formulae involving the polynomials and their derivatives is given below.

$$(n+1)P_{n+1}(u) + nP_{n-1}(u) = (2n+1)uP_n(u)$$

$$P_{n+1}'(u) - P_{n-1}'(u) = (2n+1)P_n(u)$$

$$nP_{n+1}'(u) + (n+1)P_{n-1}'(u) = (2n+1)uP_n'(u)$$

$$(1-u^2)P_n'(u) = nP_{n-1}(u) - unP_n(u)$$

(3.7)

3.4 The Design Method.

Using the expressions from the previous sections it is now possible to calculate the field from current carrying loops, solenoids, and thick section coils. However, in order to arrive at a useful method for designing magnets a closer look at the harmonic series is required. By substituting for the Legendre polynomials in equations 3.3 it is possible to see the kind of variation

produced by each term of the series. The a_o term produces a perfectly uniform H_z field with no H_ρ component. The a_1 term gives rise to a linear z gradient for H_z, with a H_ρ component that increases linearly with ρ. Each higher order term of the series represents a more complicated field shape (fig.3.2).

So in order to produce a perfectly uniform field throughout a spherical volume it is necessary to produce a coil arrangement such that every term in the harmonic series, except a_o, is equal to zero. Since the odd ordered spherical harmonics have odd symmetry, and the even orders have even symmetry, then all the odd orders

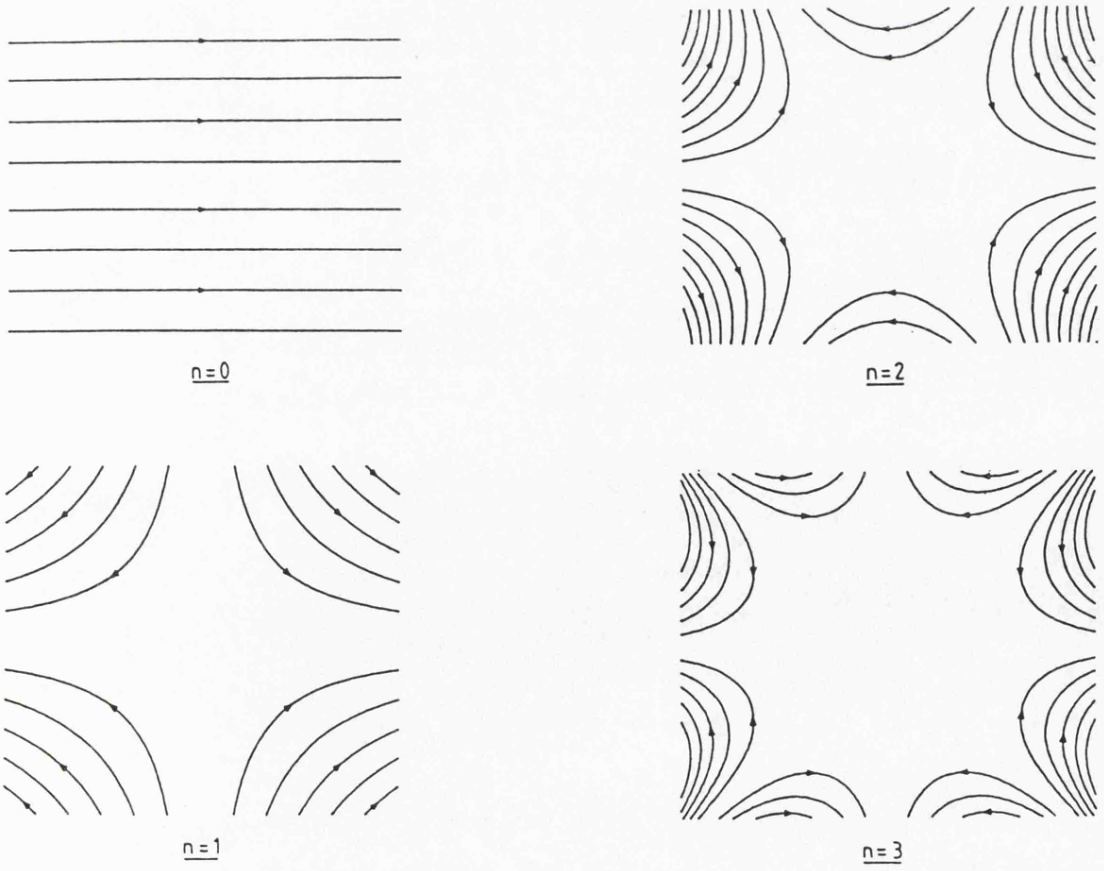

Fig.3.2 Field maps for spherical harmonics

may be removed simply by making the coil arrangement symmetrical about the origin. The number of even order terms that then need removing depends upon the degree of uniformity required.

Fig.3.3 shows the homogeneity produced by various arrangements of loops. The single coil has every even order harmonic present, whilst the coil pair has the 2nd order term cancelled because of the coil spacing. This arrangement is the well known Helmholtz pair. Three coils allow the 2nd and 4th orders to be cancelled, whilst 4 coils can cancel the 2nd,4th and 6th order terms. There is at least an order of magnitude improvement in homogeneity with every extra order that is cancelled.

It is usual to refer to a magnet by the order of the first error term in its field distribution. Thus the Helmholtz pair is a 4th order system, whilst the 4 coil arrangement is 8th order. In general, 8th order magnets will be required to produce the homogeneity required for nmr imaging.

The design process therefore reduces to simultaneously solving the non-linear equations

$$\sum_{\substack{\text{all}\\\text{coils}}} a_2 = 0$$

$$\sum_{\substack{\text{all}\\\text{coils}}} a_4 = 0$$

$$\sum_{\substack{\text{all}\\\text{coils}}} a_6 = 0 \qquad (3.8)$$

Contours: ±10,000ppm

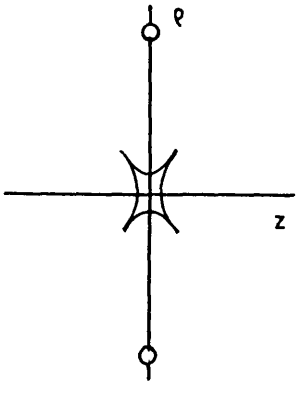

2nd Order

Contours: ±1,000ppm

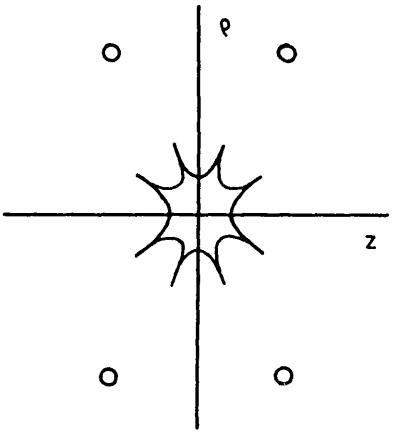

4th Order

Contours: ±100ppm

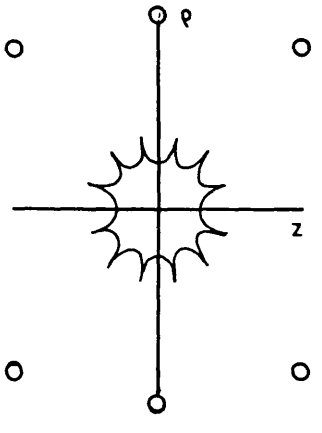

6th order

Contours: ±10ppm

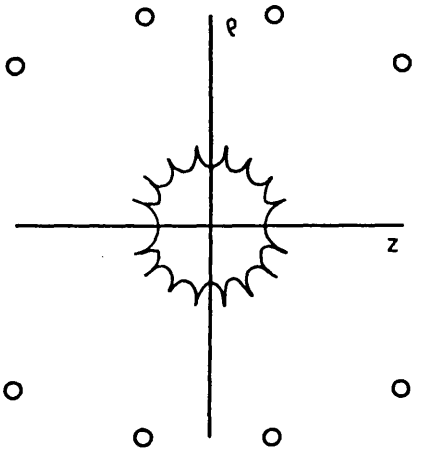

8th Order

Fig.3.3 Field uniformity produced by arrays of current loops

The method adopted for solving these equations is to use an optimising procedure to minimise the expression

$$\sum_{\substack{\text{all}\\\text{coils}}}(a_2^2 + a_4^2 + a_6^2) \qquad (3.9)$$

3.5 Notes on Optimisation.

The mathematical procedure of optimisation is achieved by adjusting a set of variables until some function, f, of those variables is at a minimum. Maximising a function would be equivalent to minimising the function -f. The methods used for this process depend on the nature of the problem to be solved. Adby and Dempster[3.3] give a useful introduction to optimisation methods and an extensive bibliography. The major objective is to reach the minimum with as small a number of function evaluations as possible, since these calculations usually account for the majority of the computational cost.

Further considerations include whether the derivatives of f with respect to each of the variables exist, are they available for use, or can they be reasonably approximated. For many problems the variables may be constrained to lie within certain limits, and in this case the problem is best transformed into an unconstrained one. Having reached a minimum there is a question of uniqueness, and if the solution is not unique

has a global minimum been reached. In general there can be no guarantee that the minimum found is a global minimum.

Since many of the multivariable techniques reduce to a single variable minimisation at some stage, it is worth looking to see how this is performed. The two basic methods are that of searching and of approximation. One approach to searching would be to use the Secant Method[3.4] to find the zero of the derivative of f. The rule uses two evaluations of f'(x) at the points x_a and x_b, and gives an approximation to the minimum

$$x_{min} = x_a - (x_b - x_a) \frac{f'(x_a)}{f'(x_b) - f'(x_a)} \qquad (3.10)$$

This rule is used iteratively using the latest value of $f'(x_{min})$ to replace the larger of $f'(x_a)$ or $f'(x_b)$. It can be shown that this method is more efficient than the classical Newton-Raphson method for finding the zero of f', for which the second derivatives of f would be required.

Approximation methods attempt to fit the function with a low order polynomial. The coefficients of a cubic could be found from the solution of four linear equations using four evaluations of the function f. Alternatively, the function and its derivative could be evaluated at two points giving the same information. The minimum of the function is then found algebraically by differentiating

the polynomial and setting the result to zero. A check of the second derivative may be required to check that the point found is not a maximum. However, since the method only uses an approximation to the function it will be necessary to use the technique iteratively.

The multivariable optimisation problem may be tackled by two methods, search and gradient techniques. A simple search method would be to adjust each variable, one at a time, until a minimum is reached. One of the previously described methods may be used for finding the minimum at each stage. The whole process is repeated until no further improvement can be obtained. Figure 3.4 shows a set of contours for a two variable function and the path taken towards the minimum using this method. It is clear that the direction taken at any one time is rarely in the direction of the minimum. The method is therefore rather inefficient, especially as several evaluations are required at each stage.

A more efficient method that again only requires function values is the Simplex Method. For an n variable problem a simplex may be regarded as an equilateral polyhedron with n+1 vertices in n dimensional space. A two dimensional case where the simplex is a triangle is shown in fig. 3.5. Function evaluations are obtained at each of the vertices. The vertex with the largest value is then reflected about the remaining vertices, and the function value obtained at the new point. This process is

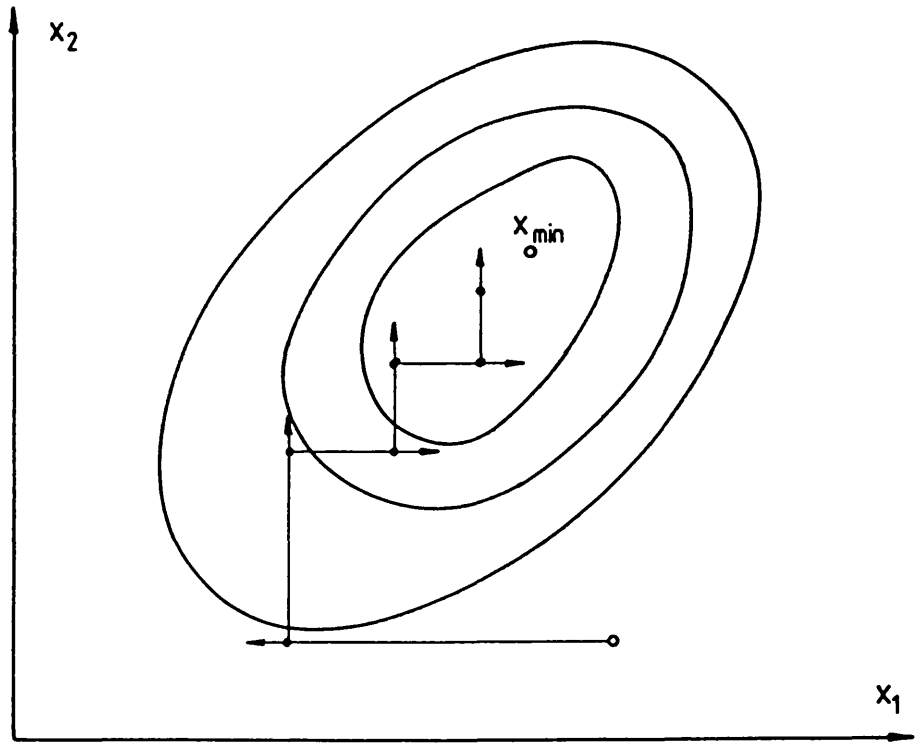

Fig.3.4 A 'one at a time' search

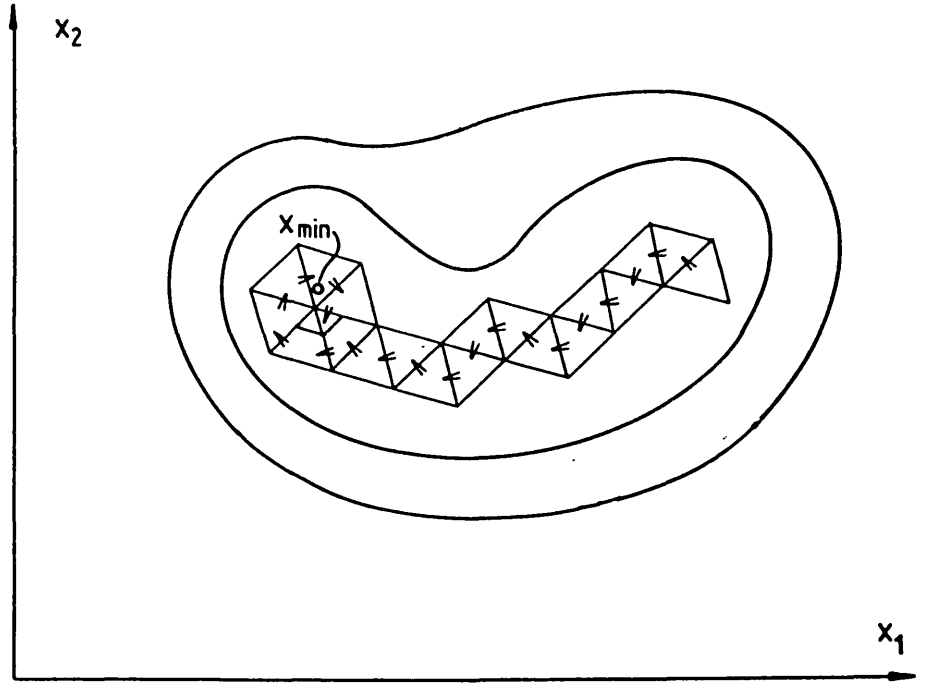

Fig.3.5 A Simplex search

continued until a minimum is reached, usually indicated by one vertex being used continuously as a pivot. The advantage of this method is that a decision about the direction of descent is made at each iteration. Improvements to the method include changing the size of the simplex as the minimisation procedes, and performing a search in the direction of the reflected vertex. With these modifications this relatively simple and compact procedure competes with more complex methods when the number of variables is very large (greater than 100).

The starting point for gradient methods is the multivariable form of the Taylor series expansion for f

$$f(x+dx) = f(x) + g^T dx + 1/2 dx^T H dx + \ldots \quad (3.11)$$

where

g is the column Jacobian matrix

with elements $g_i = \partial f/\partial x_i$

H is the square Hessian matrix

with elements $H_{ij} = \partial f/\partial x_i \partial x_j$

The function at a new point f(x+dx) nearer the minimum may be considered as the function at the present point f(x) plus some correction. For first order methods the correction will be $g^T dx$ which can be regarded as the scalar product of two vectors

$$g^T dx = |g||dx| \cos\theta \quad (3.12)$$

where θ is the angle between the directions g and dx. The largest reduction in f will occur when $\theta = 180$ degrees, that is when the direction of the minimising change is in

the direction of the negative gradient -g. It then remains to find dx in this direction so that f(x+dx) is a minimum. This amounts to a single variable minimisation that may be tackled using one of the above methods. The procedure is known as the "steepest descent" method, and since the direction taken will not generally be in the direction of the minimum, it needs to be used iteratively.

A second order method may be derived by differentiating and setting to zero equation 3.11. The first two terms on the right hand side yield

$$g + Hdx = 0$$

$$\text{or} \quad dx = -H^{-1} g \qquad (3.13)$$

Thus the adjustment to x needed in order to find the minimum is given in terms of g and H. In practice a search in the direction of dx is used since the method is only an approximation, but if f were quadratic the minimum would be reached in one step. Nevertheless, it is undesirable to have to evaluate the Hessian and its inverse at each iteration, so an approximation to the inverse is usually used. The approximation is derived from the Jacobian values subject to the constraint that H^{-1} needs to be positive definite to assure convergence. As a starting point H^{-1} is often assumed to be the identity matrix, so the method starts as one of steepest descent.

Ensuring that H^{-1} is positive definite is not an easy task especially when errors may be introduced by

using central or forward difference formulae in order to approximate the derivatives. Gill and Murray [3.5] have considered these problems and have produced an unconstrained optimisation procedure that requires only function values, and uses an approximation to H^{-1} that guarantees positive definiteness.

3.6 Field Calculations Using Elliptic Integrals.

Direct analytic expressions for the field from axisymmetric conductors generally involve complete elliptic integrals (for example Smythe [3.1]). The integrals of the first, second and third kind are defined by

$$K(k) = \int_0^{\pi/2} \frac{d\phi}{\sqrt{1 - k^2\sin^2\phi}} \qquad 0<k<1$$

$$E(k) = \int_0^{\pi/2} \sqrt{1 - k^2\sin^2\phi}\; d\phi \qquad 0<k<1$$

$$\Pi(n,k) = \int_0^{\pi/2} \frac{d\phi}{(1 + n\sin^2\phi)\sqrt{1 - k^2\sin^2\phi}} \qquad 0<k<1 \qquad (3.14)$$

Garrett [3.5] has collected together from the literature many unconnected formulae and produced a set of equations for fields, forces and mutual inductances between loops and thin section solenoids in terms of these integrals. In order to obtain results from thick section coils the

expressions for a thin solenoid must be numerically integrated (section 4.3). The formulae of present interest are shown in Appendix 3.2.

The evaluation of these may be performed by successively transforming the integral until the modulus k reaches unity, whereupon the expression may be integrated analytically. Bulirsch [3.7] has developed a general, efficient, computational scheme that allows all three kinds of integral to be evaluated using a single routine. More importantly this generalisation allows linear combinations of the three kinds to be calculated without loss of accuracy due to cancellation. The procedure is defined by

$$\mathrm{cel}(k_c,p,a,b) = \int_0^{\pi/2} \frac{a\cos^2\phi + b\sin^2\phi \quad d\phi}{(\cos^2\phi + p\sin^2\phi)\sqrt{\cos^2\phi + k_c^{\,2}\sin^2\phi}} \tag{3.15}$$

where k_c is the complementary modulus given by $k^2+k_c^2=1$.

The transformation is accomplished using the formula

$$cel(k_c,p,a,b) = \int_0^{\pi/2} \frac{a_j^2 u_j^2 \cos^2\phi + b_j^2 u_j^2 \sin^2\phi \quad d\phi}{(u_j^2 \cos^2\phi + p_j^2 \sin^2\phi)\sqrt{\cos^2\phi + k_c^2 \sin^2\phi}} \qquad (3.16)$$

with the recurrence relations

$$u_{j+1} = u_j + v_j \qquad a_{j+1} = b_j/p_j + a_j$$
$$v_{j+1} = 2\sqrt{u_j v_j} \qquad b_{j+1} = 2(u_j v_j a_j/p_j + b_j)$$
$$p_{j+1} = u_j v_j/p_j + p_j$$

and using the initial values

$$u_o = 1;\ v_o = |k_c|;\ p_o = \sqrt{p}\ ;$$
$$a_o = a\ ;\ b_o = b/\sqrt{p}\ .$$

At each iteration u is replaced with twice the arithmetic mean of u and v, while v is replaced with twice the geometric mean (the factor of two is simply to avoid an unnecesary division). The method is therefore also known as the method arithmetico-geometric means. As the iteration proceeds the values of u and v approach a common limit, i.e. $u/v \rightarrow 1$. When this limit has been achieved to the required degree of accuracy the process

terminates and the integral is given by

$$\mathrm{cel}(k_c,p,a,b) = \frac{\pi}{2} \frac{a_j u_j + b_j}{u_j(u_j + p_j)} \qquad (3.17)$$

For example, in evaluating K(0.5) the values of u and v at each iteration are given by

	u	v
0	1.0	0.866 025
1	3.727 234 3	3.727 231 2
2	7.454 465 5	7.454 465 5

and cel(0.866025,1,1,1) = 1.685 750 7

The process has converged in only two iterations to give 8 significant figures of agreement between u and v. Bulirsch suggests that the relative error in cel will be less than $1 - v/u$, and so the answer should also be accurate to 8 figures.

The advantage of using the elliptic integral formulae is that they are valid anywhere in space, whereas the harmonic approach is limited to central regions. They therefore allow fields to be calculated outside the magnet and within the windings. The disadvantage is that fields from thick section coils have to be evaluated by numerical integration, and this is computationally expensive when compared to using spherical harmonics. Also they give no idea as to a suitable design procedure. Comparison of the accuracy of the two methods shows that 8 or 9 figures of agreement

are obtained over central field regions when using 14 harmonic terms. This is perfectly adequate for the application. However, as the windings are approached more terms need to be included in the harmonic series to achieve the same accuracy. The harmonic method eventually fails when the windings are reached.

3.7 The Magnet Design Package.

The techniques of the previous sections have been incorporated into a single magnet design program. The user sets up an initial guess at a possible design and the computer adjusts the allowable variables until the required harmonics are cancelled. Using a graphics terminal connected to a Rutherford Laboratory's Prime 750 computer all the operations can be performed interactively as even the most complex tasks take less than half a minute to be executed. It is therefore very easy for the user to become familiar with nmr magnet design restrictions without recourse to a lot of algebra that has previously become necessary.

The first step in the design process is to set up a coil system that is likely to produce the required results, perhaps using the models of fig 3.3 as a starting point. The coils may be loops, solenoids or thick section coils.

Before letting the computer optimise this initial geometry so as to cancel the required harmonics it is

possible to fix any of the currents or dimensions. It is also possible to tie any group of them so that they take on the same numerical value, with or without a change of sign. In this way symmetry can be enforced on the problem, whilst at the same time reducing the number of variables taking part in the optimisation.

The objective function for the optimisation procedure is usually the sum of the squares of the harmonic coefficients that need to be cancelled. Weights can be applied to each of the terms but this has not been found to be necessary. Alternatively, the sum of the squares of the deviations of field from the central value at a number of user specified points may be used. This is useful for obtaining a region of uniform field that is different from the slightly oblate spheroid that is usually obtained using the harmonic cancellation method. It does of course involve the calculation of the field from the harmonics, which means another stage of computation.

Gill and Murray's unconstrained procedure [3.5] has been used for the optimisation, and this only requires function evaluations. Since the coils have to lie within certain well defined areas for harmonic cancellation to occur then the problem is already, in a sense, constrained (section 3.10 and fig. 3.14). This has been born out in practice since it has not been found necessary to use a constrained optimisation procedure.

The system geometry determined by the optimisation program will almost certainly not be unique. Since the set of equations (3.8) that the program is in effect solving is generally overdetermined there will be an infinite number of solutions. The user is therefore able to adjust the design to fit the requirements whilst still being able to obtain a solution.

Having obtained that solution contour maps and graphs of fields and field uniformity can be drawn. Again the harmonic approach is convenient since the coefficients are only calculated once, whereas the elliptic integral method has to start from scratch for each field point. However, for points outside the magnet elliptic integrals have to be used. In this case loop and thin solenoid approximations are useful since they cut the computational cost. The reduced accuracy of the model can usually be tolerated since the stray external fields are rarely required to a great degree of accuracy. In addition to graphical output it is possible to obtain conductor masses and dissipation figures for any current loading and packing factor of the conductors. Preset figures are available for aluminium and copper, but these may be adjusted if required.

3.8 Three coil magnet systems.

In an attempt to produce a design for a 0.1 Tesla magnet with a 1.0 metre internal diameter, the 3 coil, 6th order arrangement of fig. 3.3 may be used as a starting point. The coils are given a finite cross-section and the computer is used to choose the radius of the inner coil, and the thickness and axial positions of the end coils. Figure 3.6.1 shows the result of doing this, along with contours of the $\pm$10ppm field error. The arrangement produces 0.1 Tesla central field with an arbitary $2A/mm^2$ current density, and packing factor of 75%.

A whole series of designs may be obtained by increasing the length of the centre coil to form a solenoid, and adjusting the coil dimensions so as to keep a 0.1 Tesla central field. The remaining parts of fig. 3.6 show the effect of doing this. Plots of field uniformity, power dissipation and conductor weight (assumed to be copper) versus the length of the centre coil are shown in fig. 3.7. It can be seen that there is a steady increase in field uniformity with solenoid length, however, this has to be paid for with extra material weight and power dissipation.

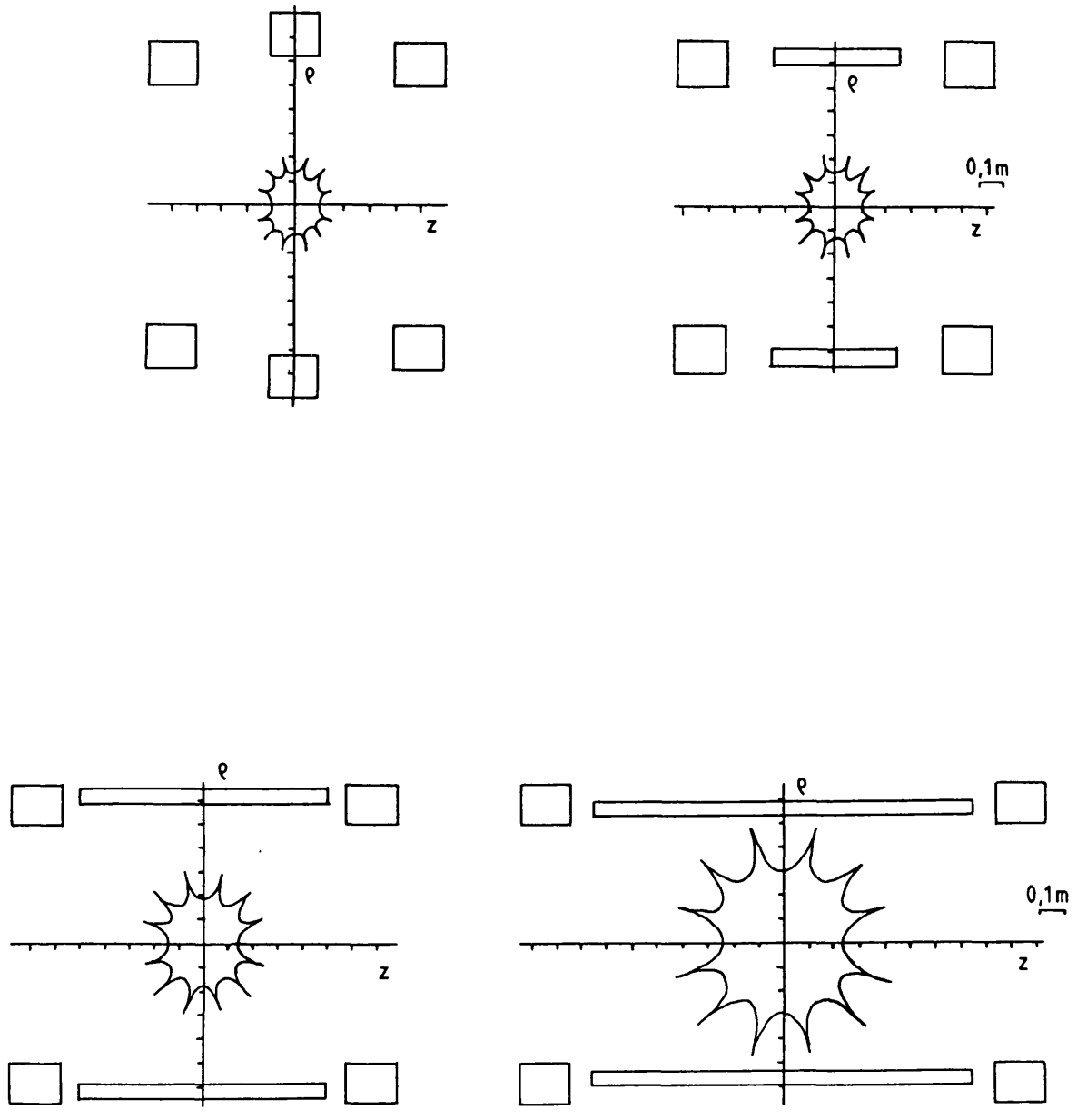

Fig.3.6 6th order, 3 coil magnets with different centre coil lengths (±10ppm contours)

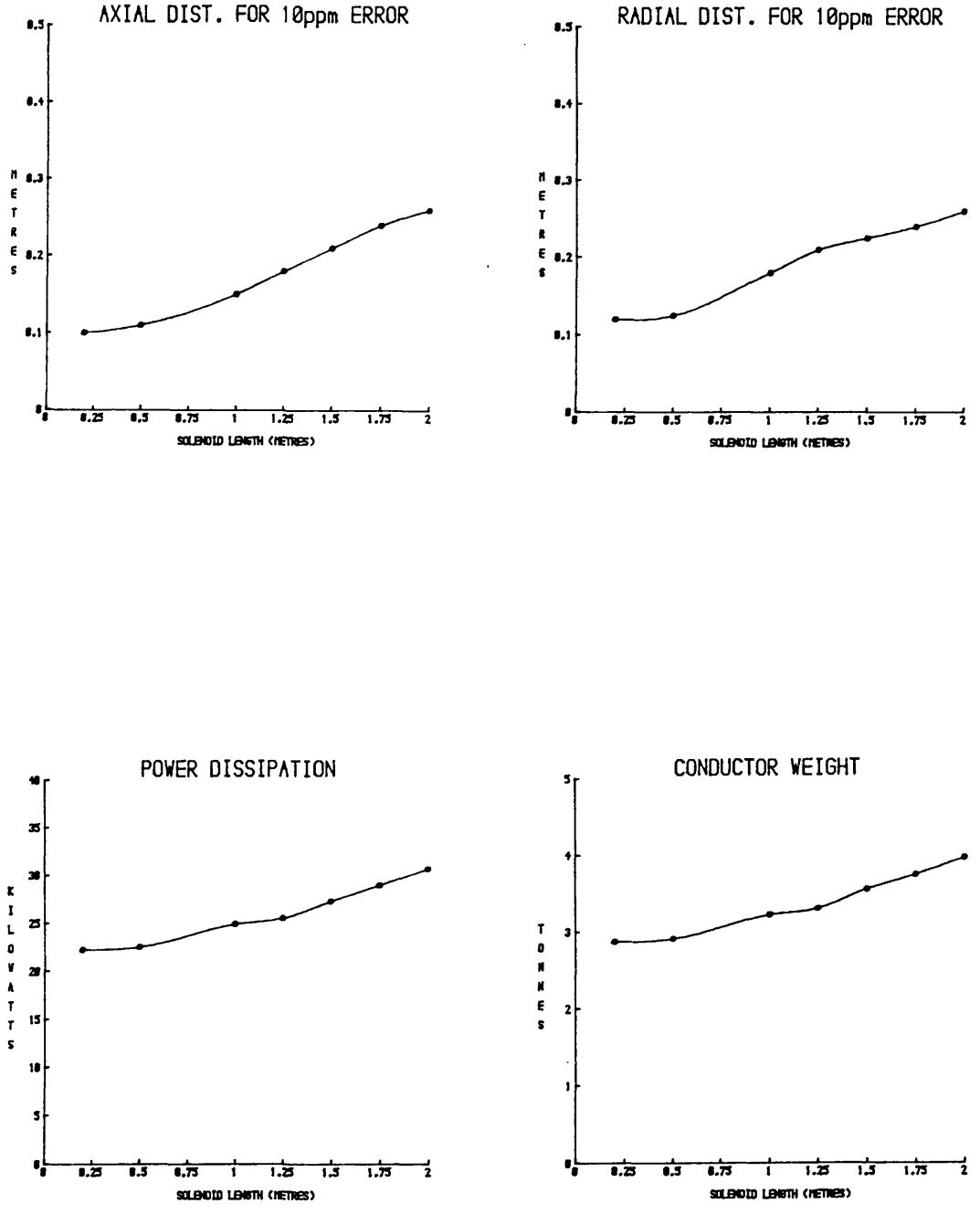

Fig.3.7 Variation in performance of 6th order magnets with length of centre coil

When the solenoid length is greater than about 0.6m it is possible to use the outer coils to cancel the 6th order term in addition to the 2nd and 4th terms. Fig.3.8 shows three cases where this has been done, and fig.3.9 gives graphical information for a range of these designs.

In all cases the radius of the uniform region in the 8th order system is at least 1.5 times that in the corresponding 6th order system. For magnets with a solenoid length of about 1 metre this increase is obtained with no increase in power or weight. As the coil length is increased up to 2 metres the weight and power of the 8th order magnet rises to about 1.2 times that of the 6th order. However, the increase in homogeneous volume with solenoid length is not smooth, with the result that the performance of a corrected 2 metre long solenoid may nearly be achieved with a solenoid only 1.5 metres long. The reason for the unusual behaviour of the homogeneity curves in fig.3.9 is that the 8th and 10th order terms generated by the complete system are small (fig. 3.10) when the central coil is in the order of 1.5 metres long. Hence the corresponding increase in uniform volume.

As the solenoid length of the 8th order system is decreased from 1 metre, the size of the required correction coils becomes excessively large. This results not only in a large increase in power and weight, but an impractical mechanical structure. Thus it becomes

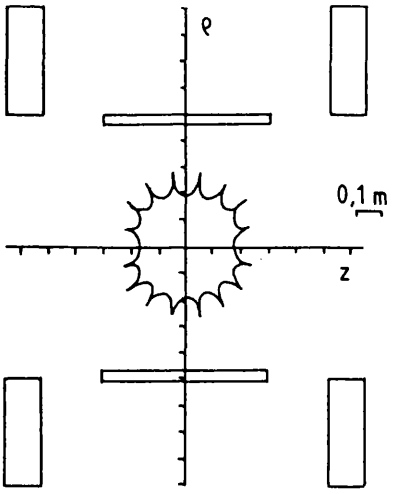

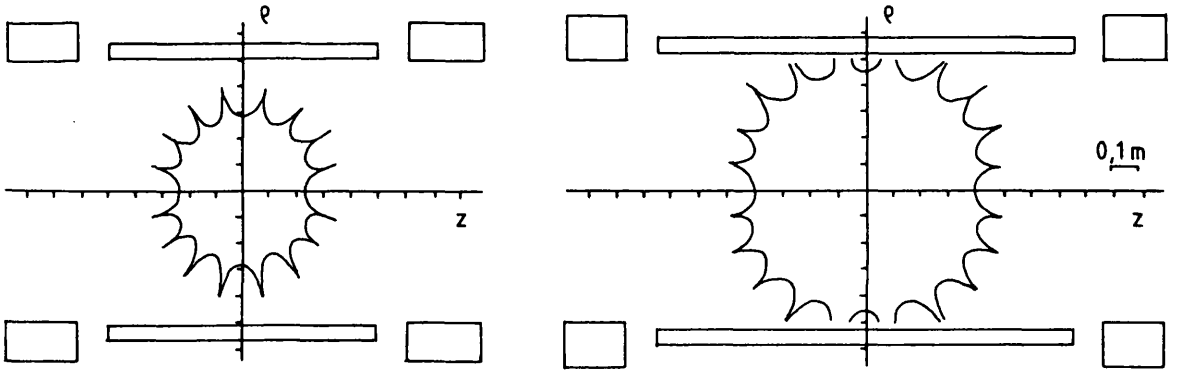

Fig.3.8 8th order, 3 coil magnets with different centre coil lengths (±10ppm contours)

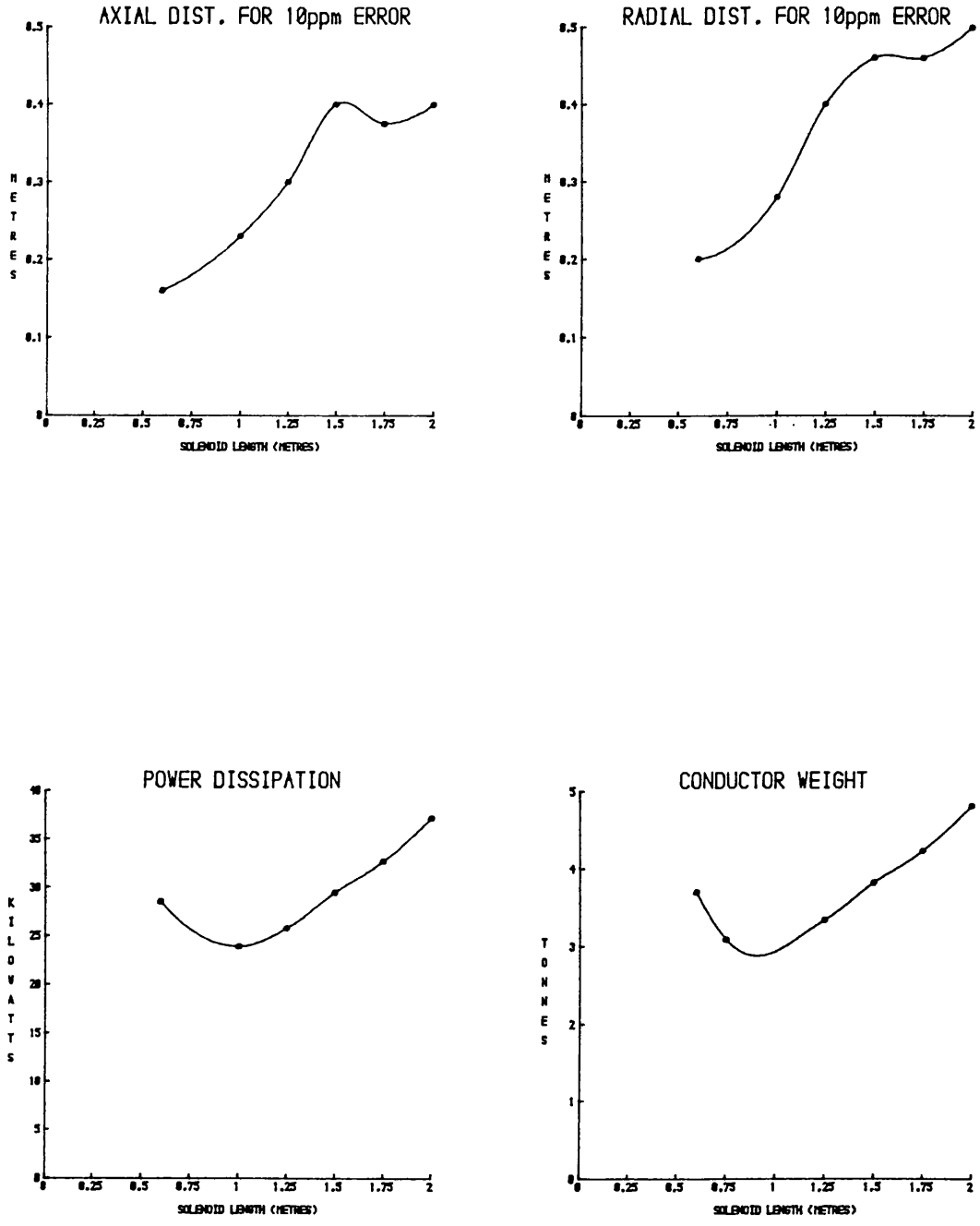

Fig.3.9 Variation in performance of 8th order magnets with length of centre coil

unrealistic to make 8th order magnets of this bore with a solenoid length of less than about 0.8 metres.

It is clear that the 3 coil arrangement is capable of meeting a wide range of performance requiremets. However, for the cases where the solenoid length is greater than about 0.8 metres long it is more economical to obtain a given field homogeneity with an 8th order rather than a 6th order system. Theoretically, a solenoid of about 1.2 metres length is required to meet the $\pm$10ppm maximum field error at 25 cms radius, as was set out in chapter 1. In practice it is desirable to leave some margin in order to allow for defects in manufacture, and so it may be tempting to consider a solenoid length approaching 1.5 metres. The large increase in uniformity obtained with a relatively small increase in weight and power makes the system very attractive if field homogeneity is the overriding concern of the designer.

3.9 Four coil magnet systems.

A series of 8th order, four coil designs may be derived, again using the filamentary models of fig.3.3 as a starting point. This sort of arrangement may be considered as an approximation to a spherical current sheet with sinusoidal current distribution. However, it will seen that more general results than this may be obtained. Figure 3.11 shows a thick coil version of the 4

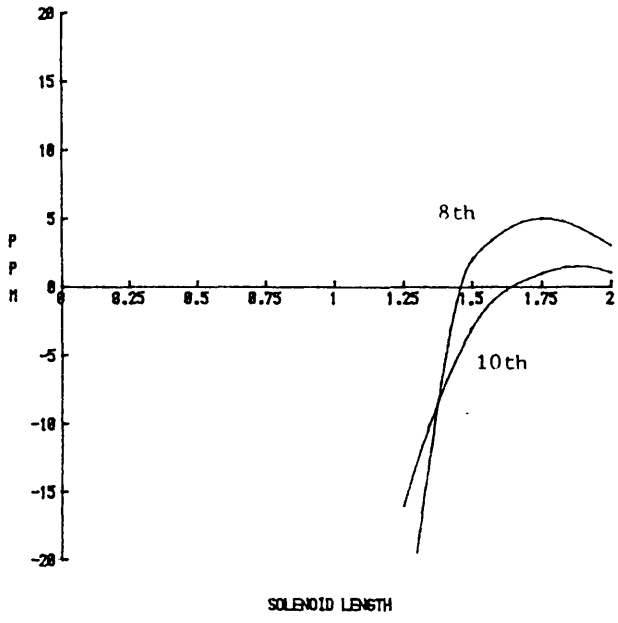

Fig.3.10 Variation of 8th and 10th order errors with centre coil length

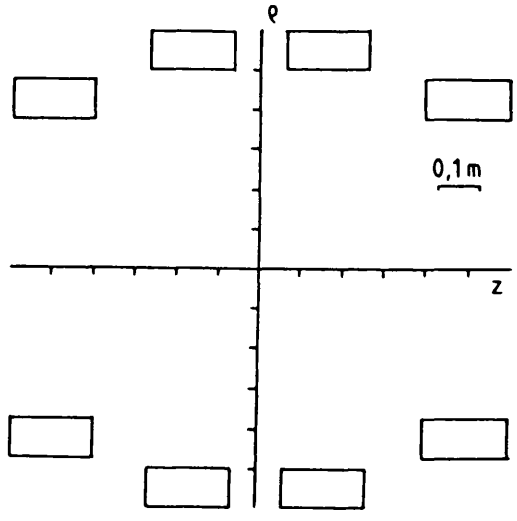

Fig.3.11 Thick coil version of 8th order 4 coil magnet

loop arrangement. The coil widths are set at 0.2 metres, inner coil radii at 0.5 metres, and the coil thicknesses chosen to give a 0.1 Tesla central field.

Anodised aluminium tape might be used to wind the coils, or alternatively copper tape with a thin layer of insulation (eg. Kapton). Such an arrangement would be expected to give very high a packing factor. Assuming the coils to be copper wound carrying $2A/mm^2$ (as in the 3 coil case) and having a 90% packing factor, the required 0.1 Tesla central field is obtained with a dissipation of 15.2kW, and a copper weight of 1.97 tonnes. The four coil arrangement is therefore much more efficient and lighter than the 3 coil, simply because the conductors are closer to the region of interest. However, because of the discrete nature of the coils the homogeneity is much worse, $\pm$10ppm field errors occur at 0.14m on axis and 0.16m on the radius. This sort of uniformity is typical of the systems that are described here, and would be acceptable for for making images of the human head. At 0.2m radius the errors are about $\pm$50ppm, and whilst this area covers most of the human torso, it must be accepted that the making of high resolution pictures is made more difficult by the increased field errors.

The bore of this magnet has rather restricted access, so in order to improve this the outer coil radii may be increased, as shown in fig. 3.12.1. As the radius increases the coil section also increases, and the coil

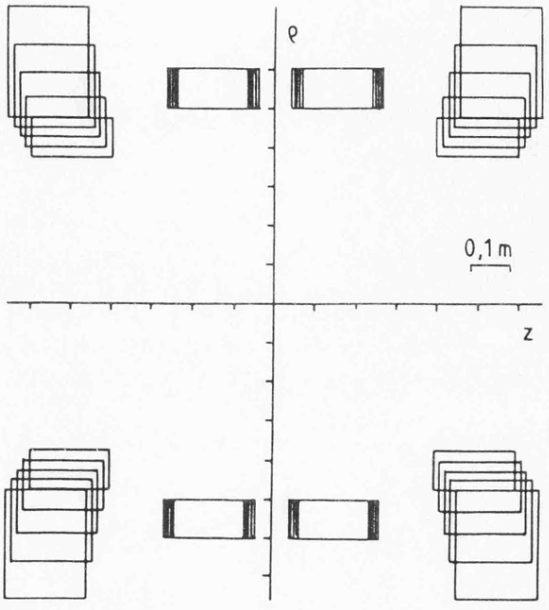

Fig.3.12.1 Variation of coil geometry with axial access

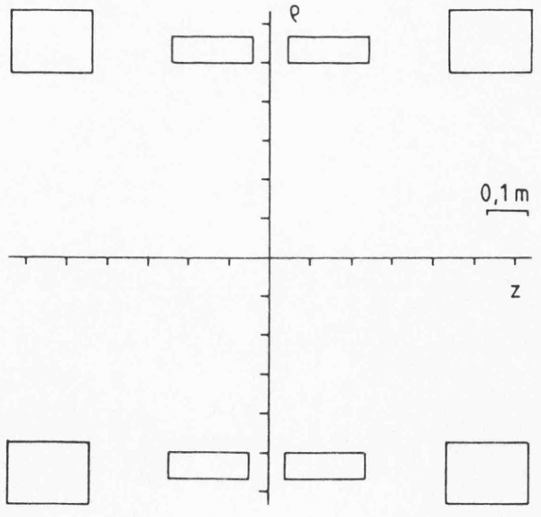

Fig.3.12.2 A four coil magnet with good axial access

moves slightly away from the centre plane. The penultimate arrangement, adjusted to give a 0.1 Tesla central field, is shown in fig. 3.12.2.

Alternatively, the same starting point may be used to obtain a magnet with good radial access. (fig. 3.13.1.) Here the inner coils have been forced axially outwards, the coil radii and inner coil thickness being allowed to vary. A magnet that produces 0.1 Tesla central field, and whose inner and outer coils have the same separation is shown in fig. 3.13.2.

Although access to the central field is improved in the latter cases, it must be paid for with increased power dissipation and conductor weight. This is particularly true for the radial access system where both of these quantities have more than doubled.

A summary of the 4 coil systems and a 6th order, 3 coil system with comparable homogeneity is shown in table 3.1. The current density and packing factor are assumed to be $2A/mm^2$ and 90% in all cases.

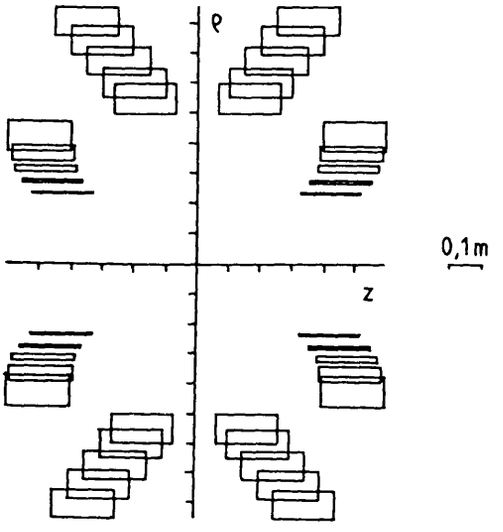

Fig.3.13.1 Variation of coil geometry with radial access

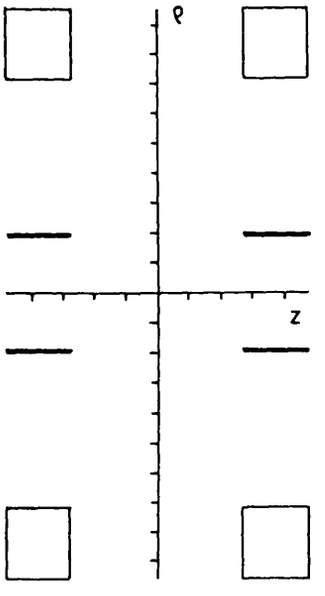

Fig.3.13.2 A four coil magnet with improved radial access

Table 3.1 Comparison of 3 and 4 coil systems.

	Dist. for 10ppm error(m)			
	axial	radial	Power(kW)	Weight(t)
Spherical				
4 coil	0.14	0.16	15.2	1.97
Axial access				
4 coil	0.15	0.17	20.0	2.59
Radial access				
4 coil	0.12	0.15	32.3	4.18
6th order 3 coil	0.14	0.17	23.4	3.03

3.10 The design of shim coils.

In any practical magnet there will almost certainly be some defects in the field uniformity that will require correction, either by the movement of individual coils from their theoretically ideal positions, or by the addition of small "shim" coils. The defects that occur will be due to the limited mechanical tolerances that may be reasonably achieved during construction, and due to ferromagnetic material that will inevitably be present in

nearby equipment, or in the structure of the building in which the magnet is housed.

A convenient way of tackling the problem of removing the unwanted inhomogeneity is to measure the actual field and obtain harmonic values from the measurements. Coils that produce only one harmonic term may then be used to cancel the unwanted harmonics one at a time. The adjustments made with the coils will not interact with each other since the harmonics that they produce will be orthogonal.

A method for obtaining harmonic values from field measurements is described in section 4.4, where they are represented as the peak to peak contribution that the harmonic makes (in ppm) to the inhomogeneity over the surface of a sphere of given radius. This is a fairly convenient representation as it has a physical interpretation. The a_ns of eq. 3.3 may be converted into this form by means of

$$c_n = a_n \; W_n \; r_o^{\,n} \; 10^6 \; / \; a_o \qquad (3.18)$$

where c_n represents the peak to peak amplitude of the nth harmonic over a sphere of radius r_o. If the weight W_n is taken as unity for the present, the c_n will represent the peak variation over the sphere. The a_ns actually represent the contribution of the nth harmonic over a sphere of unit radius.

In order to show typical values for the harmonics generated by incorrect coil dimensions, +0.1mm errors

were introduced into the 4 coil model of fig.3.11. The unwanted harmonics generated at 0.25m radius by these errors are shown in table 3.2.

Table 3.2 Harmonics generated by incorrect coil positions in the model of fig. 3.11 (ppm wrt 0.1T at 0.25m radius)

Harmonic	Axial error		Radial error	
	inner coil	outer coil	inner coil	outer coil
c_1	33.4	-29.7	-46.5	-5.0
c_2	31.0	-9.0	9.9	-16.4
c_3	-1.2	1.0	16.8	-9.9
c_4	-7.3	2.3	1.6	-3.0
c_5	-1.4	1.2	-3.0	0.0
c_6	1.0	0.3	-0.9	0.4

Clearly, the homogeneity is very sensitive to dimensional errors. Even though the unwanted harmonics may be reduced by the deliberate movements of the magnet coils, shim coils would still be necessary as it is improbable that new positions could be found that completely cancel the unwanted terms.

In order to design appropriate shim coils, reference should be made to fig.3.14. These diagrams show the signs of the low order harmonics generated by a current carrying loop as a function of its angular position. They

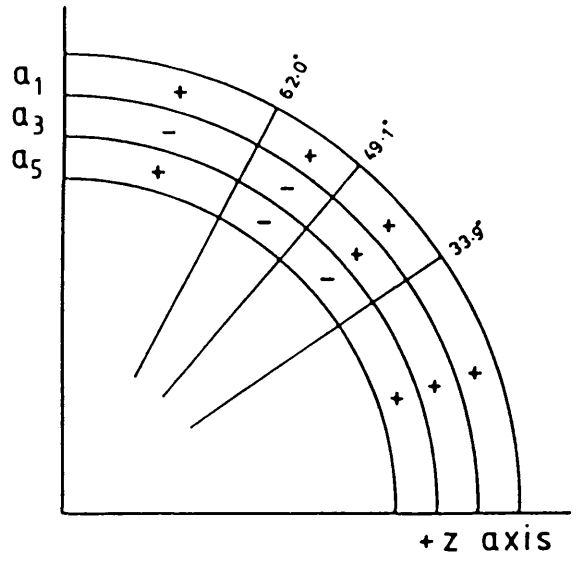

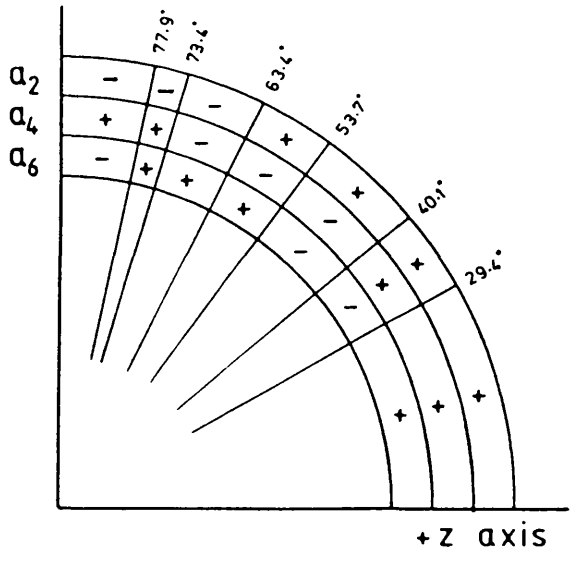

Fig. 3.14 Variation of the signs of spherical harmonics with the angular position of a current carrying loop

are derived from the expressions in appendix 3.1. To generate an even order harmonic, coil pairs that are symmetric about the origin are used, whilst odd orders are generated by antisymmetric coil pairs.

So, to produce a shim that substantially generates a first order gradient, a pair of opposing coils that subtend a half angle of 49.1 degrees at the origin may be used. By using this angle it is ensured that no third harmonic is generated. The amount of first and fifth orders that are produced at 0.25m radius, by 1.0m diameter coils, is given in table 3.3.

In many cases, the small amount of fifth order harmonic will be of no significance. However, it does mean that the adjustments of the coil currents will not be quite independent. If large adjustments are required then some allowance may have to be made for the unwanted harmonics. Alternatively, the addition of a second coil pair allows both the third and the fifth orders to be removed. The penalty for producing a purer gradient is that the sensitivity of the shim is reduced.

The task of designing shim coils (and magnets) can therefore be reduced to choosing likely angular postions for the coils using fig.3.14, and letting the computer program cancel the appropriate harmonics by adjusting the coil positions and currents. Sets of shims may be designed that have a common radius, where they are to fit into a solenoidal magnet; or lie on two planes

perpendicular to the z axis, where the magnet is a four coil type with radial access. There is a great deal of choice in positioning the individual coils of a multicoil shim because, just as for magnets, the set of equations that are effectively being solved by the program are usually overdetermined. The designer is therefore able to produce a shim coil set with the minimum of difficulty due to the coils being coincident, or nearly so.

The examples in table 3.3 may therefore be used as the starting point for designs with a common diameter of 1 metre. The optimisation program may be used to obtain designs with integral turns ratios, and they can be expanded into thick section coils, as was done in the case of the magnet designs.

Table 3.3 Harmonics generated by 1.0m diameter shimcoils (in ppm/ampturn wrt 0.1T, at 0.25m radius)

Angular Position (degrees)	Current Ratio	c_1	c_3	c_5
1st order				
49.1	-	4.03	0	-0.13
63.8	1			
37.4	6.7	2.48	0	0
3rd order				
69.75	1			
56.9	-1	0	0.67	0.27
62	1			
33.9	-3.56	0	0.42	0
5th order				
80.9	1			
65.9	-1			
49.1	0.58	0	0	0.15

Table 3.3 (contd.)

Angular Position (degrees)	Current Ratio	c_2	c_4	c_6
2nd order				
40.1	-	1	0	-0.02
73.4	-	-2.26	0	0.17
58.0	1			
34.4	18.24	0.65	0	0
4th order				
63.4	-	0	-0.65	0.17
76.8	1			
40.6	2.95	0	0.10	0
6th order				
90	-1			
52.7	-1.88	0	0	0.10

3.11 Conclusions.

The results presented in this chapter demonstrate that the interactive computer program is capable of producing designs for a wide variety of magnet systems, and shim coils, that meet a broad range of performance and mechanical requirements. A user with no previous knowledge of spherical harmonics, or optimisation methods, may easily take any of the designs described and adapt its dimensions to fit a given winding arrangement. In order to design a system from scratch the user would require some knowledge of harmonics, but reference to fig.3.14 should be all that is required to determine the angular position of the coils to achieve a given result. The computer will then calculate the unknown dimensions.

The use of spherical harmonics allows calculations to be performed quickly and efficiently. At the same time it allows the user to obtain some feel for what can produce a feasible design, and what cannot. If the elliptic integral calculations were used instead of the harmonic approach, the time taken to perform the field calculations would be sufficiently long that it would not be worth running as an interactive program. The usefulness of the program would then be greatly reduced, as this represents a strong disincentive to adopt a trial and error approach to achieving a new design.

CHAPTER 4. MODELLING OF DISCRETE CONDUCTORS.

4.1 Introduction.

Having chosen a suitable magnet design using the techniques of the previous chapter it is necessary to evaluate the effects that a real winding will have on the magnet's performance. A winding may consist of helices or spirals, it may be oval or tapered because of the effects of mechanical tolerances, and it will have interconnections between the individual coils and the power supply. All of these effects require modelling, and a unified approach is presented in this chapter.

Because of the difficulties in visualising the effects of these disturbances by looking at field values alone, a more general series of non-axisymmetric harmonics is introduced, together with a method for resolving a set of field values into harmonic amplitudes. By using harmonics it is possible to gain some insight into the sort of effect that each disturbance produces because of the high degree of symmetry that each harmonic term possesses.

Results are presented for a range of conductor geometries. From these it is possible to derive some guidelines that allow the designer to minimise the effects of real windings upon field uniformity. Shimming methods are also described that allow some of the remaining field errors to be removed, either by movement of the magnet coils, or with specially shaped shim coils.

4.2 Field calculations for practical windings.

Whilst it may be possible to obtain analytic expressions for the fields from various forms of winding, they are generally difficult to obtain, and since they usually include elliptic integrals they have to be evaluated numerically anyway. A further problem is that a complete new derivation must be performed for every new effect that requires modelling. A much simpler approach is to calculate the field by the numerical integration of the Biot-Savart law. The field of an incremental current carrying element (fig. 4.1), is given by

$$d\underline{H} = \frac{I\ (\underline{r} \times \underline{dr})}{4\pi r^3} \qquad (4.1)$$

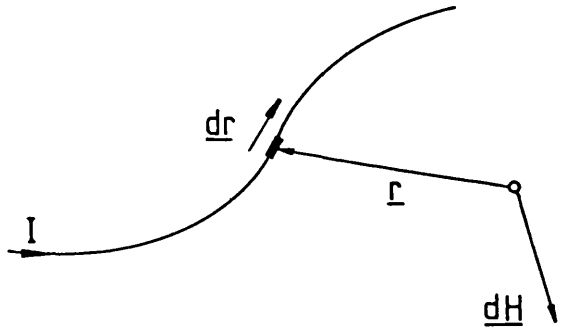

Fig.4.1 Field $d\underline{H}$ due to current carrying element $d\underline{R}$

As an example, consider the filamentary current carrying loop in figure 4.2. The components of the various vectors will be given by

$$\underline{R} = (R\cos\phi, R\sin\phi, z_o) \qquad \underline{p} = (x,y,z)$$
$$\underline{r} = (R\cos\phi - x, R\sin\phi - y, z_o - z) \quad \underline{dR} = (-R\sin\phi, R\cos\phi, 0) = \underline{dr} \tag{4.2}$$

Substituting 4.2 into 4.1 and evaluating the cross product allows the three components of $\underline{H}$ to be evaluated by integration with respect to ϕ throughout the range 0 to 2π. Thus all that is required to calculate the field of any filamentary conductor is a parametric description of the path taken by the filament, and its derivative with respect to that parameter. The rest of the procedure will be the same whatever the actual form of the wire. The parametric form for a generalised filamentary arc or loop that can have helical or spiral pitch, ovality and an arbitary starting point is given in appendix 4.1. Also given is a parametric form for a straight wire, although this could easily be tackled by analytical means.

The method may be extended to rectangular section conductors. If the conductor's parametric equation refers to its centre (fig. 4.3), then a triple integration must now be performed with one integration in width from -w/2 to +w/2, one in thickness from -t/2 to +t/2, and the third as before in ϕ. Before this can be done it is essential to know the directions in which the first two

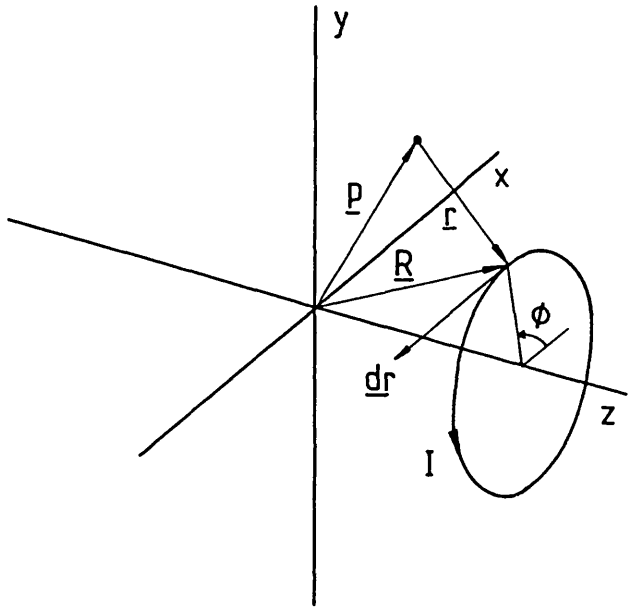

Fig.4.2 Vectors required for determining the field of a loop of wire

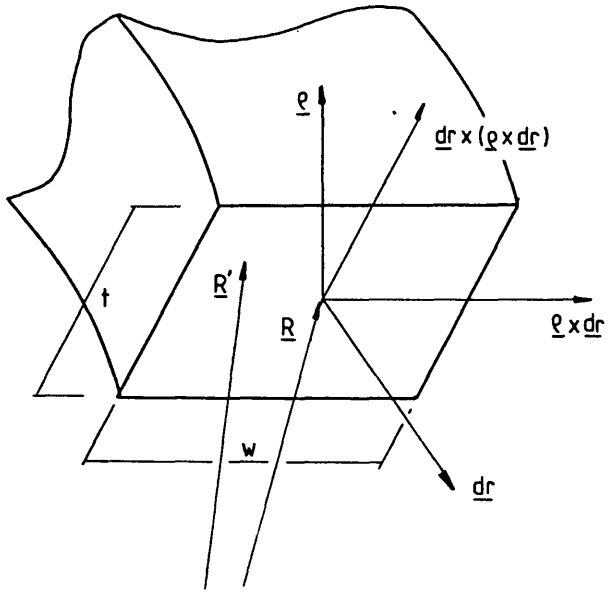

Fig.4.3 Vectors required for determining the field of a rectangular section wire

integrations are performed. In the case of a thick wire loop these directions are simply axially and radially. However, when there is a helical or spiral pitch this is no longer true. The direction required for the integral in width is given by the unit vector $\widehat{\underline{\rho} \times \underline{dR}}$ and in thickness by $\widehat{\underline{dR} \times (\underline{\rho} \times \underline{dR})}$. So the position vector $\underline{R}'$ of an incremental current element anywhere in the conductor volume will be given, after transformation of the second term, by

$$\underline{R}' = \underline{R} + a\widehat{\underline{\rho} \times \underline{dr}} + b\,(\widehat{\underline{\rho} - (\underline{\rho}.\underline{dr})\underline{dr}}) \qquad (4.3)$$

where $-w/2 \leqslant a \leqslant +w/2$ and $-t/2 \leqslant b \leqslant t/2$.

The vector $\underline{dr}$ remains unchanged since this will always remain perpendicular to the area of the conductor over which the integrations in width and thickness take place.

4.3 Methods of numerical integration.

Numerical integration [4.1] is performed by evaluating the integrand at a number of discrete points throughout the range of integration, and obtaining an estimate of the value of the integral, usually as the weighted sum of the integrand values. The points may or may not be equally spaced, and do not necessarily include the limits of integration.

Having obtained a value for the integral it is

desirable to know its accuracy. Repeating the process with more points and differencing the two results is a common method of producing an error estimate. Once the number of points required to produce a given accuracy is known then it is reasonable to expect a similar accuracy to be achieved when the same number of points are used for other similar integrals.

Alternatively, the integral may be evaluated using a few points. The number of points is then repeatedly increased obtaining error estimates at each stage until the required accuracy is reached. This approach forms the basis of automatic "iterative" techniques. Since the majority of the computational effort is usually assosciated with the integrand evaluations, it is important that the previous values are not thrown away in any subsequent estimates of the integral.

"Adaptive" methods are also available that concentrate the points at any awkward portions of the integrand. Since it is difficult to avoid losing previous integrand values with these methods, and as the functions that are being considered here are reasonably well behaved, adaptive methods will not be considered further.

In order to compare the efficiency of various rules the axial field of a filamentary loop was calculated at two points in the plane of the loop (fig 4.4) using the Biot-Savart method described in the previous section. Figs. 4.5 show the relative error achieved with a given

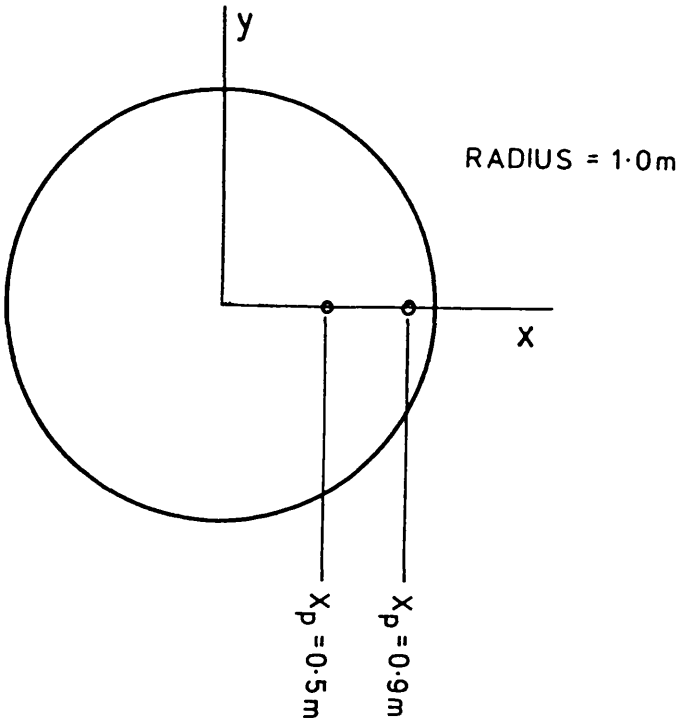

Fig.4.4 Positions used for determining the accuracy of various numerical integration methods

number of integrand evaluations for the two points, using various methods to be described below. There is a factor of two difference in horizontal scales of the graphs. It is more difficult to obtain an accurate answer as the field point approaches the wire. At the wire, some methods fail because of the singularity in the integrand. At the other extreme, only one value is required for any method on axis, as the incremental contributions from each part of the wire are equal.

The most well known integration methods are probably the first few Newton-Cotes formulae: the mid-point, trapezoidal and Simpson rules. They are easy to program

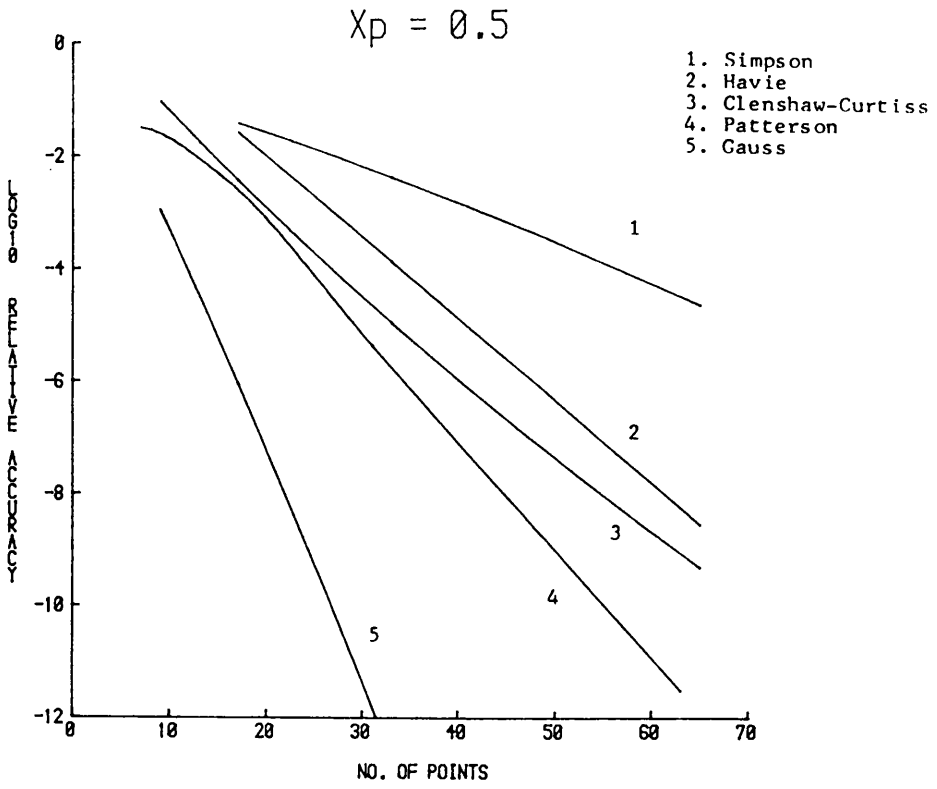

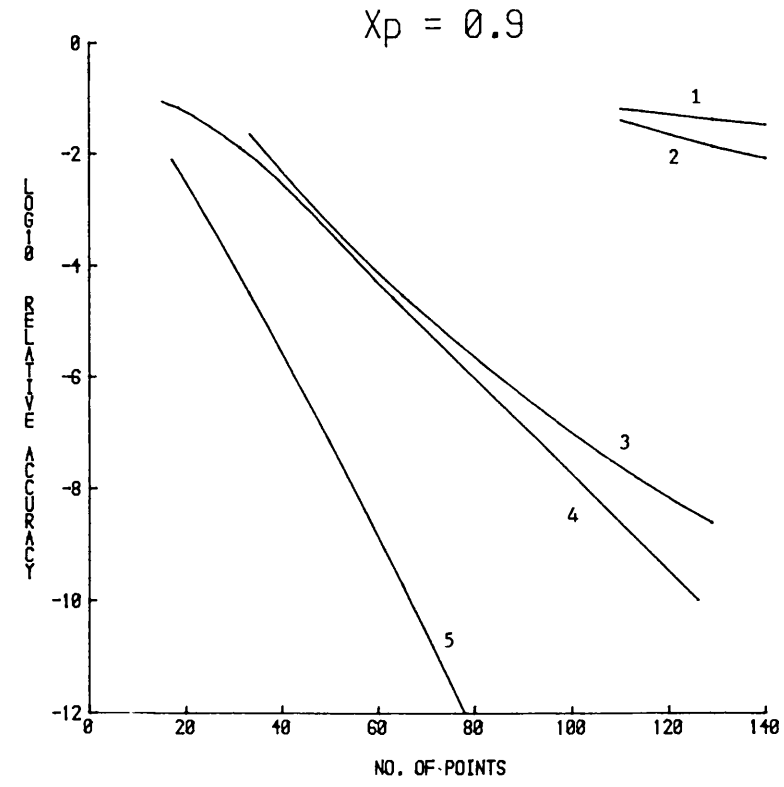

Fig.4.5 Accuracy of various integration methods versus number of points used

and since they use equally spaced points they may be used iteratively by successively doubling the number of intervals. Unfortunately they are also the least efficient.

From a knowledge of the asymptotic errors of these rules it is possible to take estimates of the integral with different numbers of points and obtain a closer estimate. This is the basis of Romberg integration, or "extrapolation to the limit". A variation of the Romberg method made by Havie [4.2] significantly reduces the number of integrand evaluations required, especially when higher accuracies are requested.

Further improvements can be made using a rule proposed by Clenshaw and Curtiss [4.3]. The integrand is expressed as a limited series of Chebychev polynomials whose coefficients may be determined from p values at non-equally spaced points that include the limits of integration. If the magnitudes of the high order coefficients are sufficiently small then it may be assumed that the integrand has been approximated well, and the integral may be evaluated from the coefficients. If this is not the case then 2p-1 points may be interlaced with the present points and a new, more accurate series calculated without any loss of previous values.

The most efficient method appears to be the Gauss rule. Integrand evaluations are made at non-equally

spaced points that do not include the limits, and the integral is given by a weighted sum of the values. Unfortunately, when the order of the rule is increased the previous set of values is lost, so it is of no use as an iterative rule. To achieve a known accuracy test runs must be made beforehand.

A p point Gauss rule is capable of integrating a polynomial of degree (2p-1) without error. Also, Gauss rules are capable of integrating some forms of singularity reasonably well, provided that they are at the end of the range of integration. The calculation of weights and points for these rules can be difficult for large numbers of points, and in these cases it is better to split the range into sections and use the fewer points per section.

Patterson [4.4] has developed a set of p point iterative rules that start with the 3 point Gauss rule and add (p+1) points at each stage. They are designed to integrate accurately the maximum order of polynomial possible, using all of the previously obtained values, and are capable of integrating polynomials up to order (3p-1)/2 without error. In common with the Gauss rules they do not use the limits of integration and will perform reasonably with singularities at the limits.

The most efficient rule to use for the discrete conductor calculations would appear to be that of Gauss. However, it does require the program user to specify in

advance the number of points required, and figure 4.5 has shown that this number is likely to increase considerably as the field point approaches the conductor. Also, there is a large variation in efficiency depending on the angular position of the field point (fig 4.6). This is line with what has already been said about the Gauss rules being able to cope more easily with awkward

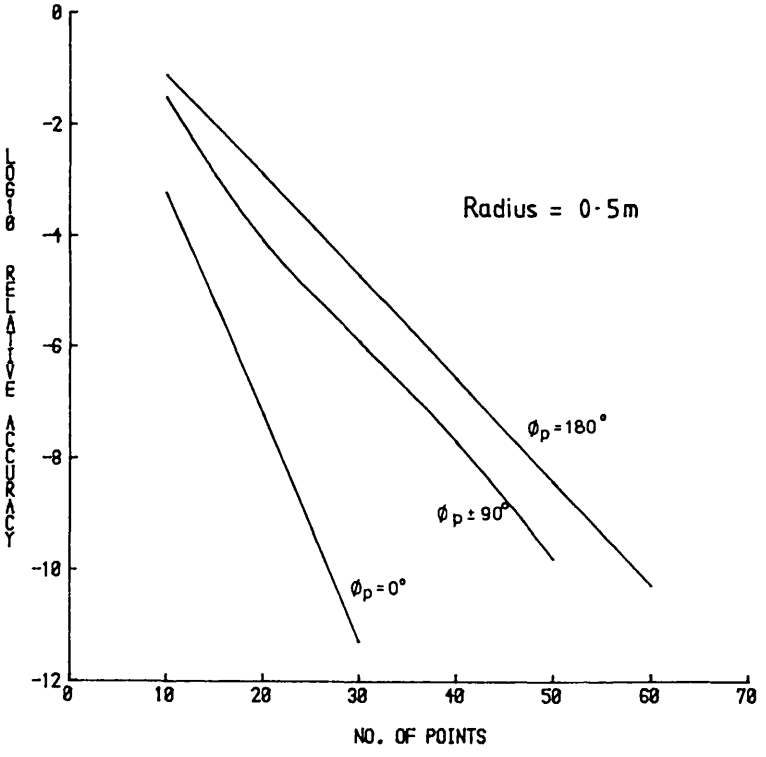

Fig.4.6 Variation of accuracy with angular position of field point

portions of the integrand at the end points of the range of integration. The least number of points are required when the field point is at ϕ=0 (+x axis), and the most points needed when at ϕ=180 degrees (-x axis). As a result of these variations, any figure chosen for the number of points per turn will inevitably be a worst case figure which will be used irrespective of how many points are actually required to achieve a given accuracy.

On the other hand the Patterson rule will automatically choose the appropriate number of integrand evaluations at each field point. It is therefore unlikely that the total amount of computation required for a complete problem at 1ppm accuracy will be as much as double that of using a Gauss rule, as was originally suggested by figure 4.5. However, it does have the advantage that no previous experience is required on the part of the user, and for this reason the method has been used for all the modelling descibed in this chapter.

In performing the integration, the range is first split into single turns and each turn, or part turn, is integrated by the Patterson method. Thus the number of points required for a given accuracy is decided on a per turn basis, rather than per conductor. This is necessary because the very high order rules that would be required for say, a long, multiturn, helical solenoid, are not available.

4.4 Obtaining Spherical Harmonics from field plots.

A magnetic scalar potential V, that satisfies Laplace's equation, is finite on axis, and not symmetric about the axis, is expressible in terms of spherical harmonics as

$$V = \sum_{n=0}^{\infty} \sum_{m=0}^{n} r^n \, P_{nm}(u) \, (a_{nm} \cos m\phi + b_{nm} \sin m\phi) \qquad (4.1)$$

where P_{nm} is an Associated Legendre Function of order n and degree m

$u = \cos\theta$

a_{nm} and b_{nm} are the harmonic amplitudes.

A table of the Legendre functions is shown in appendix 4.2. When m=0 they are the same as the Legendre polynomials of the same order. These functions may be calculated by the use of recurrence formulae, and a list of these is given in appendix 4.3.

Just as for the axisymmetric case, this series may also be used for H_z with an appropriate modification of the amplitudes. This is due to the fact that

$$\begin{aligned} &d/dz \, [r^n \, P_{nm}(u) \, (a_{nm} \cos m\phi + b_{nm} \sin m\phi)] \\ &= (m+n) \, r^{n-1} \, P_{n-1,m}(u) \, (a_{nm} \cos m\phi + b_{nm} \sin m\phi) \end{aligned} \qquad (4.2)$$

Again, it will be assumed that the series used is for H_z, as this is the quantity of interest.

It is worth looking closer at the harmonics in order to see the sort of field shape produced by the terms of this series. Expressing the lower order harmonics in terms of Cartesian coordinates produces the following table

Table 4.1 Spherical harmonics in terms of Cartesian Coordinates

n	m	cosine terms	sine terms
0	0	1	
1	0	z	
1	1	x	y
2	0	$z^2 - 1/2(x^2 + y^2)$	
2	1	3zx	3zy
2	2	$3(x^2 - y^2)$	6xy
3	0	$1/2z(2z^2 - 3(x^2+y^2))$	
3	1	$3/2x(4z^2 - (x^2+y^2))$	$3/2y(4z^2 - (x^2+y^2))$
3	2	$15z(x^2 - y^2)$	30z(xy)
3	3	$15(x^3 - 3xy^2)$	$15(3x^2y - y^3)$

When m=0 the Legendre functions are simply the Legendre polynomials, and the series is exactly the same as for the axisymmetric case (eq.3.3). These terms are

generally known as the zonal harmonics, whilst the terms where $m \neq 0$ are known as the tesseral harmonics. The field varies as the nth power of the distance along any of the coordinate axes.

For m=1 there is a one cycle sinusoidal variation per revolution in ϕ, so the harmonic has a component that varies as x or y. This is multiplied by an axisymmetric term that varies as the (n-1)th power with distance along each axis.

When m=2 the two cycle variation in ϕ gives rise to terms of the form (x^2-y^2) and xy which are multiplied by an axisymmetric expression involving terms to the power (n-2).

A general harmonic of order n and degree m will therefore have an m cycle variation in ϕ multiplied by an (n-m)th order polynomial expression that has symmetry about the z axis. If (n-m) is odd the harmonic has odd symmetry about the xy-plane, and even symmetry if (n-m) is even. The degree of a harmonic cannot be greater than its order, therefore $m \leqslant n$.

It is convenient to have a shorthand notation for these harmonics, and a useful way of refering to a given harmonic is by the leading term in its Cartesian expansion. The cosine term when n=3 and m=1 will therefore be called Z^2X, and so on. This form immediately indicates that the harmonic has a 1 cycle, cosinusoidal variation in ϕ, and has even symmetry in z. The cases

where this notation breaks down are for the (X^2-Y^2) terms, which will be refered to as X^2; and the (XY) terms, which will be called Y^2. It is emphasised that this is only a shorthand notation, and does not accurately describe each harmonic.

In order to express a given field profile in terms of these harmonics it is necessary to make use of the orthogonality properties of the so called "surface harmonics": $P_{nm}(u) \cos m\phi$, and $P_{nm}(u) \sin m\phi$.

Now,

$$\int_{-1}^{1}\int_{0}^{2\pi} P_{nm}(u) \cos m\phi \; P_{jk}(u) \cos k\phi \; d\phi \; du$$

and

$$\int_{-1}^{1}\int_{0}^{2\pi} P_{nm}(u) \sin m\phi \; P_{jk}(u) \sin k\phi \; d\phi \; du$$

$$= \begin{cases} \dfrac{2}{(2n+1)} \dfrac{(n+m)!}{(n-m)!} & \text{for } m=i \text{ and } m=j \\ 0 & \text{otherwise} \end{cases}$$

$$\int_{-1}^{1}\int_{0}^{2\pi} P_{nm}(u) \cos m\phi \; P_{jk}(u) \sin m\phi \; d\phi \; du$$

$$= \quad 0 \text{ always.} \qquad \text{(Smythe [3.1])} \quad (4.3)$$

Thus if the field distribution over the surface of a sphere of radius r_o is known and denoted by $H_z(u,\phi)$, from equations 4.2 and 4.3, the harmonic amplitudes will be given by

$$a_{nm} = \frac{(2n+1)(n-m)!}{2r_o^{\,n}\,(n+m)!} \int_0^{2\pi}\int_{-1}^{1} H_z(u,\phi)\, P_{nm}(u) \cos m\phi \, du \, d\phi$$

$$b_{nm} = \frac{(2n+1)(n-m)!}{2r_o^{\,n}\,(n+m)!} \int_0^{2\pi}\int_{-1}^{1} H_z(u,\phi)\, P_{nm}(u) \sin m\phi \, du \, d\phi \qquad (4.4)$$

Having found these amplitudes the field interior to the sphere will be given by equation 4.1. For present purposes a more useful set of numbers to use is

$$c_{nm} = a_{nm}\, W_{nm}\, r_o^{\,n}\, 10^6 \,/\, a_{oo} \qquad (4.5)$$
$$d_{nm} = b_{nm}\, W_{nm}\, r_o^{\,n}\, 10^6 \,/\, a_{oo}$$

The c_{nm} and d_{nm} represent the peak to peak contribution to the field profile of the nth order, mth degree harmonic over a sphere of radius r_o. The values are in parts per million relative to the field strength at the origin. W_{nm} is a weight that accounts for the fact that the Legendre functions can be very much greater than ± 1. The effect on the field can therefore be much larger than the amplitudes alone would suggest. A table of weights for the various harmonics is given in appendix 4.4. They are simply the peak-peak range of $P_{nm}(u)$ for $-1 \leqslant u \leqslant +1$. It can be seen that the weights get rapidly larger for

increasing m.

So, in principle, the weighted harmonic components of a magnètic field may be obtained from values obtained over the surface of a sphere. It is now necessary to determine where on a sphere these calculations should be made so that the maximum number of components may be extracted from a given number of data points.

In general, the field profile $H_z(u,\emptyset)$ will be the sum of an infinite series of spherical harmonics. The integral with respect to u in eq. 4.3 will therefore be of the form

$$\int_{-1}^{1} P_{nm}\, P_{jk}\, du \qquad (4.6)$$

where the required amplitude is for the term of order j and degree k. Ideally all the terms will vanish where $n \neq j$ and $m \neq k$ as the Legendre functions are orthogonal. Now, because of the properties of the Legendre functions, (appendix 4.2) the integrand will be a polynomial of degree 2n.

The most efficient way of integrating a polynomial from values at a number of points is by using Gaussian quadrature (sect. 4.3). A p point Gauss rule will accurately integrate a polynomial of degree (2p-1), and so a (p+1) point rule is needed to resolve accurately harmonics up to and including the pth order. The integration is then performed by taking a weighted sum of

the field values , obtained at the (p+1) points given by u equal to the Gauss points.

The form of the integral in ϕ in eq. 4.3 is that of the Fourier integral. Integration is therefore best performed by taking field values at q equally spaced values of ϕ between 0 and 2π, and then performing a discrete Fourier transform. According to the Sampling Theorem terms of degree up to m=q/2 can be resolved. However, since the sample points will lie at the zeroes of sin $q\phi/2$, this term cannot be resolved. The limit of resolution will therefore be taken as those terms of degree m=(q/2-1).

The spherical harmonics are therefore resolved using field values obtained from a set of p rings of points at a constant spherical radius. The positions of the rings are calculable from the Gauss points, and each ring has q equally spaced points on it.

Substitution into

$$c_{nm} = \frac{(2n+1)(n-m)!\ k\ W_{nm}}{2x10^{-6}(n+m)!\ q\ H_{zo}} \sum_{j=1}^{p} w_j\ P_{nm}(u_j) \sum_{k=1}^{q} H_z(u_j,\phi_k)\cos(m\phi_k)$$

$$d_{nm} = \frac{(2n+1)(n-m)!\ k\ W_{nm}}{2x10^{-6}(n+m)!\ q\ H_{zo}} \sum_{j=1}^{p} w_j\ P_{nm}(u_j) \sum_{k=1}^{q} H_z(u_j,\phi_k)\sin(m\phi_k)$$

where $k=1$ for $m=0$

$k=2$ otherwise

w_j = Gauss weight

u_j = Gauss point

$H_{zo} = H_z$ at the origin

W_{nm} = pk-pk range of $P_{nm}(u)$ for $-1 \leqslant u \leqslant +1$

(4.5)

yields the required weighted amplitudes in terms of peak to peak variation in parts per million over the sphere of measurement.

With any sampled data system it is possible for errors due to aliasing to occur, and this case is no exception. If terms of degree $(q/2 + k)$ are present in the field data then not only is it impossible to accurately resolve them, but they will cause terms of degree $(q/2 - k)$ to be in error. However, not all the $(q/2 - k)$ are affected, only those with the same symmetry in z as the $(q/2 + k)$ term.

A similar form of aliasing occurs when terms of order greater than p are present in the data from a (p+1) ring plot. A (p+k) order harmonic will influence not only the (p-k) order terms, but those of order between (p-k) and p. This happens provided they have the same symmetry in z, and the same degree. The one exception is the term of order (p+1) and degree zero. Since the Gauss points are at the zeros of $P_{p+1,0}$, it is not possible for this component to cause any aliasing errors, nor is it possible to resolve this term.

In order to decide how many rings of points are needed, a 1m diameter loop at z=0 was modelled, and plots taken at 0.25m radius. Eighteen rings were required to obtain an accuracy of 1ppm in all terms up to and including Z^8. For a 1 metre long solenoid of the same diameter, only 10 rings were required to yield the same accuracy. Fewer rings are required in the case of the solenoid because the magnitudes of the higher order terms are significantly less than for the loop. Thus little aliasing can occur.

Loops, solenoids and thick section coils have been modelled using this plotting technique. Provided that an appropriate number of rings is used, agreement to better than 1ppm can be achieved with the results from the axisymmetric program described in chapter 3.

4.5 Helically wound solenoids.

A variety of helical solenoids have been modelled using the techniques of the the previous sections, and harmonic amplitudes obtained from a 12 plane by 12 point per plane spherical plot of 0.25 metres radius. All have integral numbers of turns placed so that the start and finish are equidistant from the x-y plane. Table 4.2 shows the harmonics generated by a filamentary helix of pitch 2cms, diameter 1 metre, and having 41 turns. Whilst this may appear to be a rather coarse pitch, it may not be untypical of what might be used in a resistive magnet if a current of a few hundred amps is chosen.

The table shows that because of various symmetries in the winding the odd zonal harmonics are zero, as are the terms in X with odd Z symmetry, and the terms in Y with even Z symmetry. It is also clear that the amplitudes diminish as the order of the harmonic increases. The amplitudes also decrease as the length of the solenoid is increased, as demonstrated by the X and ZY terms in figure 4.7. This is of course to be expected, because if the length were extended to infinity then only the Z^0 term would remain. Figure 4.7 also demonstrates the general result that the terms involving Y are proportional to the pitch, and the terms in X to the square of the pitch. Thus, in principle, it is possible to reduce the tesseral harmonics to an acceptable level

Table 4.2 Harmonics generated at 0.25m radius by a helically wound solenoid with 41 turns of pitch 2cms.

Z1	0.0 ppm
Z2	-201114.0
Z3	0.0
Z4	2214.0
Z5	0.0
Z6	2135.4
Z7	0.0
Z8	131.6
Z9	0.0
Z10	29.8

Z0X1	86.5	Z0Y1	0.0
Z1X1	0.0	Z1Y1	-3396.0
Z2X1	15.5	Z2Y1	0.0
Z3X1	0.0	Z3Y1	-311.8
Z4X1	8.4	Z4Y1	0.0
Z5X1	0.0	Z5Y1	111.4

Z0X2	-8.9	Z0Y2	0.0
Z1X2	0.0	Z1Y2	-536.6
Z2X2	-2.9	Z2Y2	0.0
Z3X2	0.0	Z3Y2	98.6
Z4X2	0.6	Z4Y2	0.0
Z5X2	0.0	Z5Y2	13.7

Z0X3	-1.5	Z0Y3	0.0
Z1X3	0.0	Z1Y3	-114.7
Z2X3	-0.7	Z2Y3	0.0
Z3X3	0.0	Z3Y3	-30.5
Z4X3	0.1	Z4Y3	0.0
Z5X3	0.0	Z5Y3	1.5

Z0X4	0.3	Z0Y4	0.0
Z1X4	0.0	Z1Y4	-27.5
Z2X4	0.2	Z2Y4	0.0
Z3X4	0.0	Z3Y4	-9.4
Z4X4	0.0	Z4Y4	0.0
Z5X4	0.0	Z5Y4	-0.2

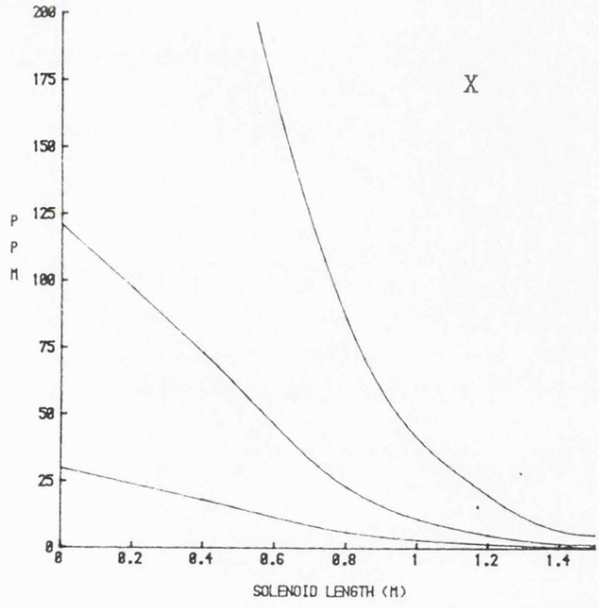

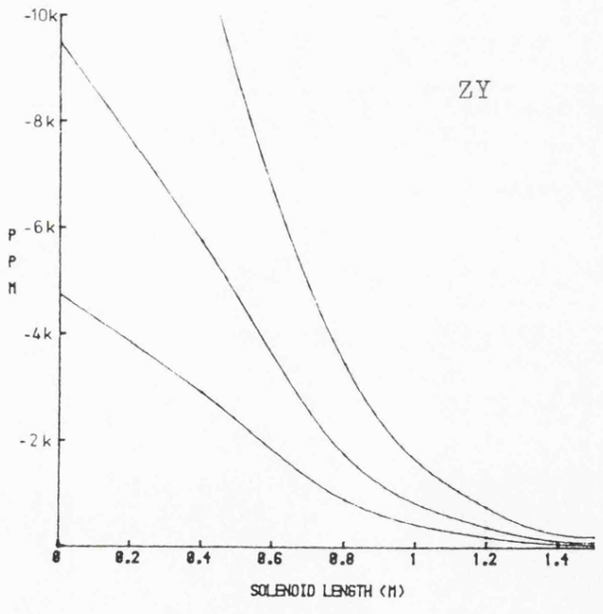

Fig.4.7 Variation of X and ZY terms with solenoid length

by reducing the winding pitch. However, this is likely to result in an impractically small size of wire.

A more fruitful approach is to consider the effect of a second filamentary, helical winding on top of the first. The helix angles of the two layers are of opposite senses, since the second layer is wound in the opposite axial direction to the first. This effect leads to a reduction in the tesseral harmonics. The result of placing another 41 turn solenoid of diameter 1.02 metres over the one previously described is shown in table 4.3. The X terms remain virtually unchanged, and the Y terms are reduced to levels comparable with the X terms. In order to obtain the best possible cancellation of helical effects, albeit physically non-realisable, the outer coil was placed coincident with the inner one. This resulted in the complete cancellation of the Y terms, leaving the others with same magnitude as for a single helix.

Further cancellation occurs when end coils are added to form a complete magnet (fig.4.8). The end coil dimensions are derived from the axisymmetric design program, and the harmonics for the complete magnet are shown in table 4.4. It can be seen that most of the tesseral terms have been reduced to a negligible level, and the remainder can probably be removed by shimming.

It would be very convenient if a helical solenoid had an equivalent axisymmetric current sheet that generated exactly the same zonal harmonics. If this were

Table 4.3 Harmonics generated at 0.25m radius by two helically wound solenoids, spaced by 2cms, with 41 turns of pitch 2cms each

Z2	-199375.9ppm		
Z4	2555.7		
Z6	2714.0		
Z8	-1449.3		
Z10	1956.8		
Z0X1	-86.0	Z1Y1	-57.3
Z2X1	-13.5	Z3Y1	-44.6
Z4X1	8.8	Z5Y1	6.5
Z6X1	0.1	Z7Y1	1.7
Z0X2	-8.8	Z1Y2	-8.0
Z2X2	-2.7	Z3Y2	-10.2
Z4X2	0.6	Z5Y2	0.3
Z0X3	-1.5	Z1Y3	-1.6
Z2X3	-0.6	Z3Y3	-2.8
Z0X4	-0.3	Z1Y4	-0.4

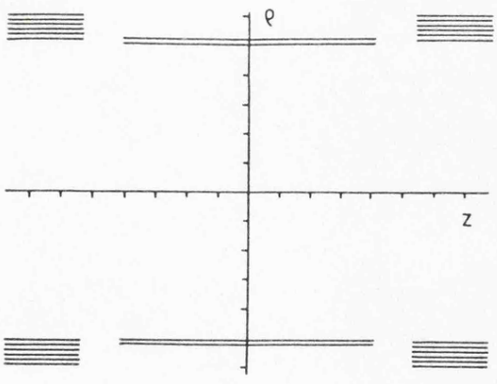

Fig.4.8 Three coil magnet used for helical models

Table 4.4 Harmonics generated at 0.25m by the helically wound magnet of fig.4.8

Z8	-97.5 ppm		
Z0X1	6.8	Z1Y1	-3.5
Z2X1	3.1	Z3Y1	0.1
Z3X1	1.9	Z5Y1	4.2
Z0X2	-0.2	Z1Y2	-4.3
Z2X2	0.1	Z3Y2	-1.8
Z0X3	-0.3	Z1Y3	-1.3

the case then the winding dimensions could be substituted directly into the optimising program of chapter 3, and vice versa. This would allow the coil dimensions and positions to be determined with little regard for their actual construction. In the case of a filamentary helix a current sheet with the same length as the overall length of the helix gives the required result.

Unfortunately, a similar simple result does not apply to a helix whose conductor has finite width (ie. as if wound from tape). In this case the length of the equivalent current sheet is approximately the distance between the centres of the beginning and the end of the wire. However, a current sheet of this length will not generate the harmonics correctly, nor will any sheet of a given length. Figure 4.9 shows the corrections to this length that must be made in order to generate the Z^2, Z^4, and Z^6 terms accurately for a helix with 2 cms pitch, and 2 cms conductor width. This shows that although it is possible to choose an appropriate equivalent sheet so as to correctly generate say Z^6, adequate shimming capability must be provided to cancel the additional Z^2 and Z^4 components that will inevitably be present. Having said this, it is worth pointing out that the corrections indicated in fig. 4.9 may be comparable to any errors in the mechanical construction due to tolerances. In these cases the required shimming is likely to be present already in any final design.

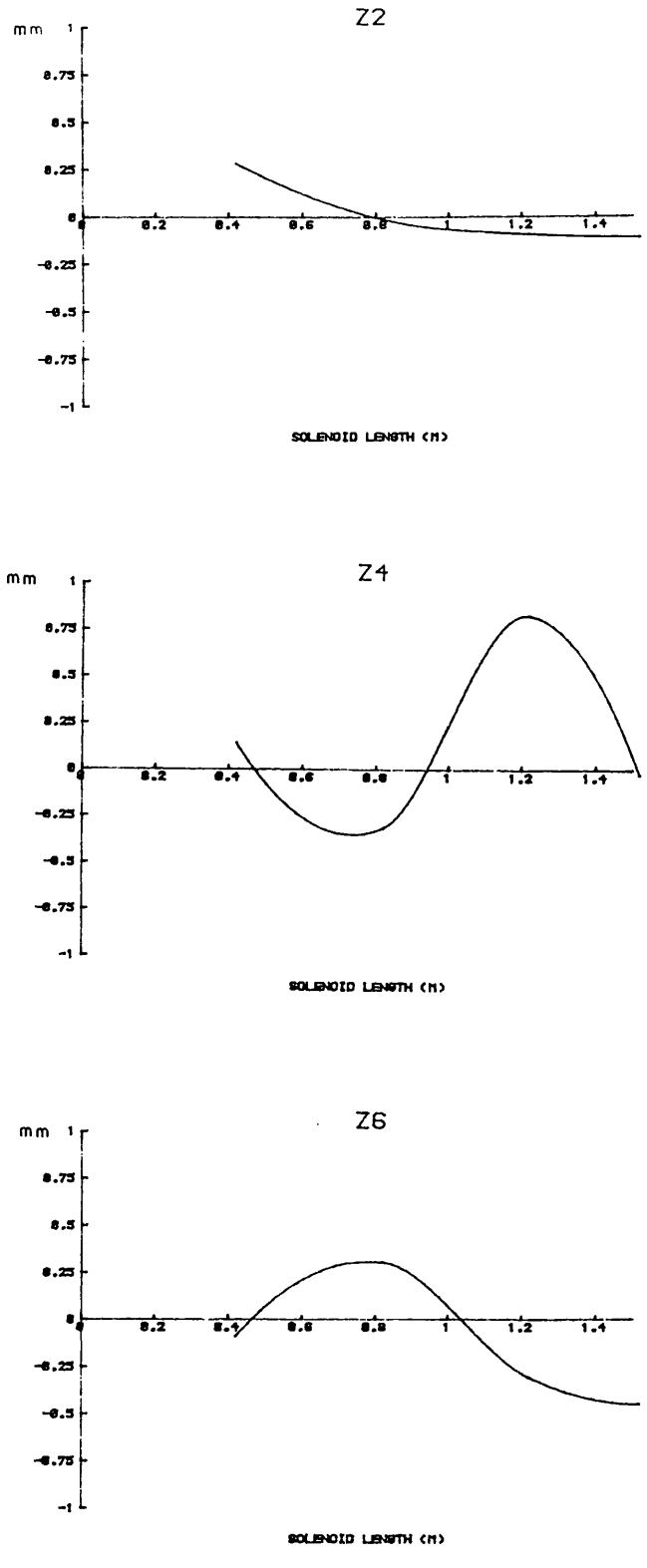

Fig.4.9 Corrections to equivalent current sheet needed to generate the same zonal harmonics as a wide helix

The case where the pitch and the conductor width are both 2 cms is an unreal situation since this does not allow any room for insulation. Reducing the conductor width to zero causes the corrections in equivalent sheet length to be reduced to zero, at a rate that is proportional to the square of the conductor width. It is noticeable that the tesseral harmonics do not vary by more than 1ppm as the width is varied. Only the zonal terms change significantly.

Modelling the complete magnet of fig. 4.8 with a 2cms wide conductor produces a set of harmonics that differ from the filamentary values only because Z^6=-1ppm. The effect of the wide conductor in the main coil has therefore been balanced out by its effect in the end coils. So, in this case, the discrepancy between the wide conductor and filamentary models may be ignored.

The addition of finite thickness to a helix would not be expected to produce an equivalent thick current sheet of a length different to that given above. This is because each helix of negligible thickness that makes up the thick helix will have an equivalent thin sheet. Each of these sheets will have the same length, as given above, and simply adding together an infinite number of them will not alter their length. Several thick, helical solenoids of different lengths have been modelled, and this expectation has been born out in practice.

It appears, from the modelling described in this

section, that there is little difficulty in taking the dimensions of a design from the axisymmetric program, and using them to generate the appropriate dimensions for a helical winding. A filamentary model is probably sufficient to indicate the amplitudes of the tesseral harmonics that will be generated, and this has the benefit of being relatively cheap in computer time. However, in order to check that the zonal harmonics generated are comparable to the axisymmetric model, then wide, if not thick, conductor models should also be used.

4.6 The effects of ovality.

Ovality may appear in a real winding simply because of mechanical tolerances on the formers that support the winding, or due to the weight of the windings themselves upon the former. A heavy winding tends to squash the former from top to bottom, which then tends to bulge outwards from side to side. It is important to know the effects that this ovality will have on the field homogeneity so that a requirement for the strength and tolerance of the former can be specified. A former that allows the winding to become too oval may produce a field disturbance that is difficult to correct. On the other hand a former that is too thick, and provides excessive stiffness, will be heavy and costly to produce.

The solenoidal magnet design used in the previous

section was used to assess the effects of ovality. Instead of having helical windings, the layers consist of thin current sheets. Introducing a diameter difference of +1mm (i.e. x diameter - y diameter = 1mm) into the two layers of the centre coil produces the following significant changes (in ppm) to the harmonics generated:

$$Z^0X^2 \quad -63$$
$$Z^2X^2 \quad -4$$
$$Z^4X^2 \quad +2$$

Other terms were produced, but their magnitudes were less than 1ppm.

Because the radius of the oval coils has a two cycle variation in ϕ, the field pattern also has two cycle symmetry, hence the production of terms of the form Z^pX^2. Terms like Z^pY^2 are not produced. These would arise from an oval coil rotated in ϕ by 45 degrees. Some negligible components like Z^pX^4 are also produced, which indicate that the field variation is not quite sinusoidal. Since the ovality is symmetrical in z the Z^pX^2 terms are only non-zero when p is even.

The negative sign of the Z^0X^2 term is predictable because, by the definition of diameter difference, the windings on the x axis are further away from the origin than those on the y axis. The field is therefore lower along x than it is along y. Hence the "x^2-y^2" term is negative. The small amplitudes of Z^2X^2 and Z^4X^2 indicate that the effects of the ovality change only slightly with

z. The magnitude of all the $z^p x^2$ terms are directly proportional to the diameter difference of the coils.

Using the same magnet model, but this time with all layers of the +z end coil having a diameter difference of 1mm, the following significant changes were noted (in ppm):

$$z^0x^2 \quad +33$$
$$z^1x^2 \quad +13$$
$$z^2x^2 \quad +3$$

Both odd and even terms in z are now produced because there is no symmetry in z. The magnitudes are also smaller than for the previous case because the ovality occurs further away from the central region.

4.7 Spirally wound coils

The magnets that are most suited to being constructed from spiral windings are the 4 coil designs. As suggested in chapter 3, wide, anodised aluminium tape may be used to achieve a compact winding with good packing factor. The spherical type has been used for modelling spirals, and its geometry is shown in fig. 4.10. Each coil is 0.2m wide, and 2 cms thick. The rather thin coils have been used to lower the computational cost. Spherical plots with 18 rings of 12 points per ring were taken at 0.2m radius.

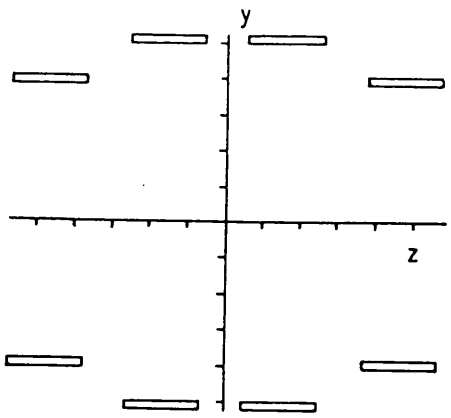

Fig.4.10 Four coil magnet used for spiral models

Table 4.5 Harmonics generated at 0.2m by the spirally wound magnet of fig.4.10

Z8	-506.0ppm		
Z10	108.1		
Z0Y1	292.0		
Z2Y1	4.9		
Z0Y2	117.3	Z0Y4	18.1
Z2Y2	1.5	Z2Y4	0.7
Z0Y3	46.9	Z0Y5	6.2
Z2Y3	1.2	Z2Y5	0.4

The first model uses 20 turns of thin conductor, and a radial pitch of 1mm. Beginning and end turn positions coincide with the inner and outer radii given by the axisymmetric program. The harmonics generated are given in table 4.5, and this shows that the first zonal error term is Z^8. Thus taking the dimensions straight from the axisymmetric program presents no difficulties.

However, there are large quantities of tesseral terms that extend up to high degree. These can be difficult to remove by shimming, although the fact that there is little variation in z does make them easier to remove. The use of 1mm thick conductor makes no difference to the harmonics generated.

Changing the winding to 10 turns of 2mm pitch leaves the zonal terms unchanged, but doubles the tesseral terms. Thus these errors appear to be proportional to the winding pitch. Once again the use of thick conductors does not change the harmonics.

The use of spirally wound conductors in this sort of magnet has significantly worsened the homogeneity of what is already a low performance design. However, the following sections show that the Y term may be removed by coil movements, and so the inclusion of a Y^2 shim coil, together with a reduction in conductor thickness (and hence pitch) may make the design more attractive.

4.8 The design of shim coils.

In the same way that shim coils for the zonal harmonics were generated by adjusting the axial (or radial) positions of current carrying loops, any harmonic may be generated by adjusting the axial or radial position of a current carrying "building block". These building blocks consist of an array of conductors that generate, nominally, harmonics of only one degree. The simplest case, that of a loop, generates harmonics only of degree 0 (i.e. m=0), and the design process for this case is covered in chapter 3.

Golay [4.5] has made use of the fact that there are distibutions of current over the surface of a sphere that will generate a given spherical harmonic throughout that sphere (Smythe [3.1]). In order to obtain a useful shim coil design, he projected these currents onto the surface of a cylinder (for use with solenoidal magnets), or onto two planes perpendicular to the z axis (for magnets with radial access). Errors that were introduced by doing this were removed by algebraic manipulation. The resulting calculations were made more difficult by the compromises that have to be made when individual coils and their interconnections obstruct each other. Also, the calculations were restricted to filamentary conductors, thick sections never being considered.

The whole process of shim coil design may be made much easier by using the tools that have been described

in this chapter. It is possible to calculate fields from virtually any coil, straight conductors and arc segments being the easiest to consider. The inclusion of thick coils is quite straightforward. The magnitudes of harmonics may be obtained from these calculations, and the coil geometry may be altered until the unwanted components are cancelled. Automatic optimisation of the coil geometry is easily accomplished, although it has not yet been included in the program. Nevertheless, the design principles involved may be demonstrated by means of examples.

A building block for an mth degree harmonic has 2m current arcs, except m=0 when there is one, a complete loop (fig.4.11). The arcs are symmetrically placed around the circumference of a circle, and the currents alternate in sign. Because of asymmetry about the centre, the m=1 block cannot generate components where m is even. By choosing the angle of the arcs to be 120 degrees, the block cannot generate any m=3 terms. The first terms that create impurities in the harmonic are therefore of degree 5. Likewise, the block for m=2 has 90 degree segments, and so does not produce terms with m=4; and the block for m=3, with 60 degree arcs, cannot produce m=6 components.

In the case of shims that fit a solenoidal magnet, all that is required is to determine the axial positions of building blocks so as to only generate the harmonic of

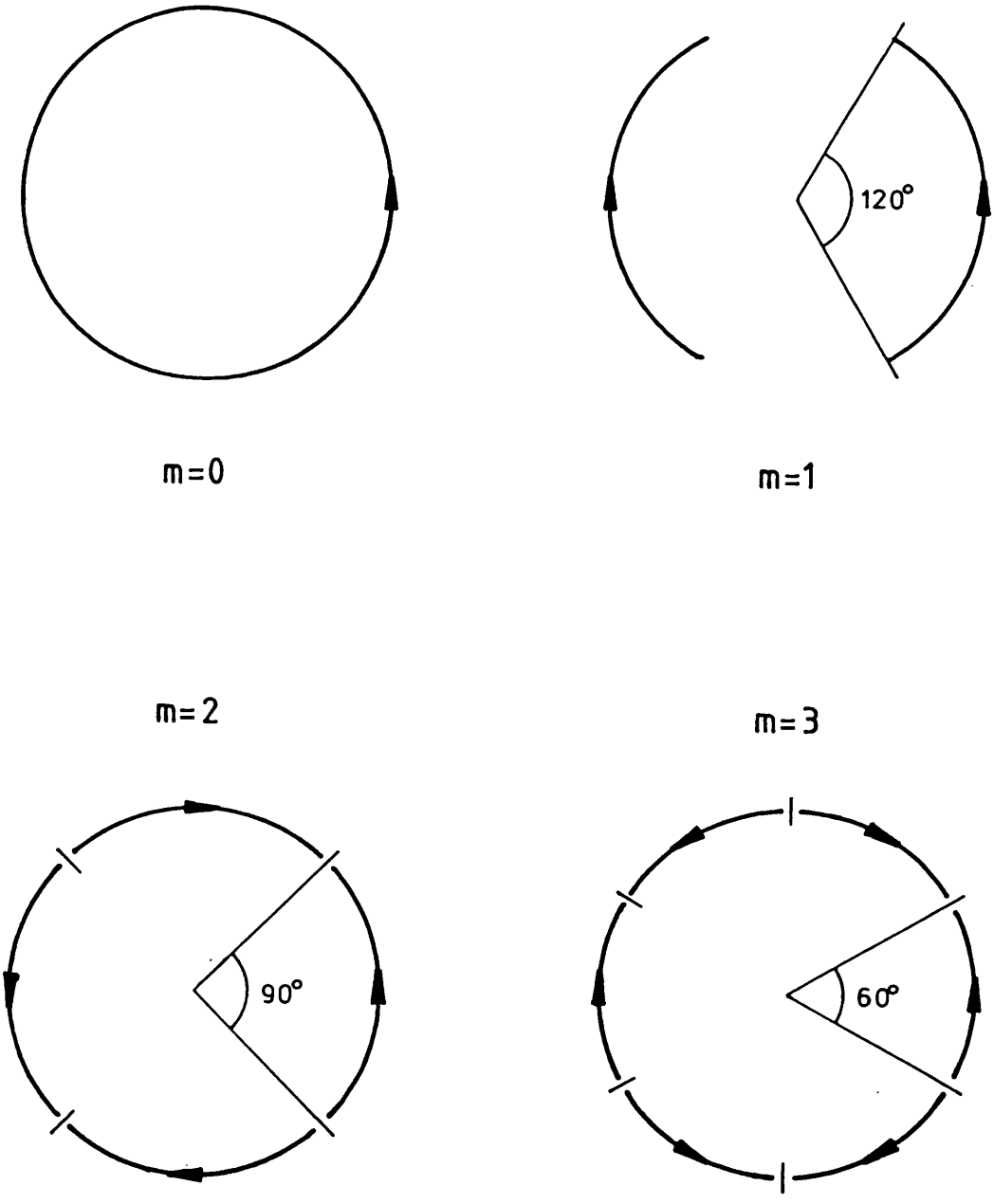

Fig.4.11 Building blocks for shim coils

required order. Once again, diagrams may be produced (eg. fig.4.12) that indicate the signs of the harmonics when the angular position of the building block is varied.

The design of an X shim (m=1,n=1) may now be considered. Two blocks of 120 degree arcs, spaced symmetrically about the origin, will produce gradients of the form Z^pX, where p is even. The odd terms in Z do not appear because of symmetry. Choosing a half angle of 68 degrees ensures that no Z^2X term is generated (fig.4.13.1) Thus the first impurities in the shim would be Z^4X and X^5.

However, these coils cannot be connected in a complete circuit as they stand without affecting their performance. In order to do this two further building blocks must be added (fig.4.13.2). The ends may now be connected with straight wire segments running parallel to the B_o field. Because of their direction, these segments will not produce any z component of field. Therefore, for small currents, they will have negligible effect on B_o.

Since the senses of the currents in the two sets of building blocks are opposed, then to cancel Z^2X the blocks must be in regions that have the same sign for Z^2X. Thus they must either both be between 20 and 68 degrees; or one must be between 0 and 20 degrees, whilst the other is between 68 and 90 degrees. The latter option is not feasible because the overall length of the shim would be in excess of 2.75 metres. Looking at the values

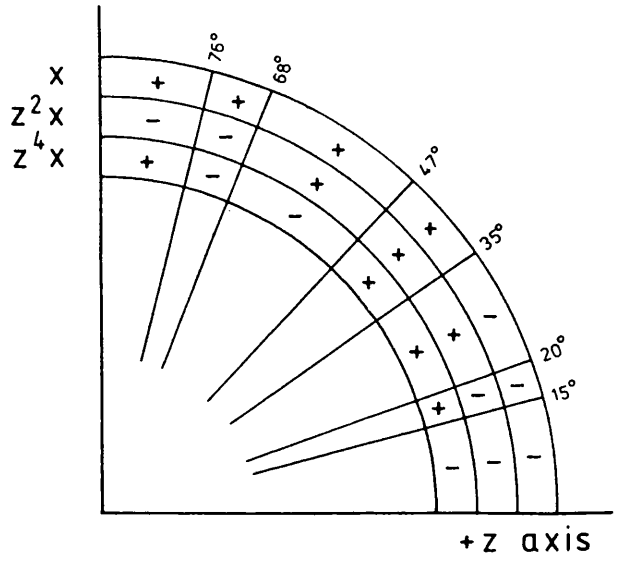

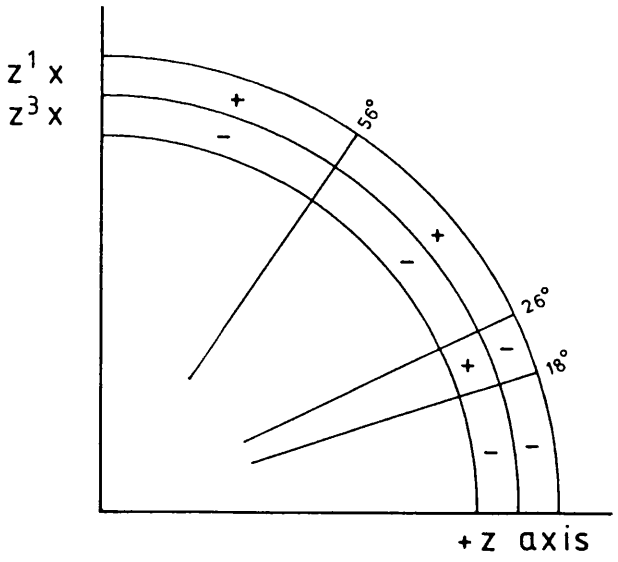

Fig.4.12 Variation of X terms with angular position of building block

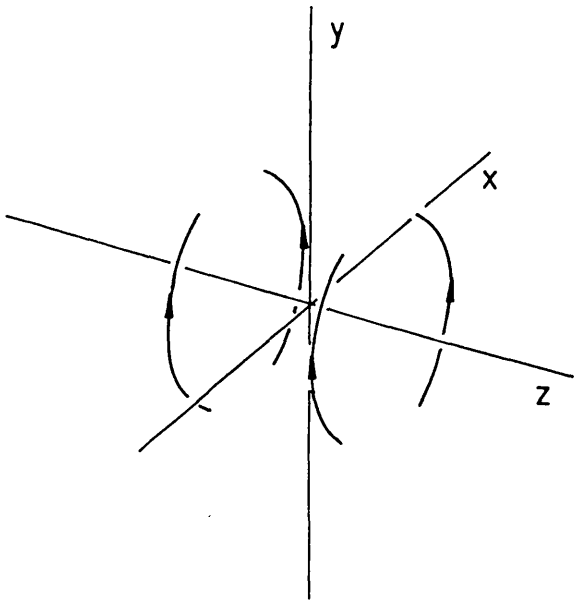

Fig.4.13.1

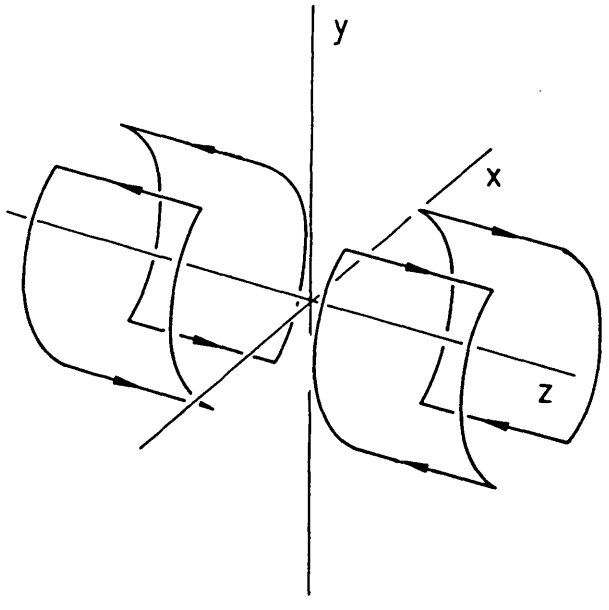

Fig.4.13.2

Fig.4.13 Design of X gradient coils from building blocks

of Z^2X throughout the first region indicates that the blocks must lie on either side of 55 degrees to be in a position to achieve cancellation. A variety of designs may therefore be obtained, with varying sensitivities and power dissipations. One possibility is that one of the sets of arcs should lie at 61.2 degrees, and the other at 49.6 degrees. The arrangement gives a weighted sensitivity of 7.6ppm of X gradient/ampturn at 0.25m radius, and in a 0.1 Tesla field.

Shim coils that generate other gradients may be designed in exactly the same manner. Some possibilities are shown in fig.4.14.

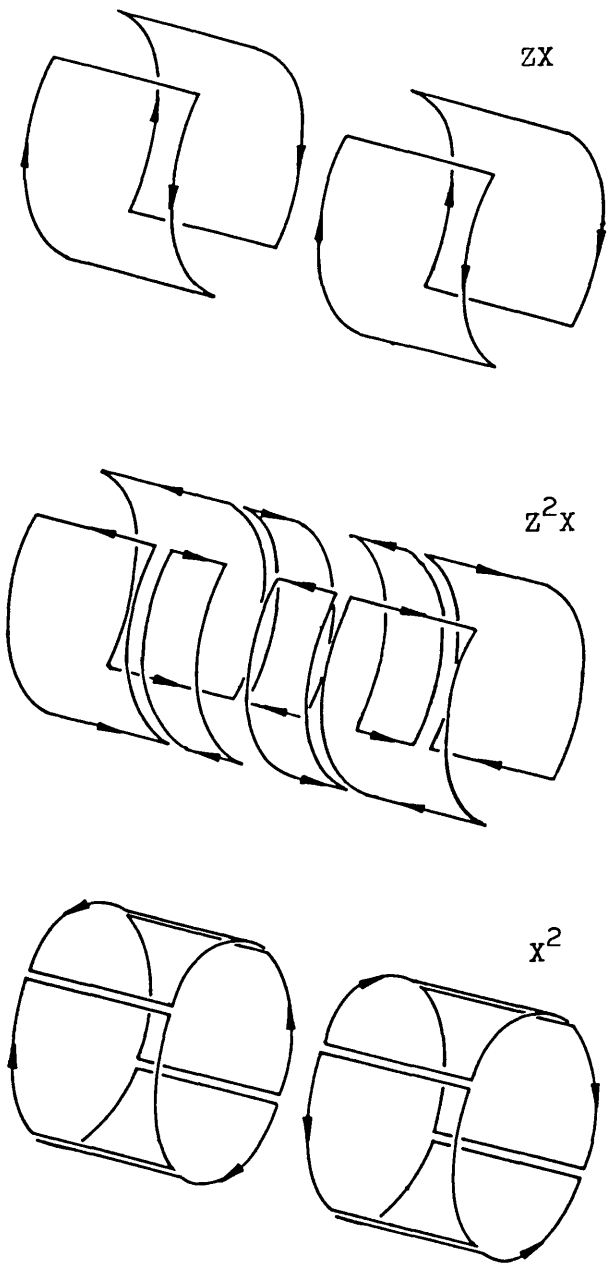

Fig.4.14 Shim coils built from building blocks

4.9 Shimming using the magnet coils

The main magnet coils may be used for shimming in one of two ways. Firstly, current may be shunted from individual coils, or tappings on the coils; and secondly by movement of the coils. In order to study these effects a program has been written that takes the magnet data from the axisymmetric program, and allows the coils to be moved off axis, or twisted about an axis. The effects of changing the currents in the coils may also be modelled.

All the field calculations are performed using the elliptic integral method (section 3.6) in conjunction with coordinate transformations of the field point and the calculated field components [4.6] that simulate the coil movements. The spherical plotting method of section 4.4 is used to obtain harmonic amplitudes from the field values.

In general, the movement or shunting of current from a coil will alter the amplitudes of many components. The higher the order of the harmonic, the less its amplitude will be affected. Thus it is only practical to alter the low orders by this method. Adjusting more than one coil at a time, with some symmetry in the adjustments, allows virtually only one harmonic to be altered. It is unlikely that all the unwanted harmonics will be completely removed, partly because of the inability to tackle some terms, and partly because of the difficulty in making minute adjustments to heavy coils accurately. As a result

the final stages of shimming will probably be made using shim coils. However, by making crude adjustments with the main coils, the range of adjustment provided by the electrical shims may be substantially reduced. As a result, the cooling of the coils will present fewer problems, and the power supplies needed to drive the coils will be smaller and less costly.

Figure 4.15 shows the adjustments required to alter some of the harmonics in the solenoidal magnet used for the helix models. Arrows indicate the direction of the coil movements, and the resistors indicate the shunting of current from a coil. Only the low order terms of degree m=0 or m=1 can be altered. Some higher degree terms are produced by some of the non-axisymmetric movements, but these are insignificant compared with the m=1 terms. Although the diagrams only show harmonics involving Y, the X terms may obviously be produced by making the same movements with respect to the x axis. A similar set of diagrams (fig. 4.16) may be produced for the four coil spherical design used in the spiral winding models. Again, only terms with m=0 or 1 can be influenced.

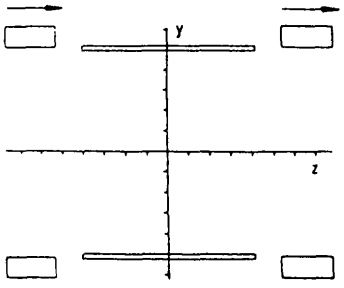

Z^1

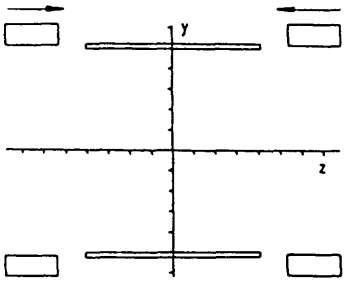

Z^2 and Z^4

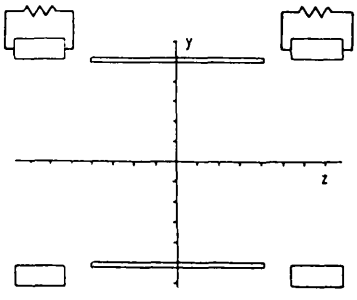

Z^2

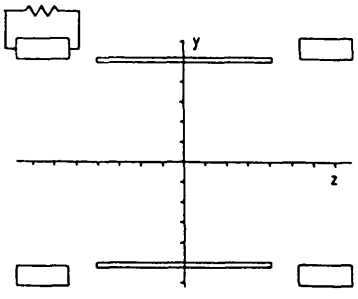

Z^1, Z^2 and Z^3

Fig.4.15 Shimming of three coil magnet using main coils

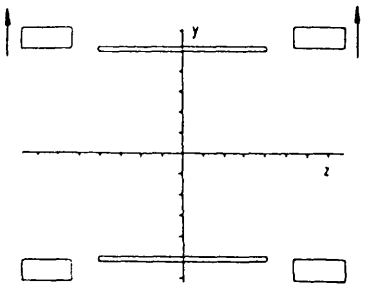

Y

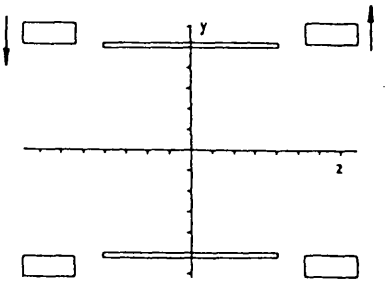

ZY

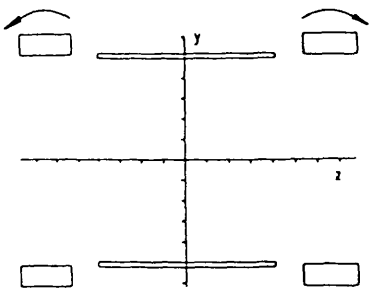

Z^2Y

Fig.4.15 (contd.)

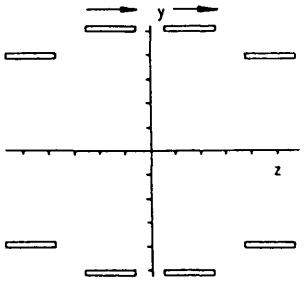

Z^1

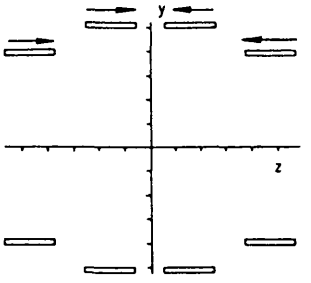

Z^2

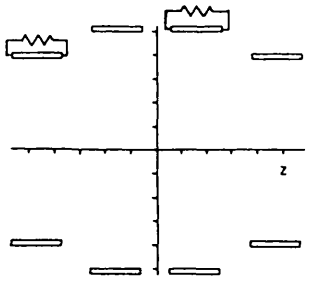

Z^3 and Z^1

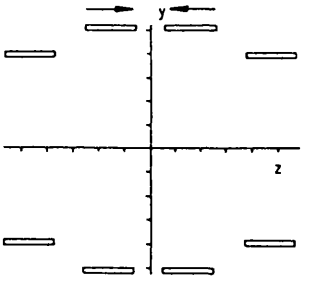

Z^4 and Z^2

Fig.4.16 Shimming of four coil magnet using main coils

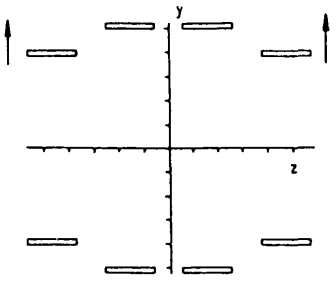

Y

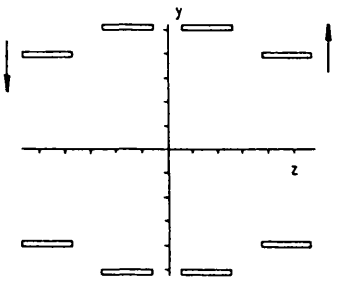

ZY

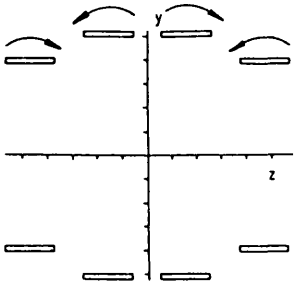

Z^2Y

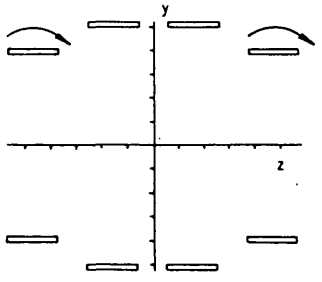

Z^3Y

Fig.4.16 (contd.)

4.10 Conclusions

It is clear that it is essential to calculate the field from an exact model of a magnet's windings in order to assess its homogeneity properly. Whilst the numerical integration method may appear to be a "brute force" approach, it does have the merit of having a simple mathematical derivation, and is therefore easily adaptible to other forms of winding. The method used for performing the integrations is the most efficient of the automatic prodedures, and only needs the required accuracy to be specified in advance. Thus the program may be run by inexperienced users with the minimum of difficulty.

At first, it may appear that the reintroduction of spherical harmonics is an unecessary complication. Nevertheless, the ability to convert sets of field values into harmonic amplitudes does have significant benefits. The visualising of the shape of a uniform field region from field values is virtually impossible. However, the knowledge that a homogeneous region is disturbed by the sum of a number of field profiles, with a well defined and highly symmetrical form, permits such a visualisation. Combined with the work on shimming methods, it becomes a straightforward matter to determine whether the inhomogeneity produced by a real winding can be removed simply, or whether further refinement to the design needs to be carried out to ensure that the terms

that are difficult to remove do not arise in the real magnet.

Perhaps the most important result that has been demonstrated by the models presented in this chapter, is that an axisymmetric design from the interactive program may be transformed into a practical winding with the expectation that the errors in the zonal harmonic components will be minimal. Thus the iterations between axisymmetric and discrete conductor models, that will inevitably be performed during the design process, may be readily made without the need for complicated corrections to be applied to the magnet dimensions.

CHAPTER 5 THE DESIGN AND TESTING OF A RESISTIVE MAGNET SYSTEM.

5.1 Introduction.

This chapter is concerned with the practical application of the design and measurement methods that have been described in the preceding chapters. The design of a full size magnet with good homogeneity has been undertaken in conjunction with GEC Stafford Laboratory and GEC Power Transformers. It is intended that the magnet should replace an existing four coil design with rather poor performance. Versions of the design software have been installed on the Laboratory's computer, and a prototype has been built by GEC Power Transformers.

The main points of the magnet design are described, and its theoretical performance determined. Using the nmr probe system the magnet's actual performance was measured. Known coil movements were made, and the changes in the field's harmonic components compared with the theory. As the magnet has no shim coils, an example of electrical shimming is given by the zonal correction coils in the NEPTUNE scanner.

5.2 The prototype magnet design.

In order to achieve good field homogeneity, a long solenoid with end coils is used. The bore of the magnet is determined by the size of the gradient coils that are fitted, these being a standard production item, and should be at least 1.05m diameter adjacent to the coils in order to minimise the eddy current losses from the pulsed gradient fields. However, the end coils will have a smaller diameter than the main solenoid, and a minimum of 1.04m needs to be allowed in order to insert the gradient coil assembly into the magnet. Once the thickness of the coil formers is determined, the minimum inside diameters for the three coils may be specified.

A preliminary axisymmetric design shows that the total conductor weight to be in the order of three tonnes of copper. Using this figure in a finite elements stress analysis program shows that a former thickness of about 25mm of aluminium is required. This provides adequate stiffness to support the windings without excessive distortion. Thus the minimum diameters for the coil windings can be determined.

The solenoid length is nominally 1.47m, as this is near the peak of the "bump" in the 8th order homogeneity curves shown in figure 3.9. If this design is run using a current density of $2.7A/mm^2$, giving a central field of 0.1 Tesla, then the power dissipation is approximately 40kW. It was felt that the running costs of the magnet

and its cooling plant would be excessively large at this dissipation, so the field magnitude has been reduced to 0.075T, giving a current density of $2A/mm^2$. Alternatively, the copper section could be increased to achieve a reduction in current density. However, the increase in conductor weight is not acceptable. As it stands the conductors, formers, supporting structure and coolant weigh nearly 6 tonnes. Any further increase in weight makes the installation very difficult. One other solution is to reduce the length of the solenoid. However, the reduction in field performance outweighs the advantages gained by the reduction of dissipation and weight. This option was therefore not adopted.

The cooling of the windings is performed in much the same manner as a conventional power transformer. The windings have interlayer gaps, through which transformer oil is passed. The three cooling circuits are connected in parallel, with baffles in the pipe connections to ensure balanced oil flow. Circulation of the oil is provided by a pump which is capable of producing a flow of greater than 500 litres/min. This rate guarantees that no part of the magnet becomes hotter than the inlet oil by more than a few degrees. Thus with an expansion coefficient of 23ppm/°C for aluminium, a temperature rise of 4° C means that the difference in diameter of either end of the solenoid will be no more than 0.1mm. Thus any shimming problems that might be caused by a tapered

former are avoided. The warm oil is passed through a heat exchanger with a secondary circuit containing water. This water is cooled by an outdoor refrigeration unit, which in turn discharges the heat to the atmosphere.

The windings are supported by a series of precision mouldings that lie on top of accurately machined aluminium formers. These mouldings locate each conductor in the winding to within 0.1mm of its correct position. Therefore, there are no cumulative winding errors due to the tolerance on the wires. So, once the formers have been machined and checked, the mouldings can be attached and winding can be performed quickly. No special winding techniques are required. These mouldings are the subject of a patent application by GEC Power Transformers, and are not described further.

The main coil is rigidly fixed to a supporting aluminium frame. Support for the end coils is provided by the frame, but they are able to move with respect to the main coil. The weight of the end coils is taken on large springs, thus the coil position adjusters do not take a large load and are designed to give a fine degree of adjustment. The attractive axial force between the solenoid and end coil is only 1.5kN, and so this too does not present any difficulty in the design of the adjusters.

There are six adjusters in all. Three, arranged at 120 degree intervals around the end of the coil, space

the end coil away from the main coil. They can also twist the end coil about the horizontal or vertical axes. Two adjusters provide vertical movement of the coil, whilst the last provides horizontal adjustment. It is therefore possible to move the end coils into any desired position over a range of a few millimetres.

The photograph on page 170 shows the completed magnet. Each of the three coils is contained in an aluminium sleeve with an O-ring oil seal. The coil spring pairs, on which the end coils are mounted, are clearly seen, together with a vertical adjuster positioned between them. Three inch bore pipe carries the cooling oil to the bottom of the magnet, the return pipe coming from a box on the top of the magnet. This box contains resistors for shunting current from the coils. The resistors will be kept at a constant temperature by the cooling oil.

5.3 Theoretical performance of the prototype magnet

The thick coil model that is used as a starting point is shown in figure 5.1. It is clear that a sphere of 0.25m radius falls easily within the $\pm$1ppm contours. The magnitudes of the significant error terms in ppm are:

$$Z^8 = -0.4$$

$$Z^{10} = -0.1$$

Thus the zonal error terms should not be a significant source of error. All the harmonic magnitudes given in

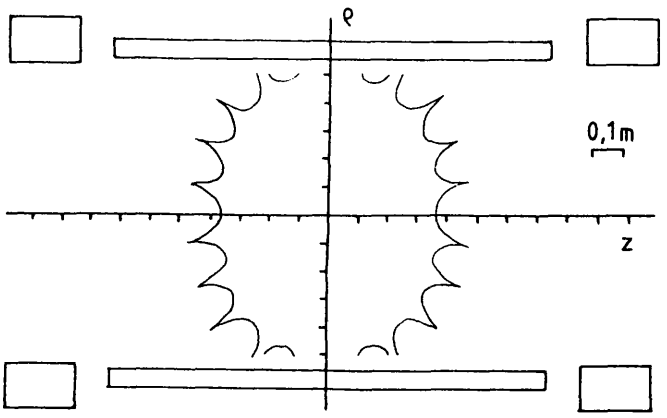

Fig.5.1 Initial model of prototype magnet

this chapter will be at a radius of 0.25m.

The current in the winding is 240A, and so the conductor will have a substantial cross section. As a result, the helix pitch is quite large, being in excess of 2cms. Even though an even number of layers is used in each of the coils, the tesseral field components are significant, as shown by the results from a filamentary helix model:

Z^8 = -0.4ppm

X = -6.7	ZY = 0.8
Z^2X = -2.6	Z^3Y = -0.2

X^2 = -0.3

Z^2X^2 = -0.2

This model took 46 mins. of CPU time on a Prime 750, using a 12 plane plot with 12 points per plane. With the same plotting points the following harmonic components were obtained by modelling the winding using thick conductors of the appropriate dimensions:

Z^2 = -4.6ppm
Z^4 = 0.4
Z^6 = 0.1
Z^8 = -0.4
Z^{10} = -0.2

X = -6.7 ZY = 0.8
Z^2X = -2.6 Z^3Y = -0.2

X^2 = -0.3
Z^2X^2 = -0.2

The tesseral terms remain unchanged, but a significant amount of Z^2 has now been introduced. This model took 6hrs. and 32mins. of CPU time on the same machine. Thus there are significant benefits in obtaining information about the tesseral terms from filamentary, rather than thick helical models. It now remains to be seen whether the quantities of Z^2,X and Z^2X can be removed simply by moving the end coils.

Moving the coil at the +z end inwards axially by 0.1mm produces the following terms from the

axisymmetric program:

Z^1	= 26.8ppm	Z^2	= 7.2
Z^3	= 2.0	Z^4	= 0.1
Z^5	= -0.2	Z^6	= 0.0
Z^7	= 0.0	Z^8	= -0.4

It is noticeable that this movement only affects the lower order terms. Thus moving both end coils inwards by 0.1mm will alter Z^2 by 14.4ppm, and Z^4 by 0.2ppm. None of the odd terms will appear because of symmetry, and there are no changes in the remaining terms. A movement of about 0.032mm would therefore provide cancellation of the Z^2 term introduced by the thick helical winding. However, it is impractical to make such a small movement accurately, so shunting current from the end coils would be a better method of providing the correction.

Reducing the current in the +z end coil by 100mA produces the following significant harmonic components:

Z^1	=-42.2ppm	Z^2	=-10.5
Z^3	= -3.4	Z^4	= 0.4

As the Z^2 component is negative, an increase in current is required to produce the required cancellation. The theoretical model of the magnet actually requires that current be shunted from the end coils, and so the

currents in the end coils may be increased or decreased to facilitate shimming. Thus the Z^2 component may be cancelled whilst only producing an insignificant amount of Z^4.

Shifting the centre of the +z coil by 0.1mm in the x direction produces the following terms:

$$X = 13.4\text{ppm}$$
$$ZX = 1.0$$
$$Z^2X = 1.0$$

Thus shifting the end coils by 0.025mm along x should cancel the X term without significantly altering Z^2X. Twisting the same coil by 0.1 degrees about the y axis gives:

$$X = -38.5\text{ppm}$$
$$ZX = -36.5$$
$$Z^2X = -17.9$$
$$Z^3X = -6.1$$

This movement gives significant quantities of Z^2X, and so may be used to cancel that term. The additional X component that this introduces can then be cancelled by a transverse shift of the coil. Thus it should be possible to remove virtually all of the effects of the helical windings simply by coil movements.

The modelling of the coil movements has only been

considered on round thick section coils, as the inclusion of helical effects is only likely to be of secondary importance. Nevertheless, the required coordinate transformations can easily be carried out on a discrete conductor model if the increase in computation time is acceptible.

The above calculations have shown that very small errors in the dimensions of a coil produce significant changes in field homogeneity. This fact calls into question the feasibility of manufacturing any of the coils with sufficient accuracy. By studying the effects of small changes in coil width, thickness and position using the axisymmetric program, it becomes clear that each of these effects only produces errors in the low order harmonics. Thus these errors will be correctable simply by coil movements and current shunting. As a result of this, and other studies, tolerances of between 0.2 and 0.5mm have been placed on various dimensions of the magnet, with the expectation that the resulting field errors would be correctable. This sort of tolerance can be met fairly easily on a structure of this size and, as a result, the magnet can be manufactured much more cheaply than might otherwise have been the case.

One effect that was not fully considered at the time of design, partly due to the lack of design tools, was the effects of the supply leads to the coils. The most significant effect appears to be due to the radial leads

that connect the inside layer of the coils to a connector on the outside of the coil. Modelling the effects that these three conductors have on a perfectly uniform field yeilds the following harmonic terms:

X	$= -37.0$ppm	Y	$= 21.4$
Z^2X	$= -2.5$	Z^2Y	$= 1.4$
X^2	$= -7.4$	Y^2	$= -4.3$
Z^2X^2	$= -0.8$	Z^2Y^2	$= -0.5$

Both X and Y terms are produced because the leads are positioned at $\phi = 60^\circ$ in the actual magnet. The X, Z^2X, Y and Z^2Y terms may be removed by the methods already outlined. However, as mentioned in section 4.9, the terms involving X^2 or Y^2 cannot be removed by coil movements. A set of shim coils would therefore be required to completely remove the effects of these leads.

5.4 Measured performance of the prototype magnet.

Initial postioning of the magnet's end coils was performed with the aid of a ruler. Nmr probes were then positioned in the magnet, the measuring probe being fixed to a plotting device that allowed it to be moved throughout the central field region. The fixed reference probe was placed in the centre plane, but near the magnet former so as not to obstruct the moveable probe.

Since the field errors in the magnet are only likely to be of low order, spherical field plots were not used

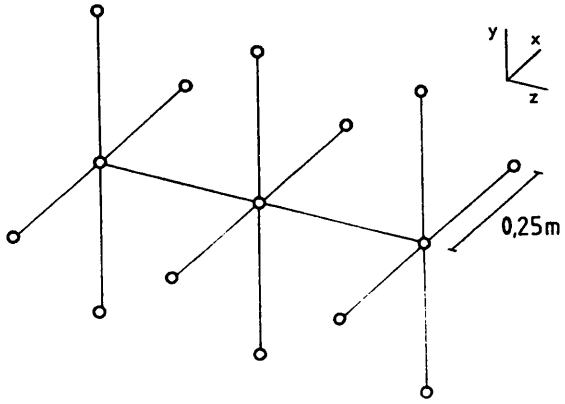

Fig.5.2 Probe positions used for setting up prototype magnet

for setting up the coils. Instead, a simple procedure involving a limited number of points allows measurements and consequent adjustments to be made quickly. Figure 5.2 shows the probe positions that are used. Taking just two positions at z=+0.25m, x=$\pm$0.25m, the +z coil is shifted in the x direction so as to make the measurements equal. The same thing is done at the -z end for the -z coil. Although the movements do slightly affect the field at the opposite end of the magnet, a few iterations yields the required result. If there is now an x gradient at the

centre plane, the end coils are tilted about the y axis and the process repeated until the gradient is minimised along the whole magnet. This procedure is equivalent to removing the X,ZX and Z^2X gradients, The Y gradients may be tackled in the same manner.

To obtain the correct axial positions of the end coils, three measurements on axis are used. Without any shunt resistors on the coils, the field at $z=\pm 0.25$m, as calculated by the axisymmetric program, should be 46ppm above that at the origin. The axial positions of the end coils are adjusted to achieve this result, and then sufficient current shunted from them to make the three measurements on axis equal.

In practice, the adjusters tend to influence each other slightly, and so removing one gradient tends to introduce another. The largest problem is making the axial coil movement where 3 adjusters have to be moved and equal amount. Thus there comes a point where making well controlled movements becomes difficult.

A 9 plane plot with 12 points per plane was taken after this setting up procedure. The following significant components were present:

Z^1	= -1.8ppm	Z^2	= 3.0
Z^3	= 6.6	Z^4	= -1.5
Z^5	= -0.7	Z^6	= 1.5
Z^7	= 0.2	Z^8	= 0.5
X	= 8.7	Y	= 2.9
ZX	= 2.5	ZY	= 1.5
Z^2X	= -1.0	Z^2Y	= 0.0
Z^3X	= -1.8	Z^3Y	= -2.1
Z^4X	= 0.2	Z^4Y	= 1.0
X^2	= -4.1	Y^2	= 2.5
ZX^2	= -1.6	ZX^2	= 2.2
Z^2X^2	= 1.1	Z^2X^2	= 0.2

It is known that the coils were not in their correct positions when this plot was made, because the shunting resistors carried unequal currents. This axisymmetric effect, being antisymmetric about the origin will generate odd ordered zonal terms, and explains the presence of of the large Z^3 component.

The large X and Y terms can easily be removed in a

complete scanner, by using the gradient coils used for scanning as shim coils. Thus, in practice, they do not represent a significant problem.

The Z^pX^2 and Z^pY^p terms are different from the results given by the radial lead model, as the model only produced significant terms when p was even. The measured values include the p=1 terms, and the X^2 have been reduced whilst the Y^2 terms have been increased. This implies that whatever is producing these additional second degree terms is only at one end of the magnet, and has different azimuthal symmetry from the effect of the leads. Ovality of one end coil may be the reason for the effect. Alternatively, the power supply leads, which are mainly at one end of the magnet, could be responsible.

No doubt some of the field errors could be removed by further shimming, using spherical field plots in conjunction with calibrated coil movements that remove individual harmonics. However, the total variation in field magnitude over the surface of, and hence throughout the 0.25m radius sphere, is only 17ppm. This within the $\pm$10ppm variation specified in chapter 1, and so the magnet is quite usable for scanning as it stands.

Sets of measurements were taken in order to check that the coil movements used for shimming produce results that agree with calculated values. A five plane plot with six points per plane was taken before and after a calibrated movement was made. By differencing the two

sets of results, the effect of the coil movement alone can be seen.

Three adjustments were made to the +z end coil; an axial shift of 1mm, a transverse shift of 1mm, and a tilt of 0.1 degrees. The difference made by each adjustment is shown below.

	Measured	Calculated
Axial movement of 1.0mm		
Z^1	-280.8ppm	-268.0
Z^2	-72.7	-71.3
Z^3	-23.1	-20.4
Z^4	-0.29	-0.8
Transverse movement of -1.0mm		
X	-139.9ppm	-134.2
ZX	-41.2	-47.6
Z^2X	-2.8	-10.5
Twist of 0.1 degrees		
X	37.6	38.5
ZX	40.3	36.5
Z^2X	19.9	17.9

Most of the measured values are within about 10% of their calculated values, and so support the theoretical model reasonably well. It would therefore be expected that further careful shimming, using these coil movements, would bring about the reduction of many of the unwanted harmonics.

5.5 The use of zonal shim coils.

Although the three coil magnet does not possess any shim coils, it would be very much easier to set up if it did. A set of shims for the zonal harmonics Z^1,Z^2,Z^3 and Z^4 have been designed and installed in the NEPTUNE machine. They are simply the single coil pair Z^1,Z^2 and Z^4 shims whose positions are given in table 3.3. The Z^3 design is not used as it adds four more coils to the arrangement. Instead, each half of the Z^4 shim is driven by a separate power supply. Currents of the same sign in each half of the shim generate a Z^4 component, whilst opposing currents generate Z^3 and Z^1. The additional Z^1 component may then be removed by the Z^1 shim.

The coil arrangement and shim sensitivities in a 0.15 Tesla field are shown in fig.5.3, and the magnitudes of the zonal harmonics before and after the use of the

shims are:

	Before	After
Z^1	11.9ppm	1.1
Z^2	-12.7	0.9
Z^3	0.9	0.6
Z^4	15.7	-0.3

Once again the remaining Z^1 component may be removed with the gradient coils. Although the Z^3 shim is not really required in this case, it was to be used later in an experiment involving the insertion of small pieces of iron inside the magnet bore to remove some of the tesseral components. The shim set is a very quick and convenient way of removing unwanted harmonic components.

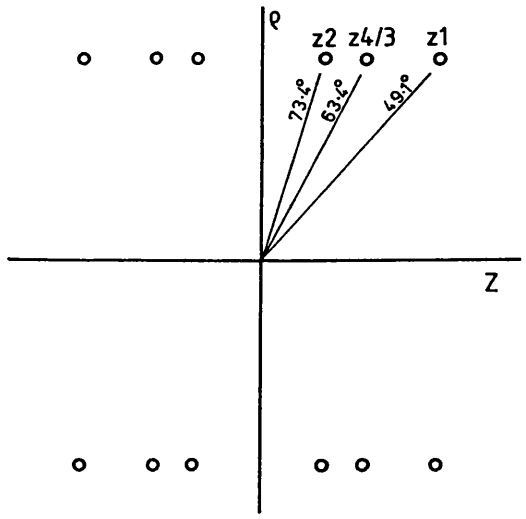

Fig.5.3 Zonal shim coil positions

Fig.5.3 (contd.)

Sensitivities with 20 turn coils in 0.15 Tesla field

Z^1 101.4 ppm/Amp

Z^2 -60.2 ppm/Amp

Z^3 -34.3 ppm/Amp

but also produces 135.9ppm/Amp of Z^1

Z^4 -15.0 ppm/Amp

5.6 Conclusions

The practical measurements made on the prototype magnet and zonal shim coils confirm the validity of the design methods described in the previous chapters. Although the measured homogeneity falls short of the theoretical calculations, it is expected that improvements may be made by making further adjustments to the end coils. Practical measurement has shown that these adjustments also produce results that support the theoretical model. Therefore the removal of the unwanted, low order harmonic terms should present few problems.

The ultimate preformance of the magnet will be determined by the higher order terms that cannot be removed by these methods. In principle, these terms could be removed using shim coils. However, the coil

arrangements become more complicated, and therefore more expensive, as the order and degree of the harmonic correction increases. As a result, the amount of correction that is made will eventually depend on the cost-effectiveness of providing the means of adjustment. It is therefore important that proper attention is given to the sources of high order terms at the design stage.

5.7 Summary and further work

A logical design procedure for iron free, high homogeneity magnets has been developed that makes extensive use of a set of computer programs. The first of these allows the dimensions of an array of axisymmetric coils to be optimised so as to produce a uniform field. A graphics terminal allows the coil geometry, design data, and graphs or contour maps of homogeneity to be viewed. By using spherical harmonics and an efficient optimisation procedure, these operations may be performed quickly, and this allows the program to be used interactively. As a consequence, the iterations needed to arrive at a suitable design may be performed with little difficulty.

Obviously, such a design will have been realised with some regard for the actual construction of the windings. For example, a helix with known conductor size

and pitch may have been chosen. A second program allows the fields from such windings to be calculated, and expressed as a spherical harmonic series. Results from this program have shown that it is a straightforward matter to transform the dimensions of an axisymmetric model into those of a practical winding. Any errors in the zonal harmonics caused by doing this will usually be negligible. However, significant quantities of tesseral harmonics will, in general, be present. It is possible that these terms will limit the magnet's ultimate performance, therefore the source of these components, and methods of cancellation, should be carefully studied at the design stage.

It is not sufficient to arrive at a suitable design without careful consideration of manufacturing tolerances. Errors in coil dimensions are inevitable since it is impractical to manufacture formers to the accuracy that the theory demands. Thus it is essential to consider methods of correcting the effects of incorrect dimensions during the design process. For a superconducting magnet virtually the only solution is to provide electrical shim coils, either superconducting or resistive. However, in the case of a resistive magnet, movement of the magnet coils is feasible in addition to electrical shims. The design programs are, or with minor extensions will be, capable of designing electrical shims using optimisation methods; whilst the program that

models displaced circular coils allows shimming movements to be determined.

Another method of shimming is by the introduction of small pieces of ferromagnetic material into the magnet. The theory is not well developed, and this is an area that merits further attention. This method would allow corrections to be made to both superconducting and resistive magnets with no extra power dissipation. It would therefore be particularly beneficial at higher field strengths.

In addition to the designing of magnets, this work has been concerned with their testing. An accurate measurement device and the spherical plotting procedure allows field measurements to be resolved into harmonic components. Thus the practical measurements can be related directly to the theoretical calculations in a manner that allows easy comparison. The use of harmonics also allows shimming to proceed in a well defined manner, by removing inhomogeneities one at a time, whilst leaving the others virtually unchanged.

To perform these measurements, a pulsed nmr probe has been developed. The performance of the probe agrees with the theory, and, in contrast to a continuously excited probe, the device may be easily incorporated into an nmr scanner with the minimum of additional hardware. The ability to measure the differences in field magnitude between two points has allowed the performance of the

prototype magnet to be assessed independently of the stability of its power supply. Incorporating other features, such as automatic tuning and an improved data collection system, would make the probe a very easy to use, versatile device with applications not only for measuring static magnetic fields, but the superimposed pulsed gradient fields.

Little attention has been given to the external field generated by an nmr imaging magnet, since it is easily calculable using elliptic integral methods. However, the effect of the field on nearby equipment, particularly if it uses electron beams (eg. X-ray tubes, television monitors, etc.) can be undesirable. Also, the field will magnetise any surrounding ferromagnetic material which, in turn, disturbs the homogeneity of the magnet. Both of these effects would be significantly reduced if the return path for the magnet's flux could be replaced by an iron core, at the same time reducing the power dissipation. However, the benefits of an iron return path would have to be paid for by a large increase in weight. The mathematical modelling of such a magnet would involve the the use of an approximation technique that uses either integral or differential methods. In either case the modelling of windings is necessary, and may be accomplished using some of the methods described here.

Calculations of limited accuracy have been performed

using the finite element method, and scale models are being built. The testing of these models will be performed using spherical plots and a probe. Thus some of the techniques for designing and testing iron free magnets are also applicable to magnets that incorporate iron. The problems of high accuracy, magnetostatic field calculations present a wide area for future research. If the problems can be solved, it is likely that iron cored magnets will form the basis for low field ($\sim$0.1T), low cost, nmr scanners in the future

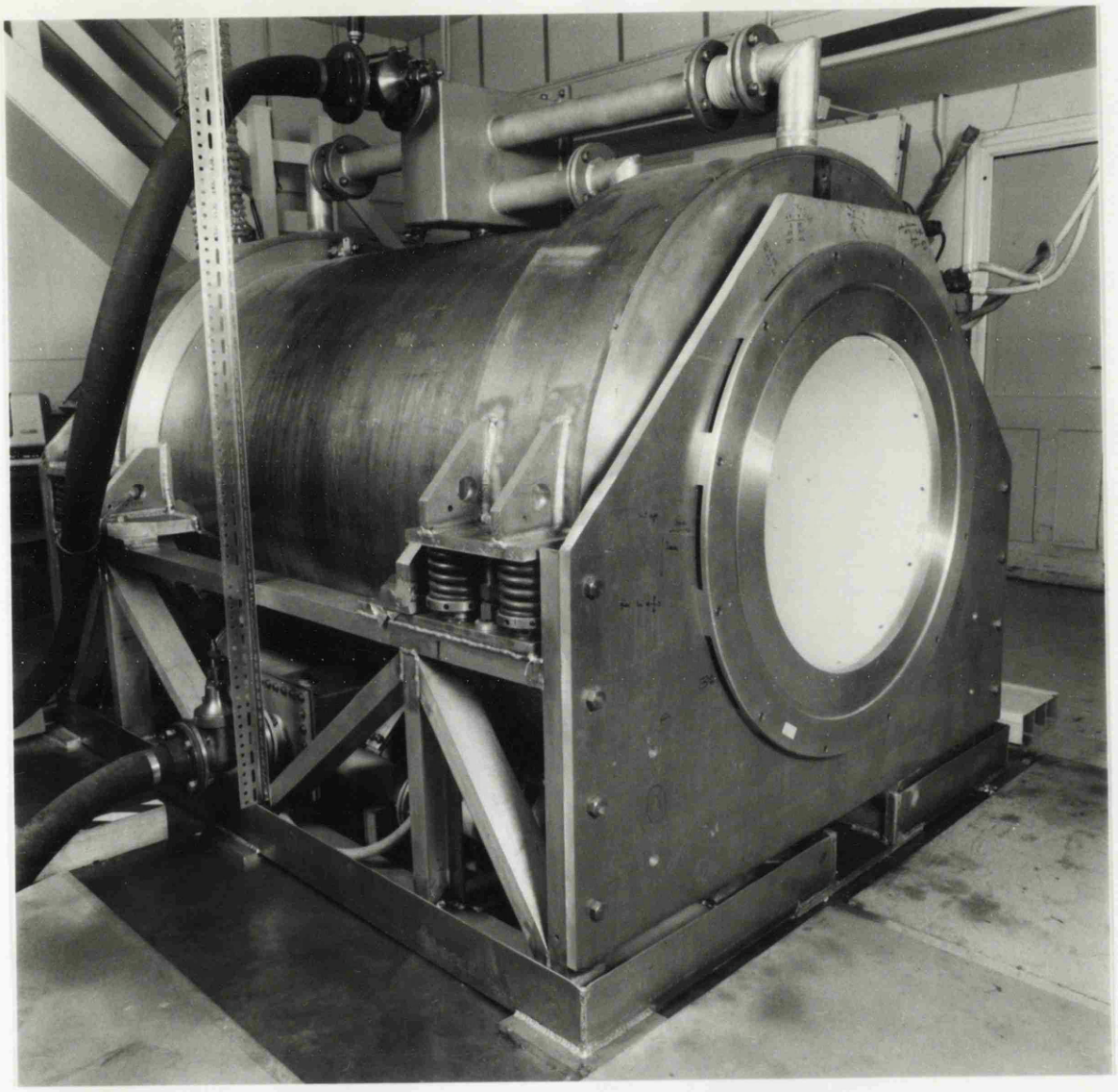

The 3 coil resistive magnet

APPENDIX 2.1

CIRCUIT DIAGRAMS FOR THE STAND ALONE PULSED PROBE SYSTEM AND AUTOMATIC TUNING

Probe amplifier

Demodulator

Baseband filters

Gated rf amplifier

Transmitter

A/D converter

Microprocessor card

Control logic card

Calculator and logic card

Magnitude generator

Auto-tuning analogue

Auto-tuning logic I

Auto-tuning logic II

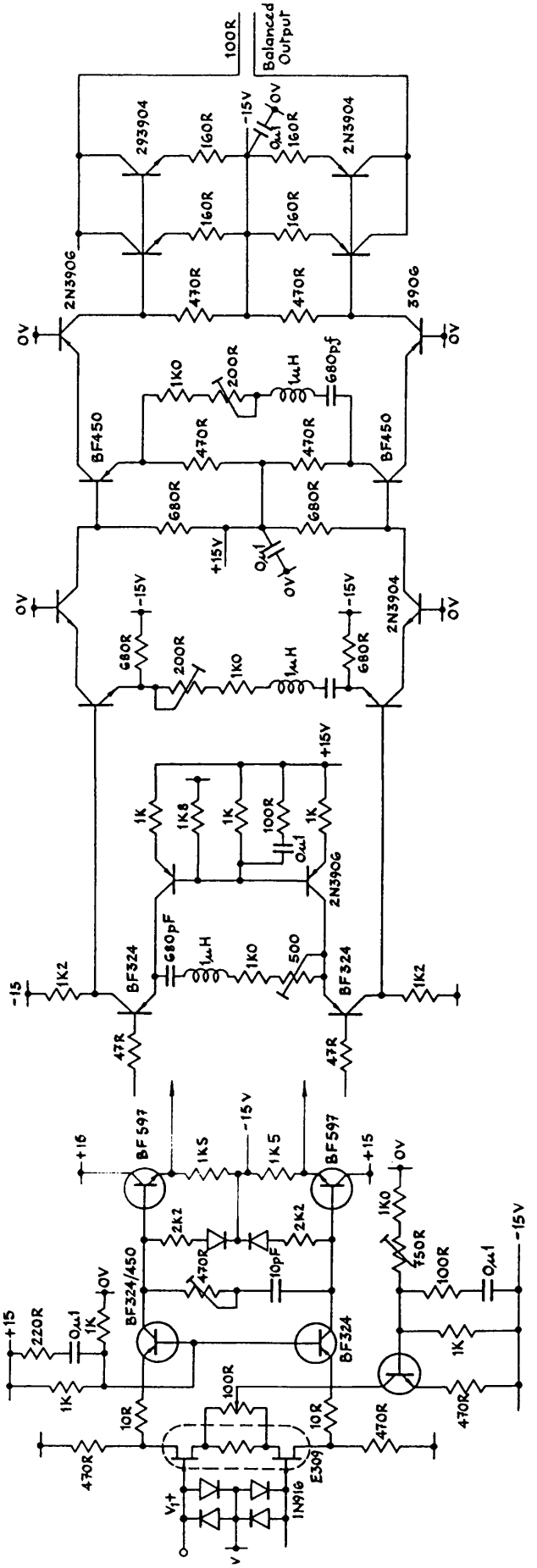

Probe amplifier

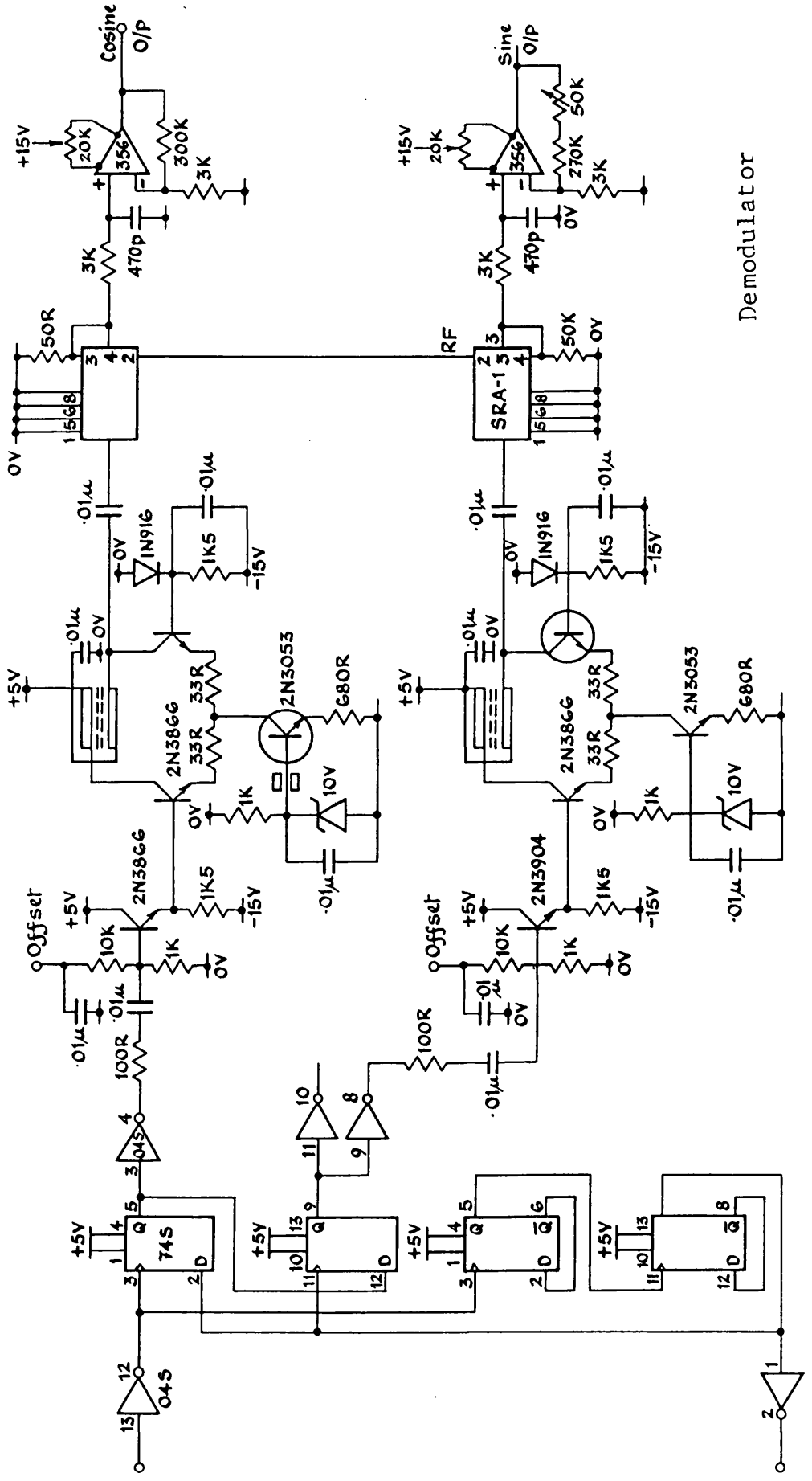
Demodulator
Cosine O/p
Sine O/p
+15V
20K
356
300K
270K
50K
3K
470p
0V
50R
SRA-1
RF
50K
.01µ
1N916
1K5
-15V
+5V
2N3866
33R
2N3053
680R
10V
1K
2N3904
Offset
10K
100R
74S
04S

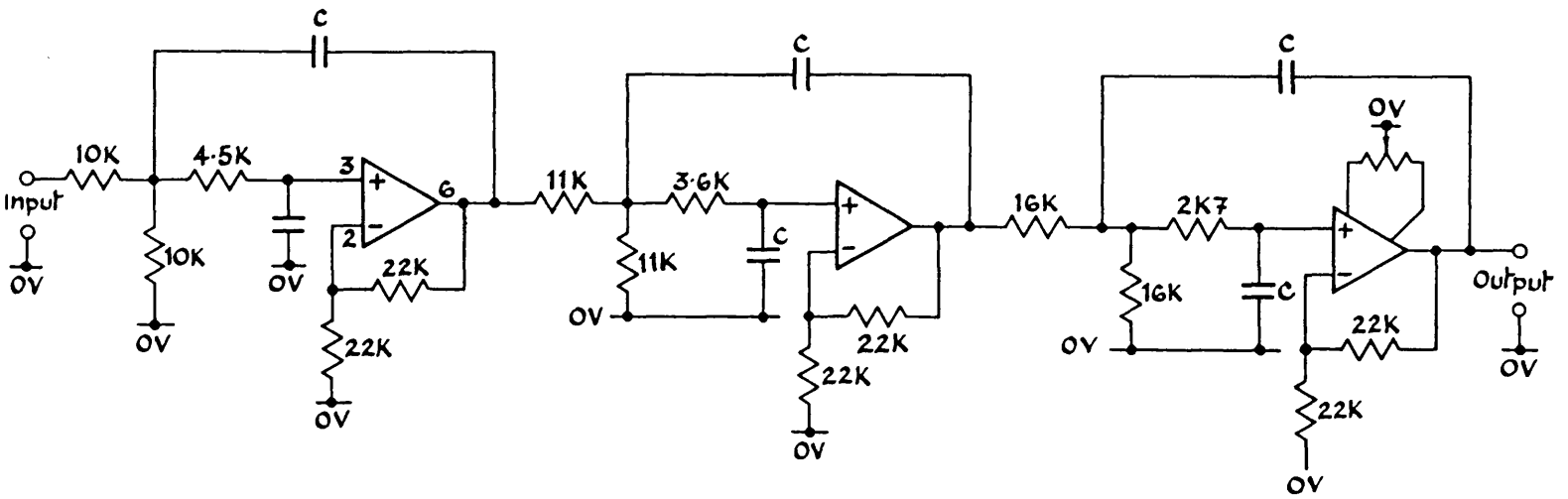

Baseband filters

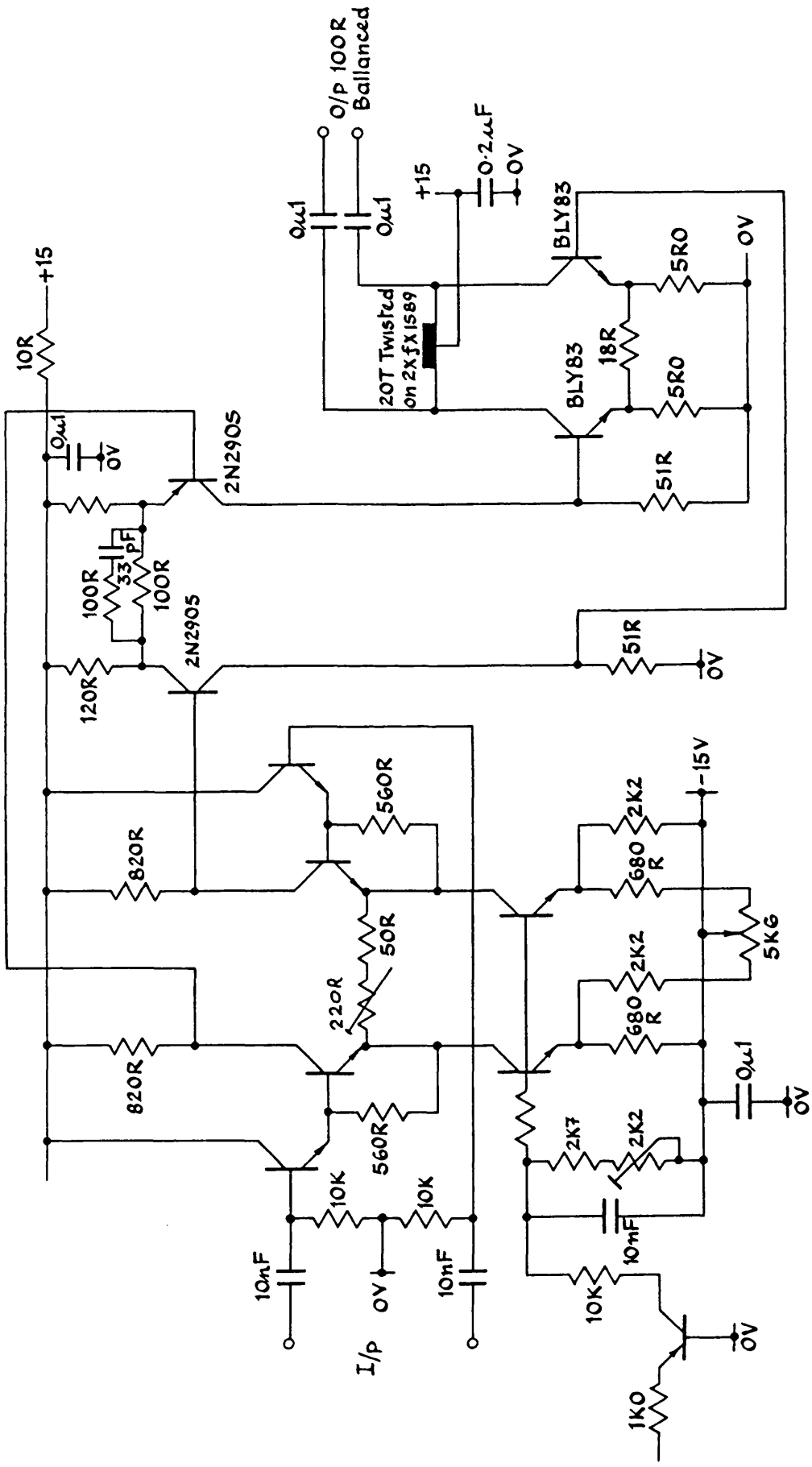

Gated rf amplifier

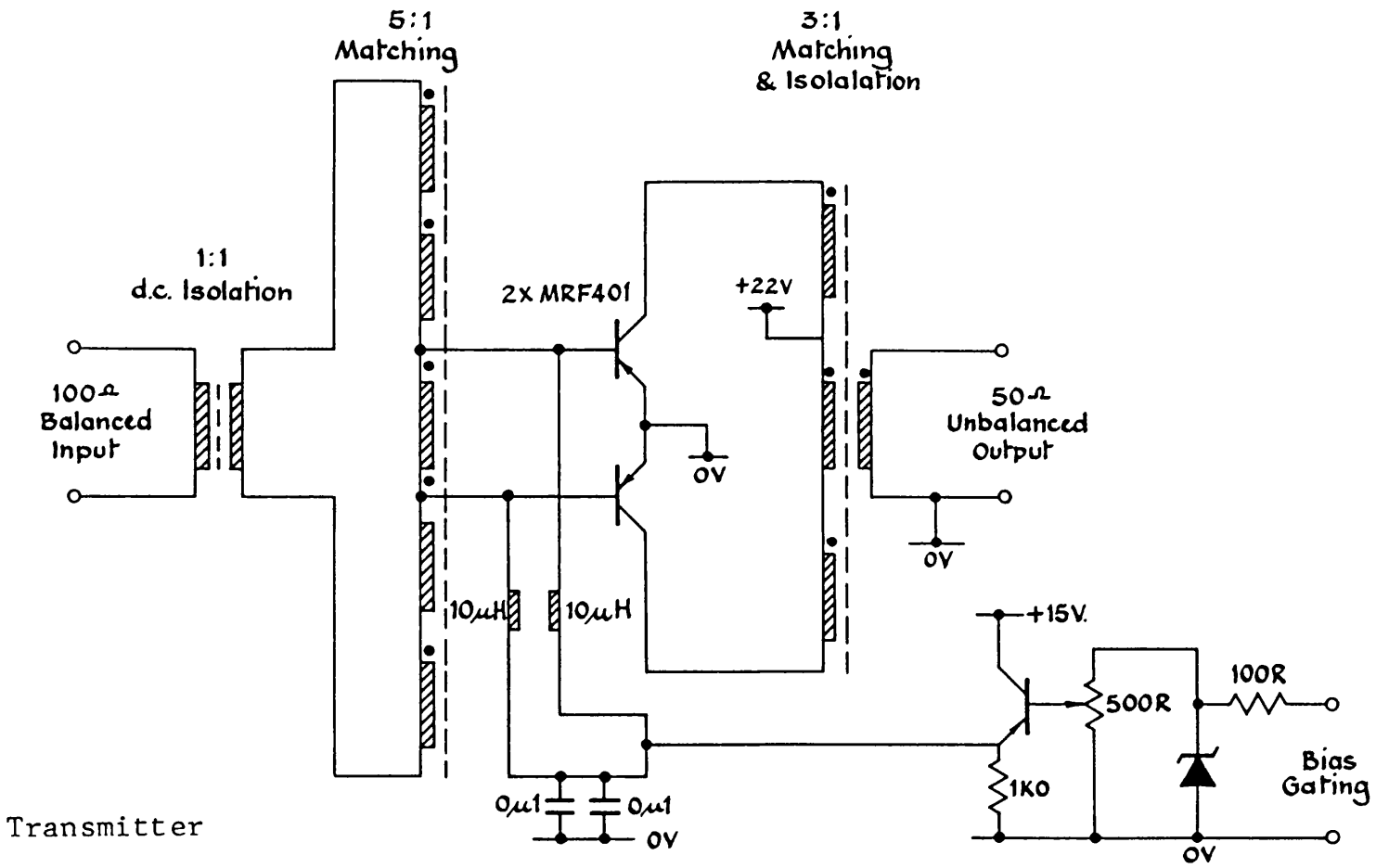

Transmitter

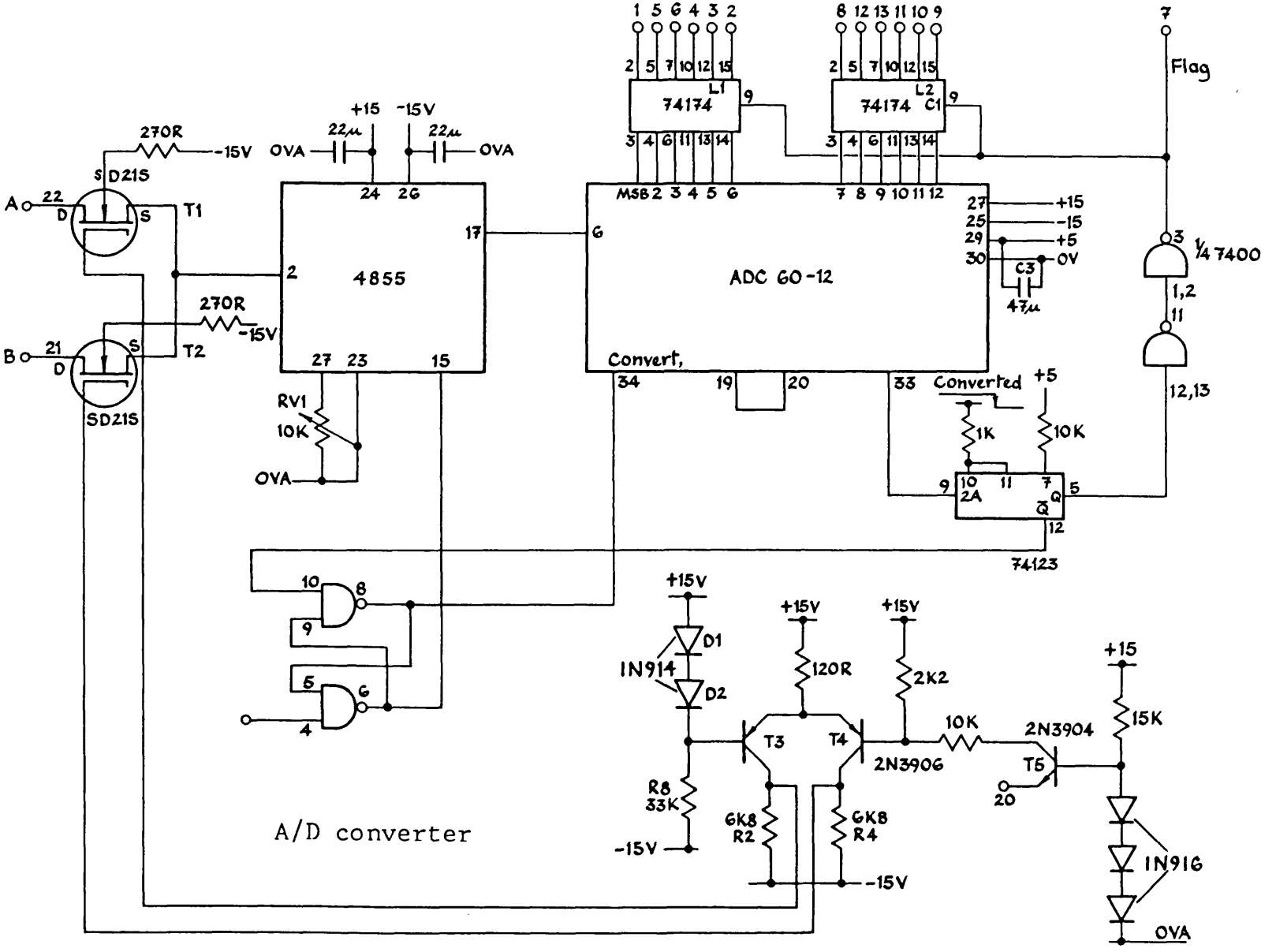
74174 L1
74174 L2 C1
Flag
270R
-15V
+15
-15V
22µ
OVA
SD215
A
B
T1
T2
4855
ADC 60-12
+15
-15
+5
0V
C3
47µ
1/4 7400
1,2
11
12,13
Convert,
Converted
RV1
10K
1K
74123
D1
IN914
D2
120R
2K2
T3
T4
2N3906
2N3904
T5
R8
33K
6K8
R2
6K8
R4
15K
IN916
A/D converter

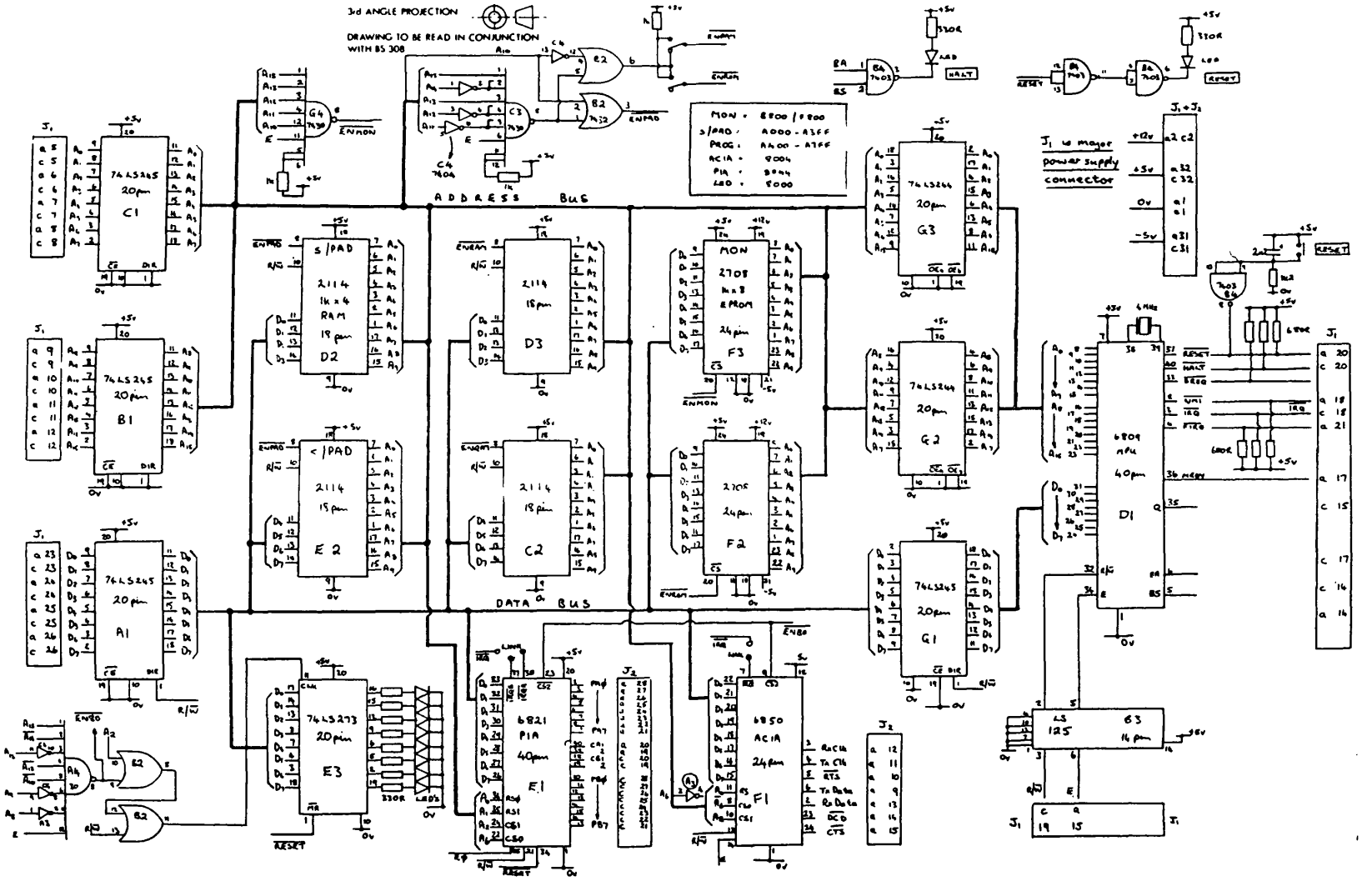

Microprocessor card

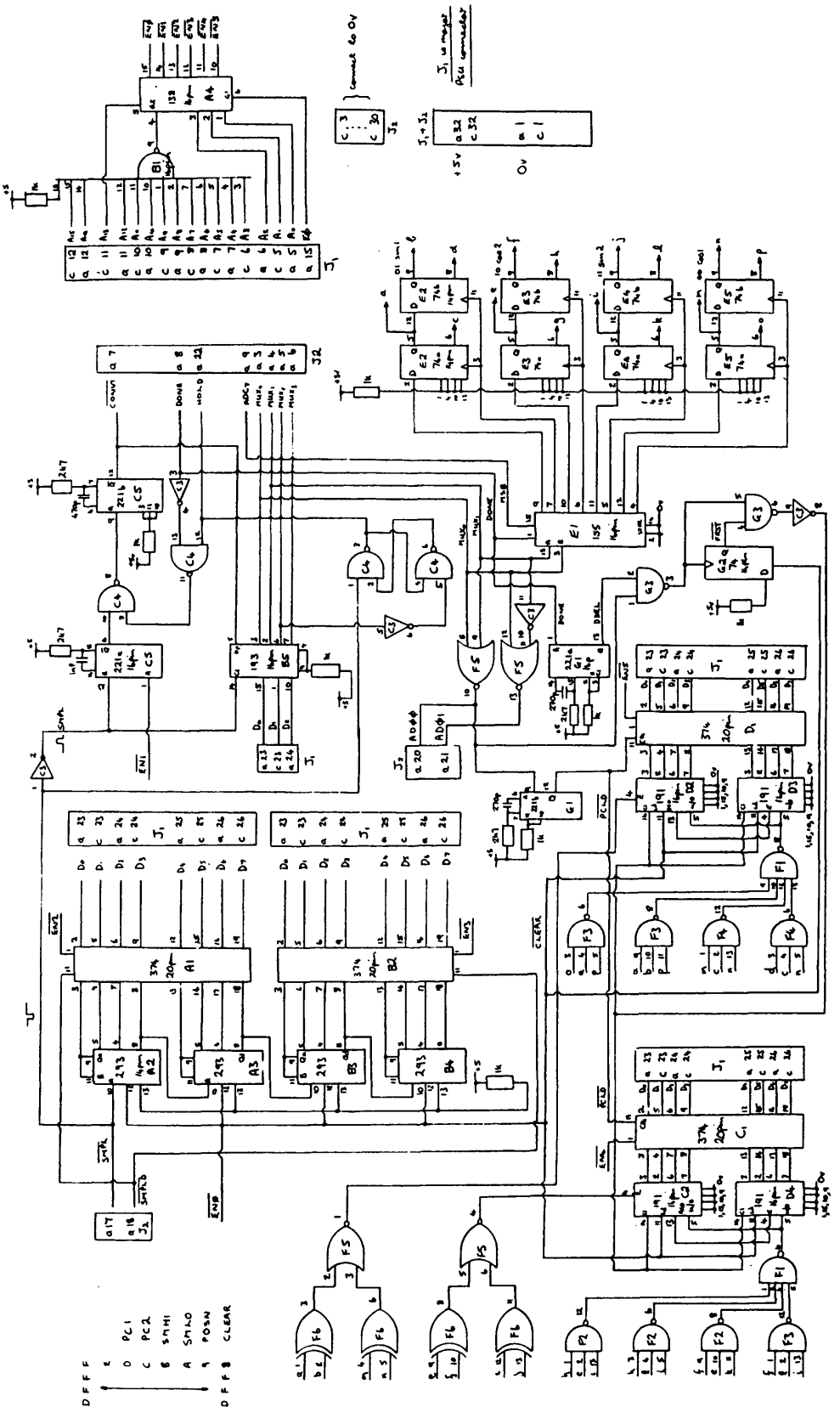

Control logic card

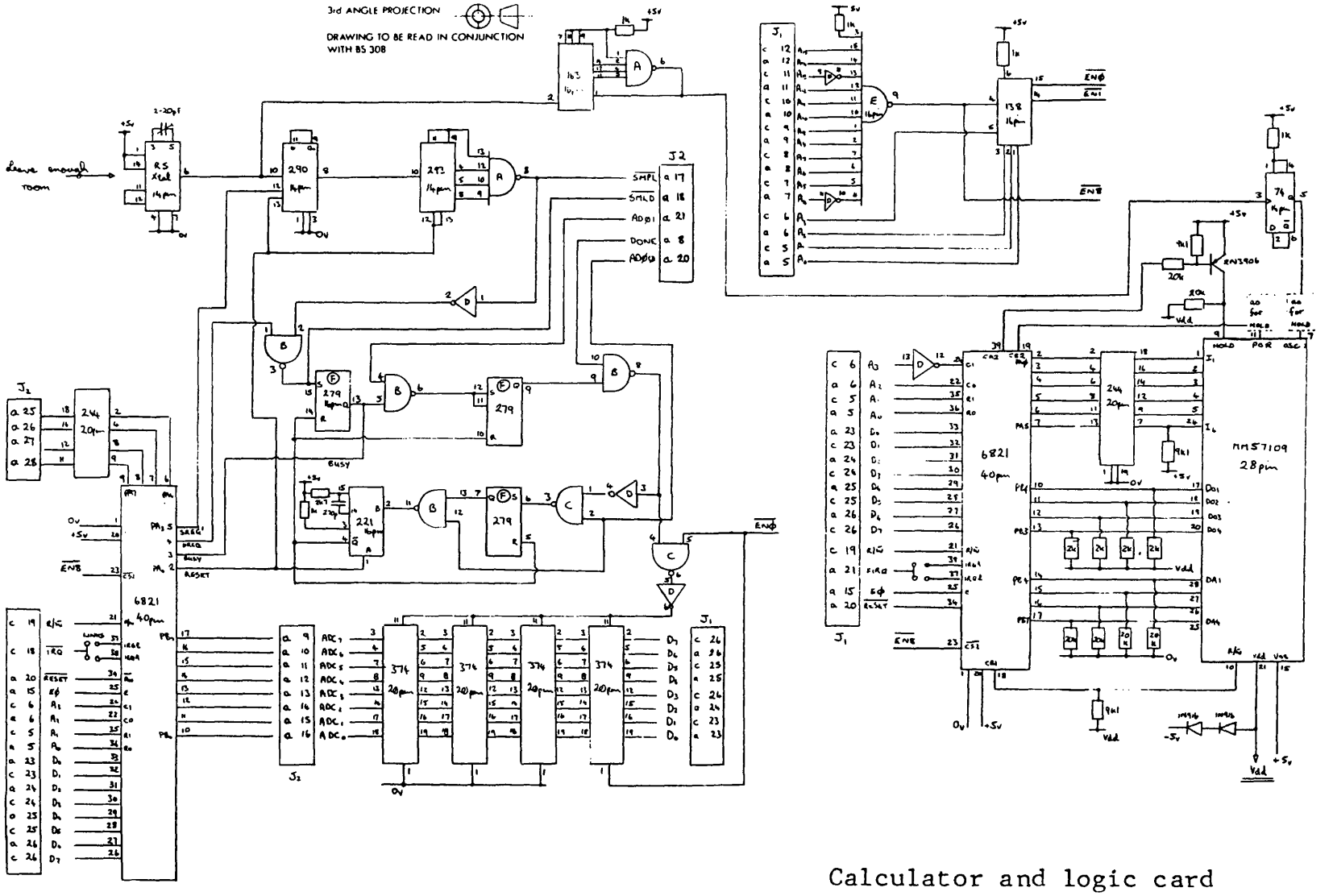

Calculator and logic card

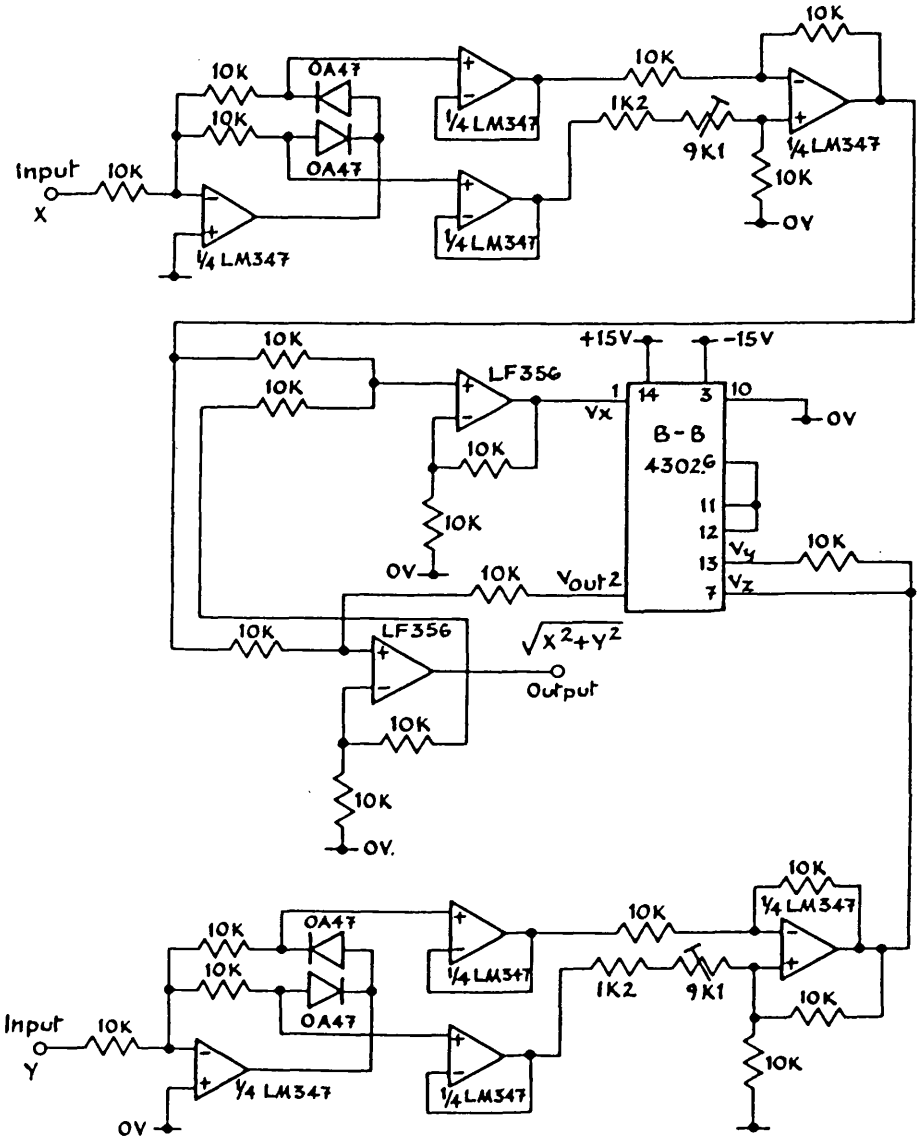

Burr Brown 4302

$V_{out} = V_y \left(\frac{V_z}{V_x}\right)^{\frac{m}{(m-1)}}$

Magnitude generator

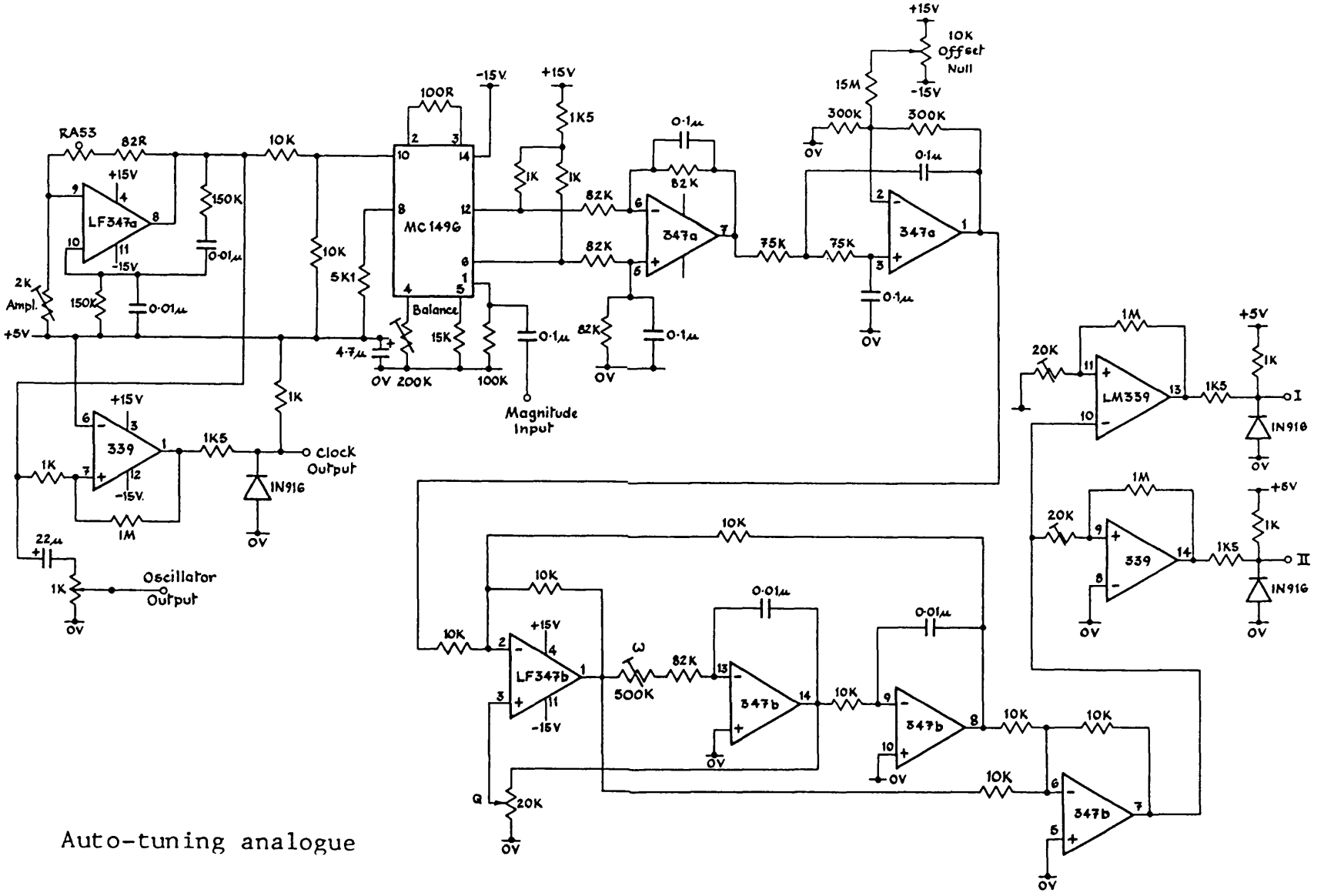

Auto-tuning analogue

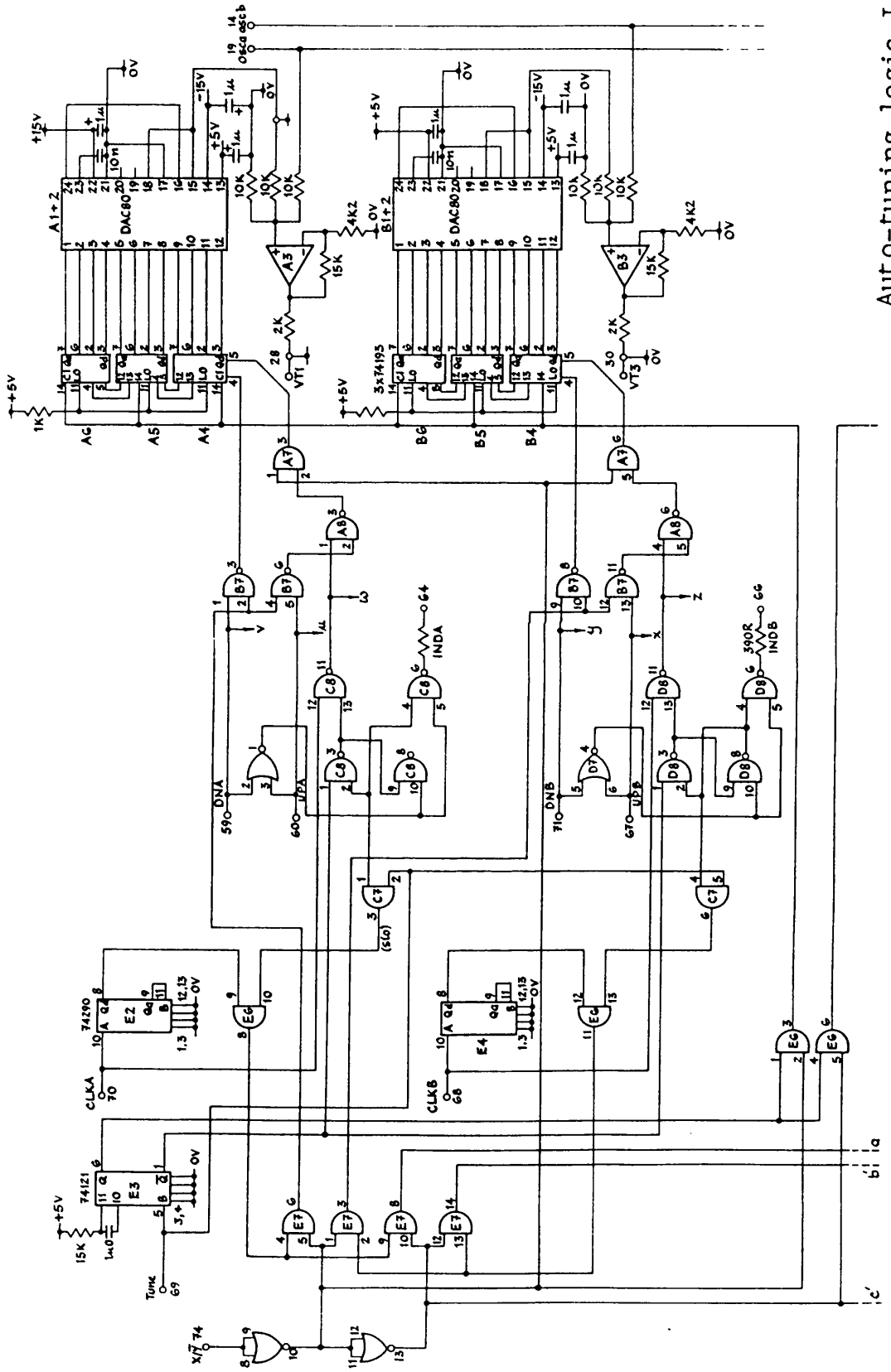

Auto-tuning logic I

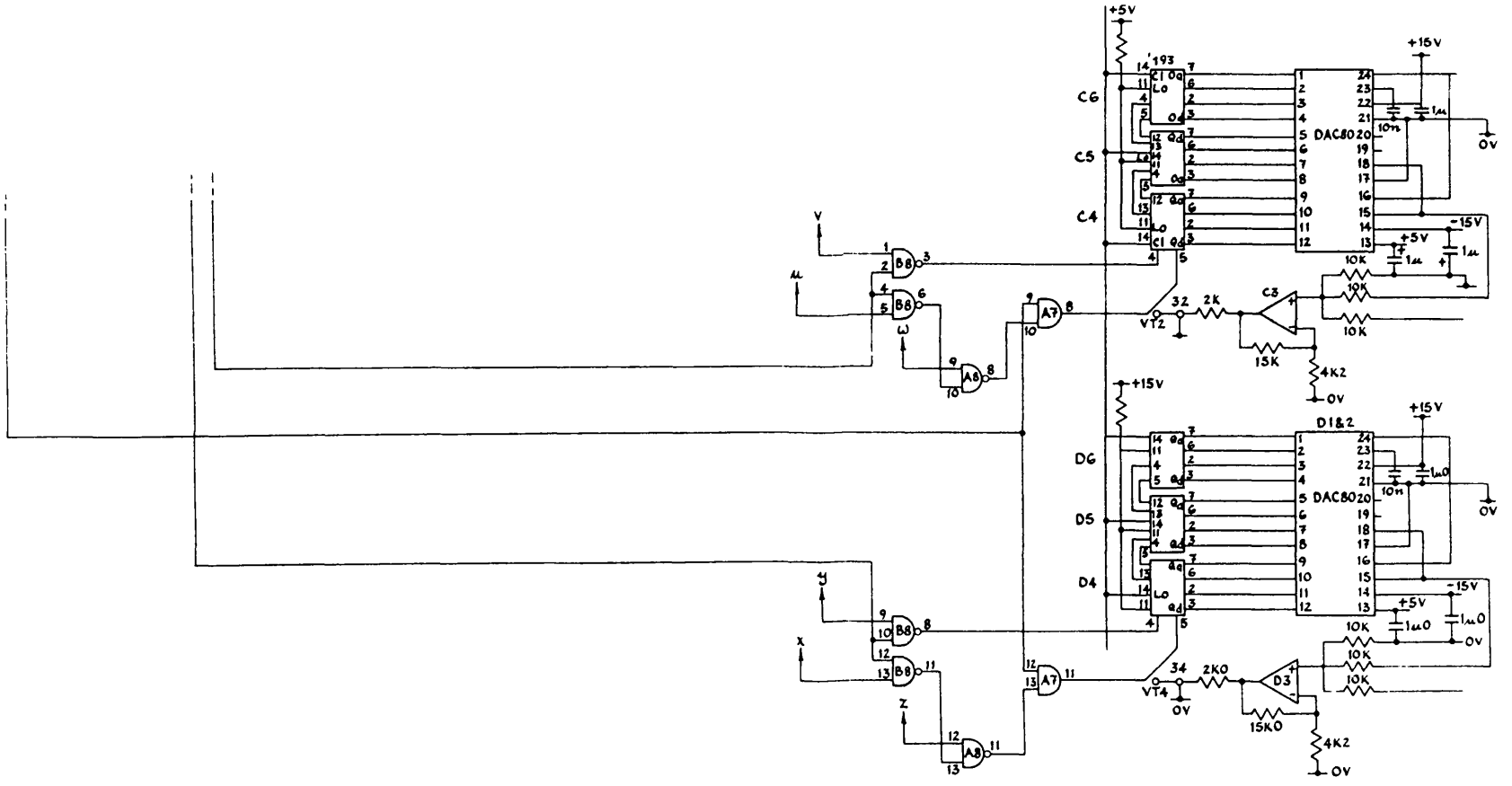

Auto-tuning logic II

APPENDIX 3.1

Harmonic coefficients for various coil geometries.

Loop

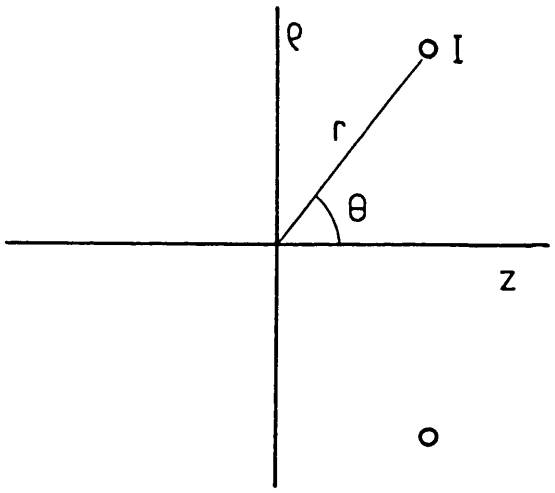

$$a_n = \frac{I}{2} \frac{\sin^2\theta}{r^{n+1}} P_{n+1}'(\cos\theta)$$

Solenoid

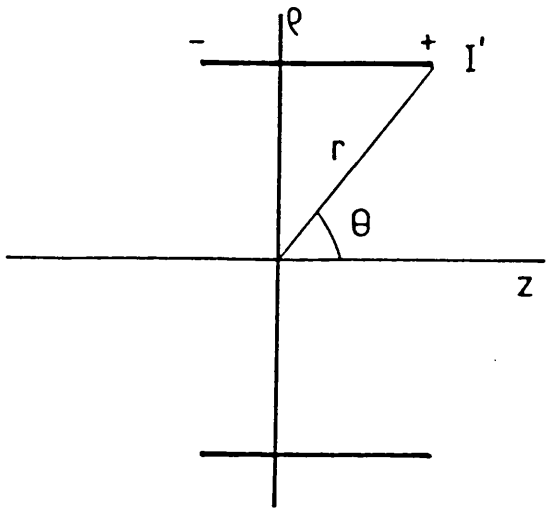

The coefficients are given by substituting the coordinates of each end of the solenoid into

$$a_o = I' \frac{\cos\theta}{2}$$

$$a_n = \frac{I'}{2} \frac{\sin^2\theta}{n\, r^n} P_n'(\cos\theta)$$

(where I' is current / unit length)

and summing the two terms using the algebraic signs shown in the diagram.

Thick section coil

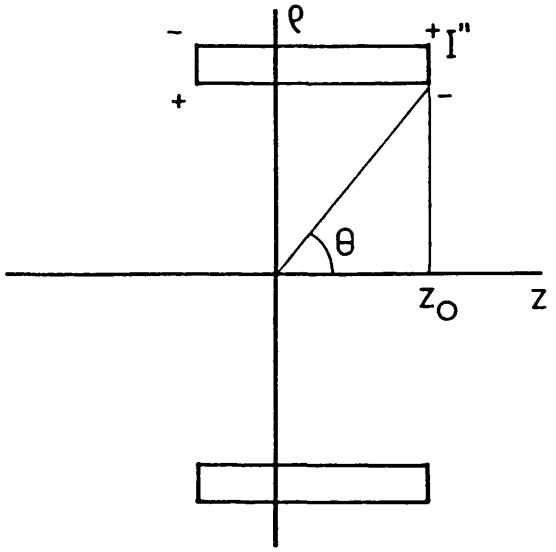

The coefficients are given by substituting the coordinates of each vertex into

$$a_o = \frac{I''}{2} z_o \ln\left[\frac{1+\sin\theta}{\cos\theta}\right] \qquad a_1 = \frac{I''}{2}\left(\sin\theta - \ln\left[\frac{1+\sin\theta}{\cos\theta}\right]\right)$$

$$a_{n+1} = \frac{I''}{2n(n+1)} \frac{1}{z_o^n} \left(1 - \sin^3\theta\right) \sum_{m=1}^{n} \cos^{m-1}\theta \; P_m'(\cos\theta)$$

(n>0) (where I" is the current density)

and summing the four terms using the algebraic signs in the diagram.

APPENDIX 3.2

Elliptic integral expressions for fields from various coil geometries.

Loop

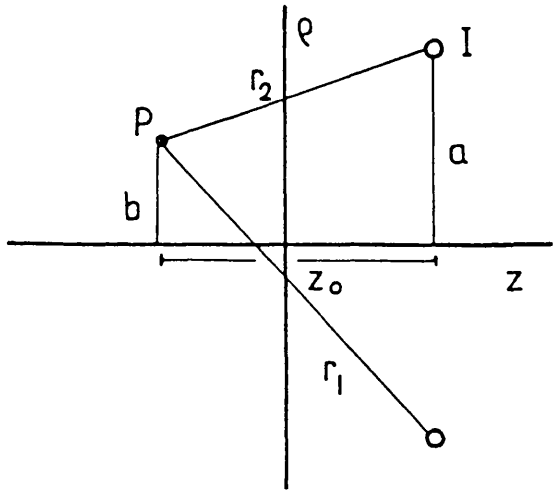

$$H_z = \frac{I\,b}{2\pi r_1}\left[(K-E) + \frac{2a(a-b)E}{r_2^2}\right]$$

$$H_\rho = \frac{Iz_o}{2\pi r_1}\left[(K-E) - \frac{2a\,b\,E}{r_2^2}\right]$$

where $k^2 = \frac{4\,a\,b}{r_1^2}$

Solenoid

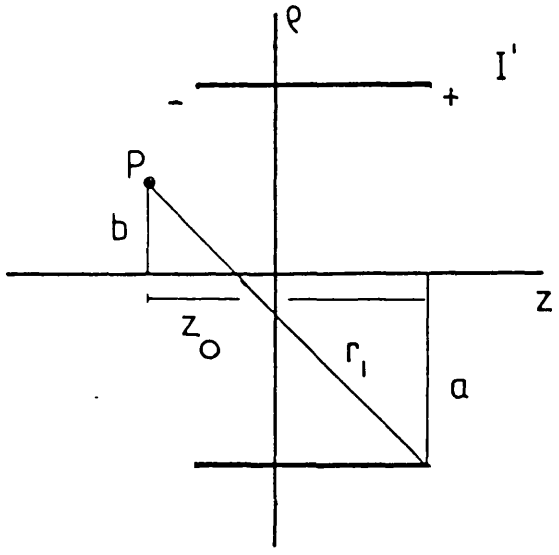

$$H_z = \frac{I' z_o c k}{4\pi} \left[K + \frac{(a - b)(II - K)}{2a} \right]$$

$$H_\rho = \frac{I' r_1}{4\pi} \left[2(K - E) - k^2 K \right]$$

where $k^2 = \frac{4ab}{r_1^2}$ $\quad c^2 = \frac{4ab}{(a+b)^2}$ $\quad n = -c^2$

APPENDIX 4.1

Parametric form for a generalised filamentary coil

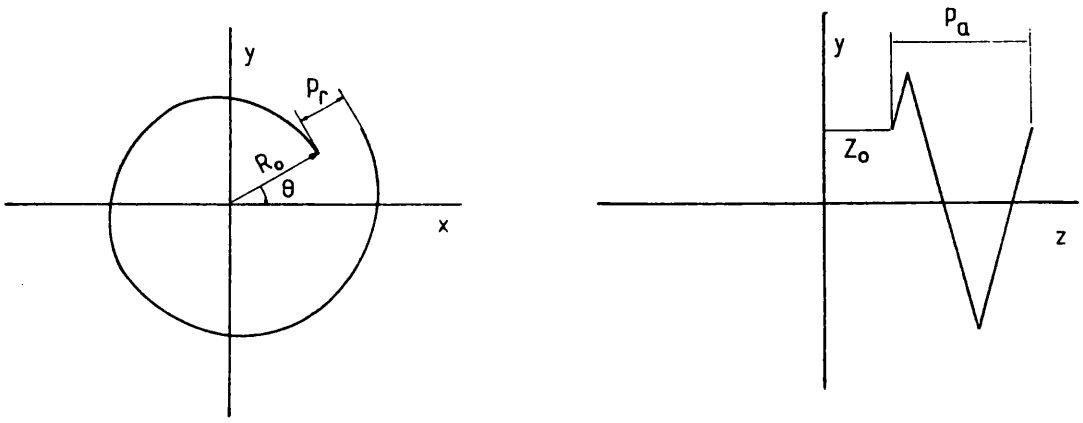

Point (x,y,z) on the coil is given by:

$$x = (R_o + p_r\phi/2\pi + d/4 \cos(2\phi + \theta)) \cos(\phi + \theta)$$
$$y = (R_o + p_r\phi/2\pi + d/4 \cos(2\phi + \theta)) \sin(\phi + \theta)$$
$$z = (Z_o + p_a\phi/2\pi)$$

and the integration is performed between $\phi = 0$ to $2N\pi$ where:

R_o = radius of coil start Z_o = axial posn. of coil start

p_r = spiral/radial pitch p_a = helical/axial pitch

d = oval diameter diff. θ = angular pos. of coil start

N = number of turns

Appendix 4.1 (contd.)

Parametric form for a straight wire

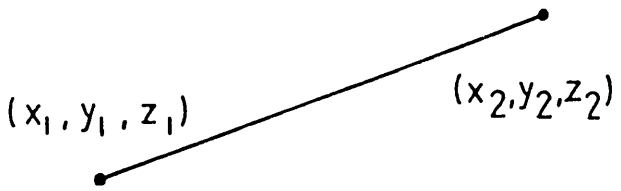

Point (x,y,z) on the wire is given by:

$$x = x_1 + u(x_2 - x_1)$$
$$y = y_1 + u(y_2 - y_1)$$
$$z = z_1 + u(z_2 - z_1)$$

and the integration performed between u = 0 to 1 where:

x_1, y_1 and z_1 are coords. of start of wire

x_2, y_2 and z_2 are coords. of end of wire

APPENDIX 4.2

The Legendre Functions

n	m	
0	0	1
1	0	u
1	1	$(1 - u^2)^{1/2}$
2	0	$1/2(3u^2 - 1)$
2	1	$3(1 - u^2)u$
2	2	$3(1 - u^2)$
3	0	$1/2(5u^3 - 3u)$
3	1	$3/2(1 - u^2)^{1/2}(5u^2 - 1)$
3	2	$15(1 - u^2)u$
3	3	$15(1 - u^2)^{3/2}$
4	0	$1/8(35u^4 - 30u^2 + 3)$
4	1	$5/2(1 - u^2)(7u^2 - 3)u$
4	2	$15/2(1 - u^2)(7u^2 - 1)$
4	3	$105(1 - u^2)^{3/2}u$
4	4	$105(1 - u^2)^2$

APPENDIX 4.3

Recurrence relations for the Legendre functions.

$$P_{n+1,m+1} = (m+n+1)\ (1-u^2)^{1/2}\ P_{n,m} + uP_{n,m+1}$$

$$P_{n+1,m+1} - P_{n-1,m+1} = (2n+1)(1-u^2)^{1/2}\ P_{n,m}$$

$$P_{n-1,m+1} = (m-n)(1-u^2)^{1/2}\ P_{n,m} + u\ P_{n,m+1}$$

$$P_{n,m+1} - 2mu(1-u^2)^{-1/2}P_{n,m} + (m+n)(n-m+1)P_{n,m-1} = 0$$

$$(m-n-1)P_{n+1,m} + (2n+1)uP_{n,m} - (m+n)P_{n-1,m} = 0$$

$$2m(1-u^2)^{-1/2}P_{n,m} = P_{n-1,m+1} + (m+n-1)(m+n)P_{n-1,m-1}$$

$$\begin{aligned}(1-u^2)^{1/2}P_{n,m}' &= -mu(1-u^2)^{-1/2}P_{n,m} + P_{n,m+1} \\ &= -1/2(m+n)(n-m+1)P_{n,m-1} + 1/2P_{n,m+1} \\ &= mu(1-u^2)^{-1/2}P_{n,m} - (m+n)(n-m+1)P_{n,m-1}\end{aligned}$$

$$\begin{aligned}(1-u^2)P_{n,m}' &= (n+1)uP_{n,m} - (n-m+1)P_{n+1,m} \\ &= (2n+1)^{-1}(m-n-1)nP_{n+1,m} + (n+1)(m+n)P_{n-1,m} \\ &= -nuP_{n,m} + (m+n)P_{n-1,m}\end{aligned}$$

and the Rodrigue's formula:

$$P_{n,m} = (1-u^2)^{1/2m}\ d^m/du^m\ P_n$$

APPENDIX 4.4

Weights used to obtain peak-peak values of spherical harmonics

Z1	2.0
Z2	1.5
Z3	2.0
Z4	1.4
Z5	2.0
Z6	1.4
Z7	2.0
Z8	1.4

Z0X1	2.0	Z0X3	30.0
Z1X1	3.0	Z1X3	68.2
Z2X1	4.1	Z2X3	130.9
Z3X1	5.3	Z3X3	222.3
Z4X1	6.4	Z4X3	347.5
Z0X2	6.0	Z0X4	210.0
Z1X2	11.5	Z1X4	540.9
Z2X2	19.3	Z2X4	1156.9
Z3X2	29.0	Z3X4	2167.6
Z4X2	40.6	Z4X4	3705.5

Y terms will have the same weights as those involving X

REFERENCES

i HOUNSFIELD, G.N.
Computerised transverse axial scanning (tomography)
Part I, Description of system.
B.J. of Radiology, 46, pp1016-1022, 1973

ii WELLS, P.N.T.
Biomedical Ultrasonics,
Academic Press, London, 1977.

1.1 ANDREW, E.R.
Nuclear magnetic resonance.
Cambridge University Press, 1958.

1.2 SLICHTER, C.P.
Principles of Nuclear Magnetic Resonance,
Harper and Row, New York, 1963.

1.3 YOUNG, I.R., et al,
(1) Initial Clinical Evaluation of a Whole Body Nuclear Magnetic Resonance (NMR) Tomograph.
J. Computer Assisted Tomography, Vol.6 No.1 Feb.1982

(2) Nuclear Magnetic Resonance Imaging of the Brain in Multiple Sclerosis.
The Lancet, 14 Nov. 1981, pp 1063-1066.

1.4 STEINER R.E., RADDA G.K., (eds.)
British Medical Bulletin, April 1984, Vol.40, No.2

1.5

(1) BLOCH, F.
Nuclear Induction,
Phys. Review, Vol.70, No.7&8, Oct.1946

(2) BLOCH, F., HANSEN, W.W., PACKARD, M.
The Nuclear Induction Experiment,
Phys. Review, Vol.70, No.7&8, Oct.1946

1.6 BLOEMBURGEN N., PURCELL E.M., POUND R.V.,
Relaxation Effects in Nuclear Magnetic Resonance Absorption.
Phys. Review, Vol.73, April 1948.

2.1 SCHWARZ, M.,
Information transmission, modulation and noise.
McGraw Hill, 1970

3.1 SMYTHE, W.R.,
McGraw Hill Book Co., N.Y., 1968

3.2 GARRETT, M.W.
Axially symmetric systems for generating and measuring magnetic fields. Part 1.
J. APPL. PHYS. Vol.22, No.9, pp1091-1107, Sept.1951.

3.3 ADBY, P.R. & DEMPSTER, M.A.H.,
Intrduction to optimisation methods,
Chapman and Hall, London, 1974.

3.5 GILL, P.E. & MURRAY, W.,
Quasi-Newton methods for unconstrained optimisation.
J. Inst. Maths & Appl., Vol.9, pp91-108, 1972.

3.6 GARRETT, M.W.
Calculation of fields, forces, and mutual inductances of current systems by elliptic integrals.
J. APPL. PHYS. Vol.34, No.9, pp2567-2573, Sept.1963.

3.7 BULLIRSCH, R.,
Numerical calculation of elliptic integrals and elliptic functions III.
Numerische Mathematik, 13, pp305-315, 1969.

4.1 DAVIS, P.J., & RABINOWITZ, P.,
Numerical integration,
Blaisdell Publishing Co., Mass., 1967.

4.2 HAVIE, T.,

On the practical application of the modified Romberg Algorithm.

BIT 7, pp103-113, (1967).

4.3 CLENSHAW, C.W. & CURTISS, A.R.,

A method for numerical integration on an automatic computer.

Numerische Mathematik, 2, pp197-205, 1960.

4.4 PATTERSON, T.N.L.,

The optimum addition of points to quadrature formulae.

Math. Comp., 22, pp847-856, 1968.

4.5 GOLAY, M.J.E.,

(1) Field homogenising coils for nuclear spin instrumentation.

Rev. Sci. Instr., Vol.29,No.4, pp313-315, April 1958

(2) Homogenising coils for NMR apparatus.

British Patent No. 1234262.

(3) Homogenising coils for NMR apparatus.

British Patent No. 1286150

4.6 MATHEWS, J.

Coordinate free rotation formalism,

Am. J. Phys., Vol.44, No.12, Dec. 1976.